Physical Principles of Remote Sensing

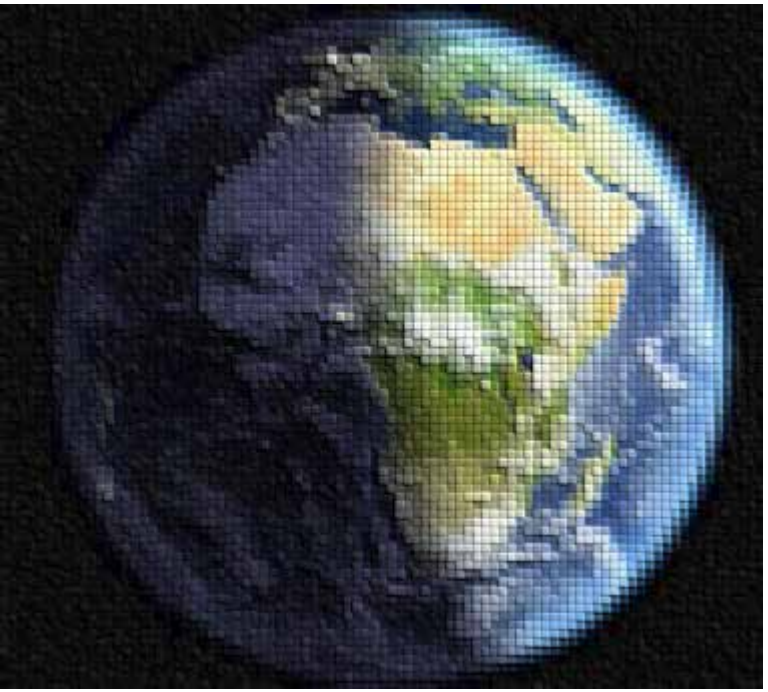

Thermal Remote Sensing

Dr. Claudia Kuenzer
German Remote Sensing Data Center, DFD
German Aerospace Center, DLR
email: claudia.kuenzer@dlr.de
fon: +49 – 8153 – 28-3280

§ TIR at high Resolution (Thermal Camera)

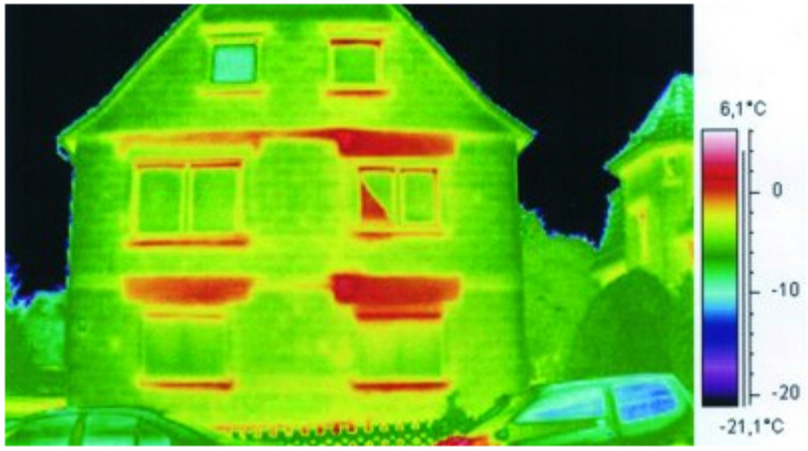

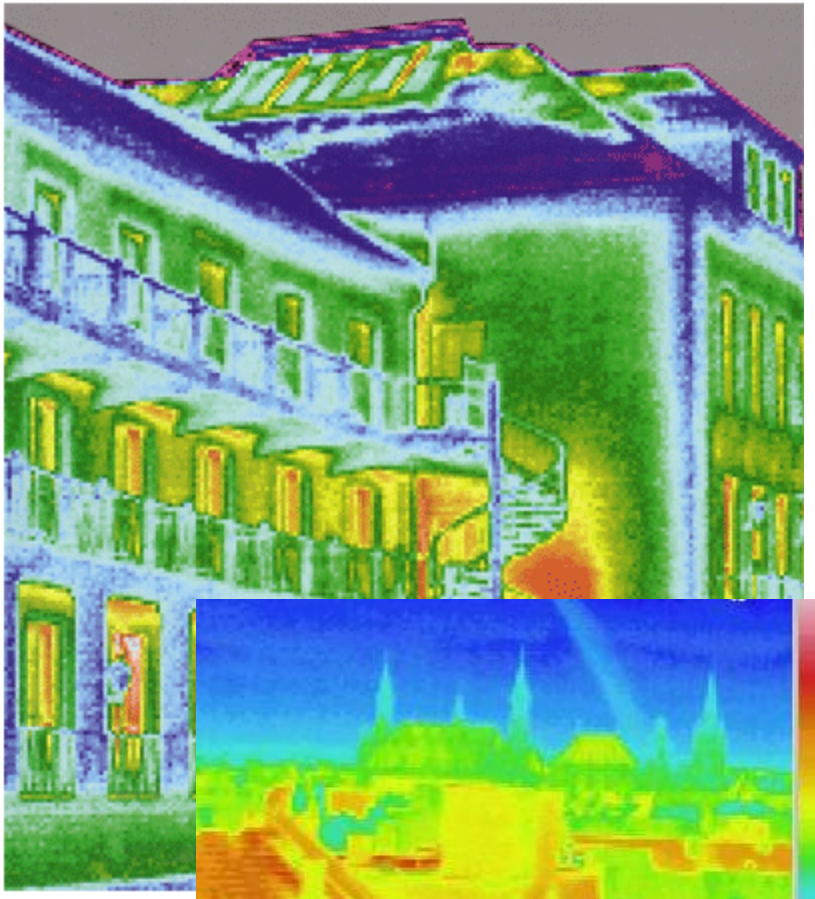

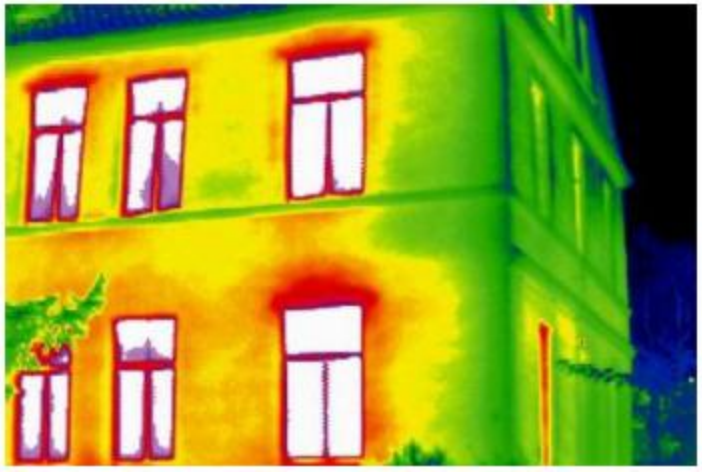

Thermal Infrared Radiation

Radiation at wavelengths between 3 - 14 µm

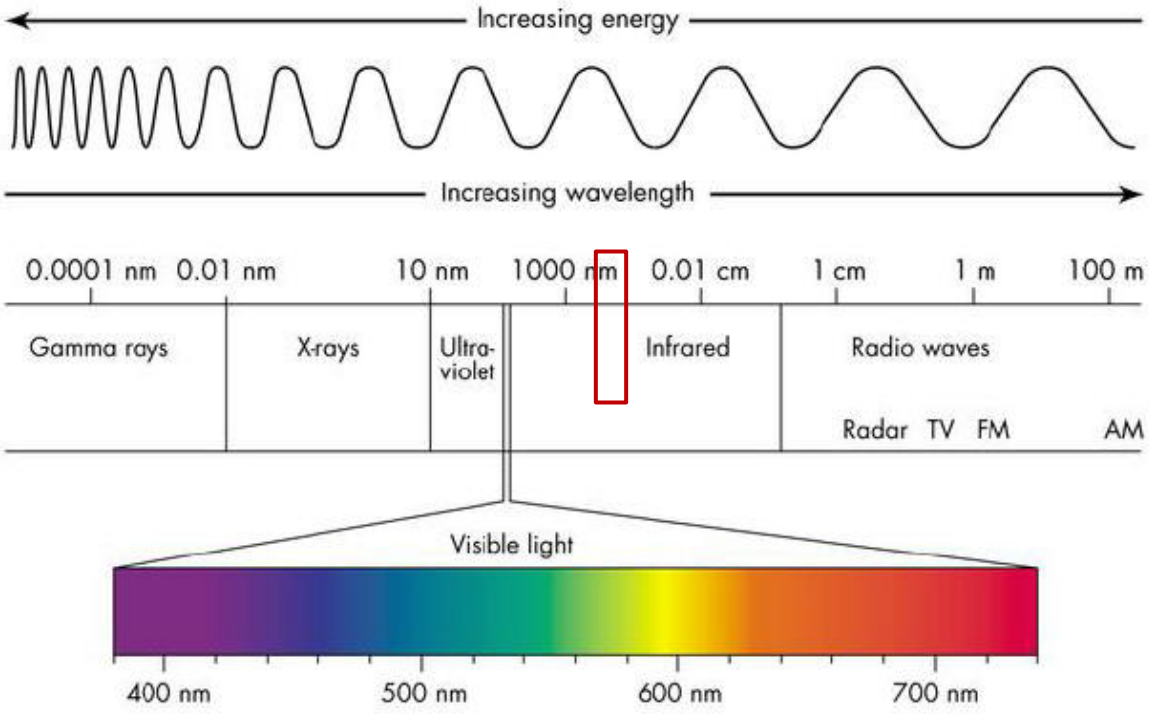

Source: http://bigfootproof.com/groups/visible-invisible-d2-ranges.html

All materials at **temperatures above absolute zero** (0 K, -273 ° C) continuously emit electromagnetic radiation. The **earth** with its ambient temperature of ca. 300 K has its **peak energy emission** in the thermal infrared region at around **9.7 µm**.

Atmospheric Windows in the Thermal IR Region

situated between 3 - 5 µm and 8 - 14 µm. The latter has narrow absorption band from 9 to 10 µm caused by ozone, which is omitted by most thermal IR satellite sensors.

Note that reflected sunlight can contaminate thermal IR signals recorded in the 3 - 5 µm windows during daytime.

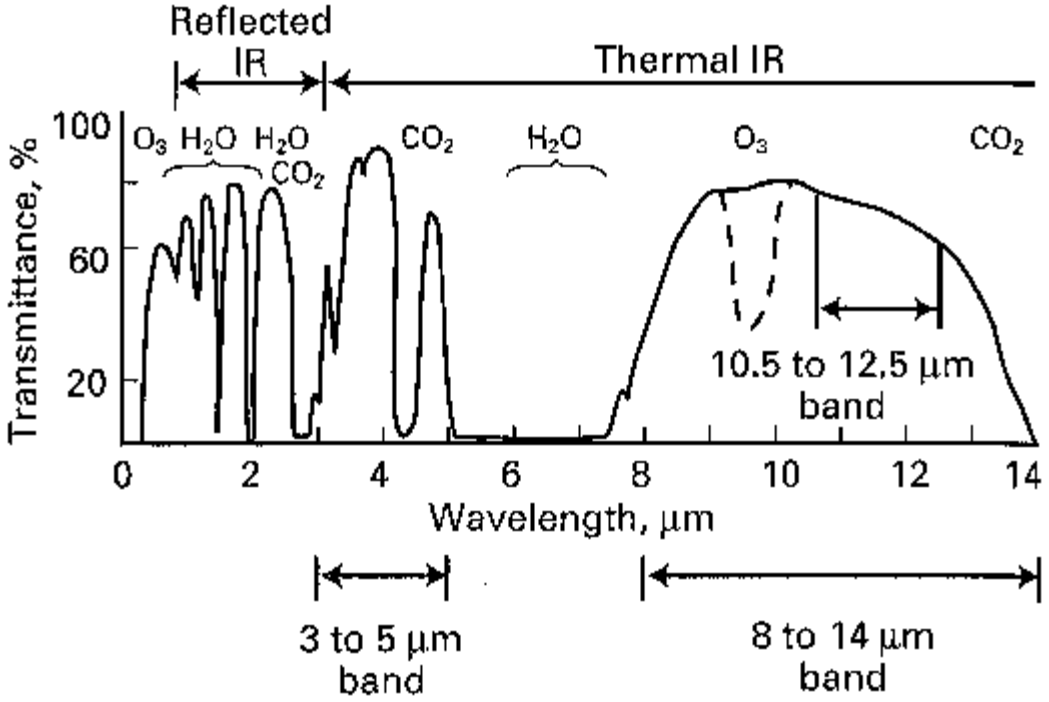

Source: Sabins (1997)

Planck's Blackbody Radiation Law

Describes the electromagnetic radiation emitted from a blackbody at a certain wavelength as a function of its absolute temperature.

$$M_{\lambda} = \frac{2 \pi h c^2}{\lambda^5 \left(e^{hc/\lambda kT} - 1 \right)}$$

M_λ = spectral radiant exitance [W m^{-2} μm^{-1}]

h = Planck's constant [6.626 x 10^{-34} J s]

c = speed of light [2.9979246 x 10^8 m s^{-1}]

k = Boltzmann constant [1.3806 x 10^{-23} J K^{-1}]

T = absolute temperature [K]

λ = wavelength [µm]

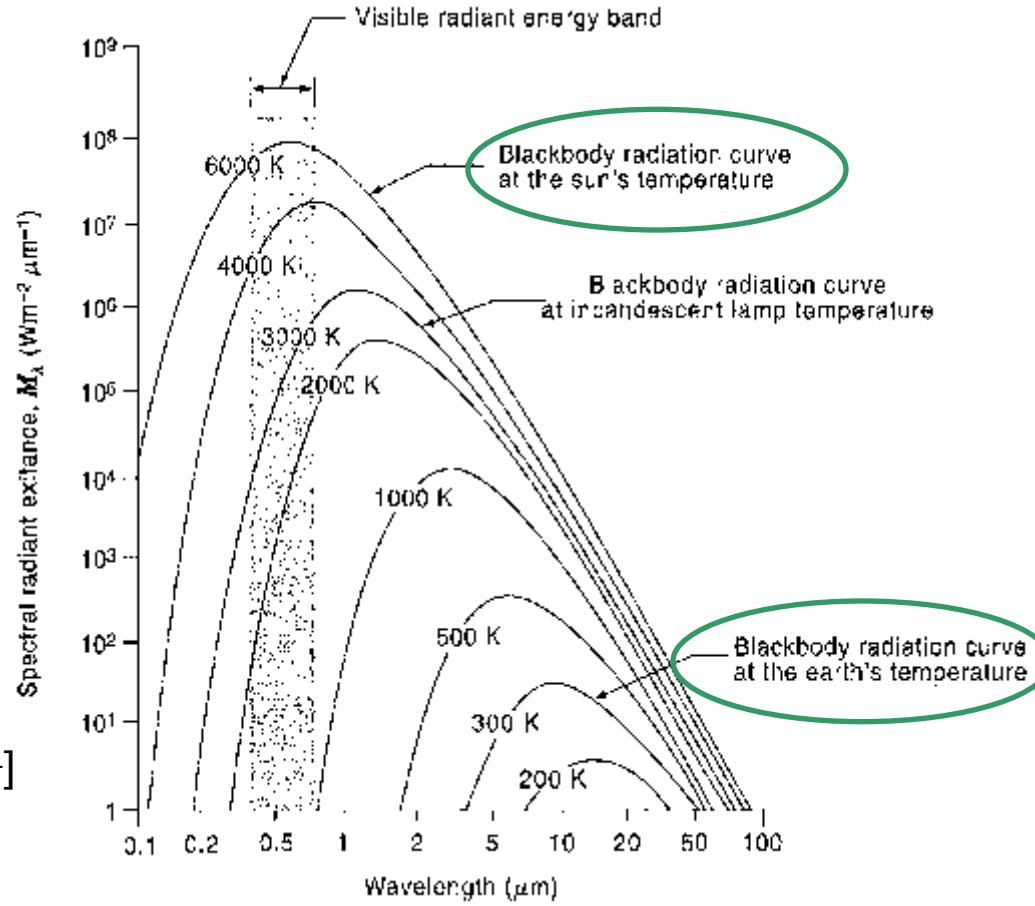

Source: Lillesand et al. (2008)

Stefan-Boltzmann Law

Describes the total electromagnetic radiation emitted by a blackbody as a function of the absolute temperature which corresponds to the area under the radiation curve (integral).

$$M = \sigma T^4$$

M = total radiant exitance [W m²]
T = absolute temperature [K]
σ = Stefan-Boltzman constant
[5.6697 x 10^{-8} W m^{-2} K^{-4}]

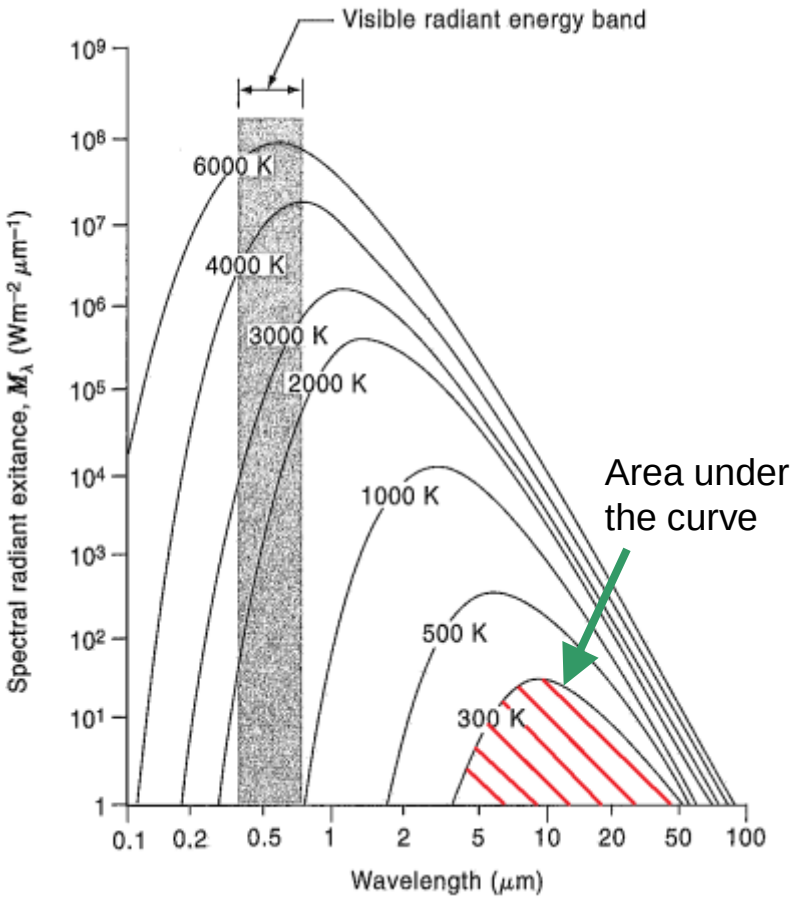

Source: Lillesand et al. (2008)

à The higher the temperature of the radiator, the greater the total amount of radiation it emits.

Wien‘s Displacement Law

Describes the wavelength at which the maximum spectral radiant exitance occurs.

$$\lambda_{max} = \frac{A}{T}$$

λ_{max} = wavelength of maximum spectral radiant exitance [µm]
A = Wien‘s constant [2897.8 µm K]
T = absolute temperature [K]

à With increasing temperature λ_{max} shifts to shorter wavelengths.

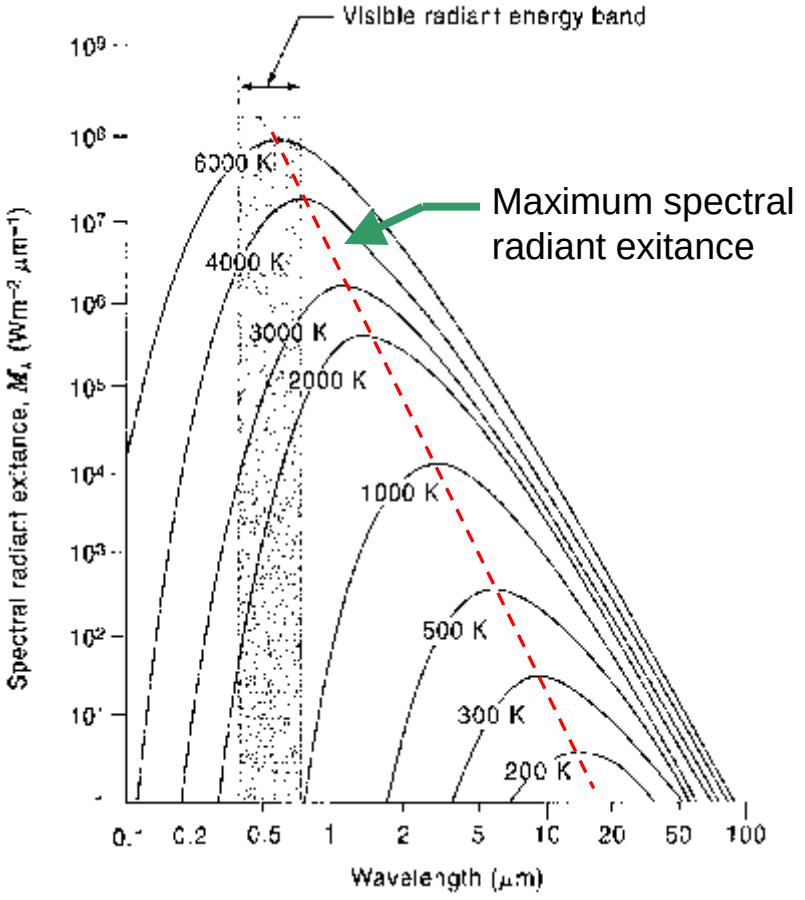

Source: Lillesand et al. (2008)

VIS versus SWIR

Landsat 7 ETM+ 14. Feb. 2000, Kilauea Volcano (Hawaii)

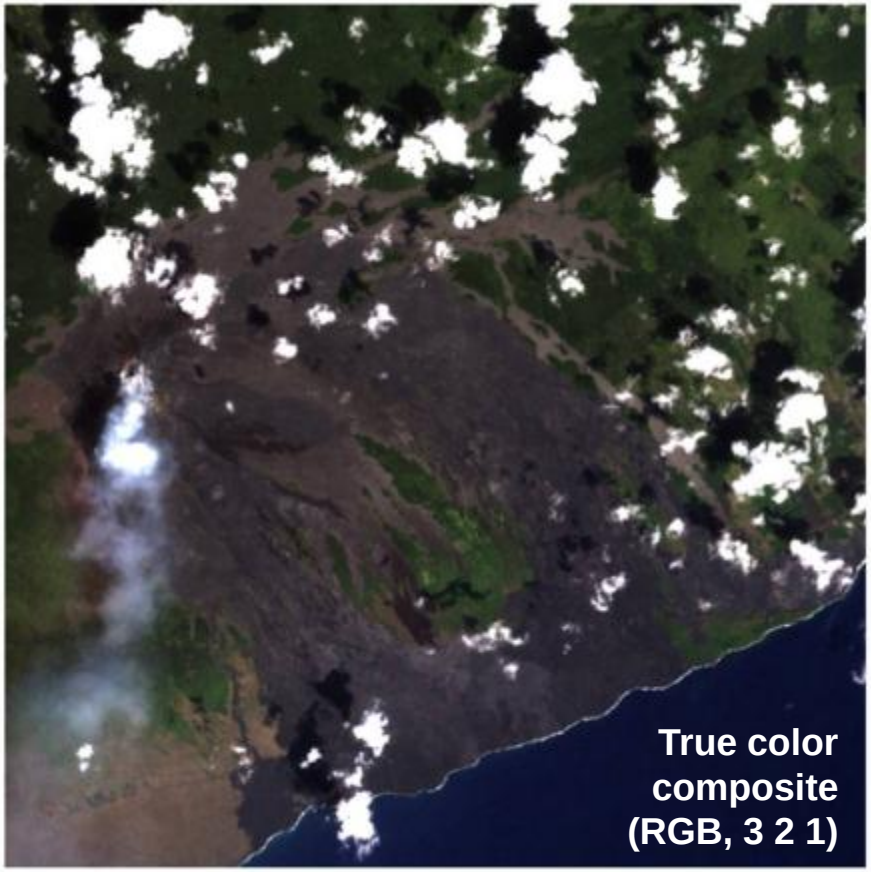

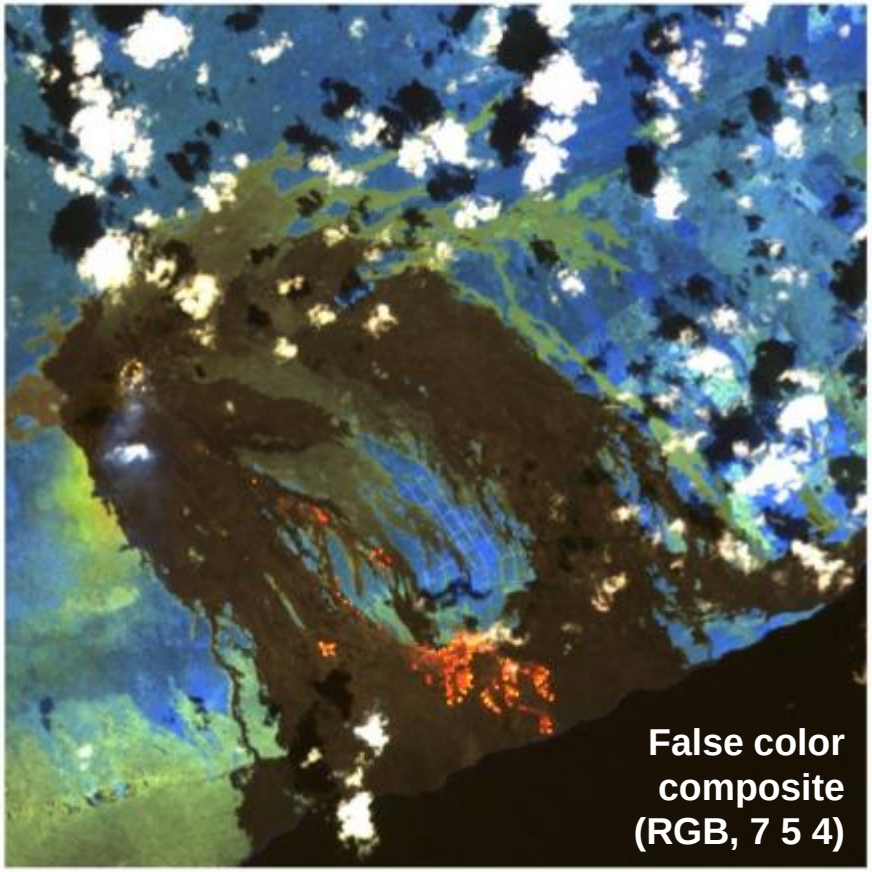

SWIR versus TIR

Landsat 7 ETM+ 14. Feb. 2000, Kilauea Volcano (Hawaii)

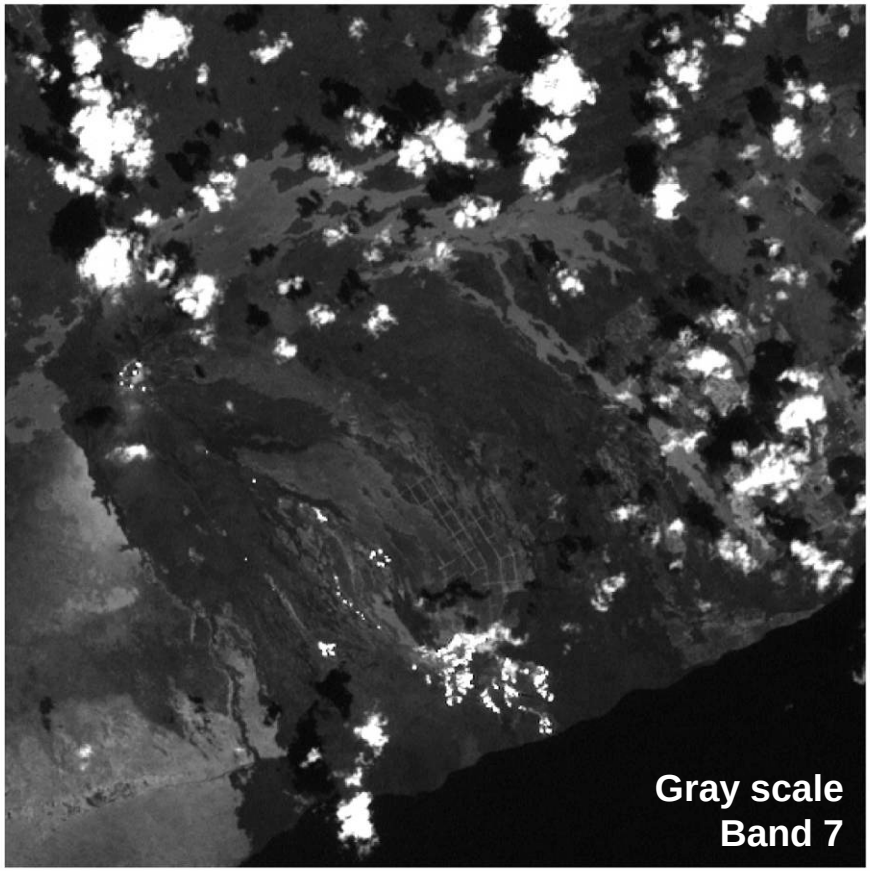

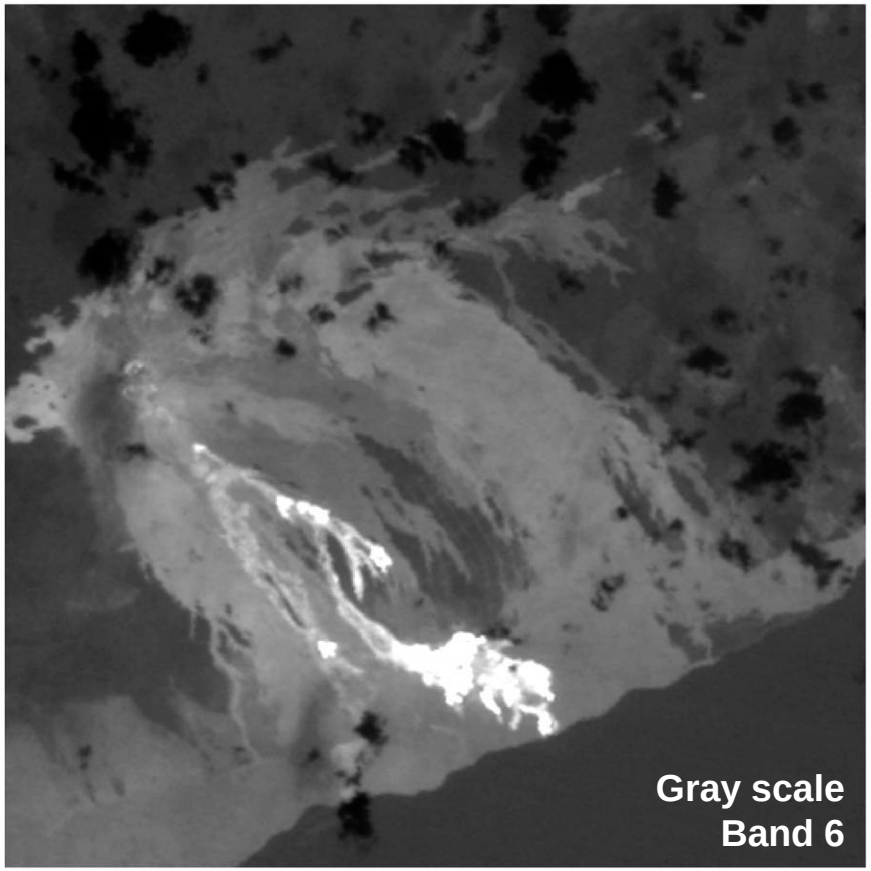

Interaction of Radiation with Terrain Elements

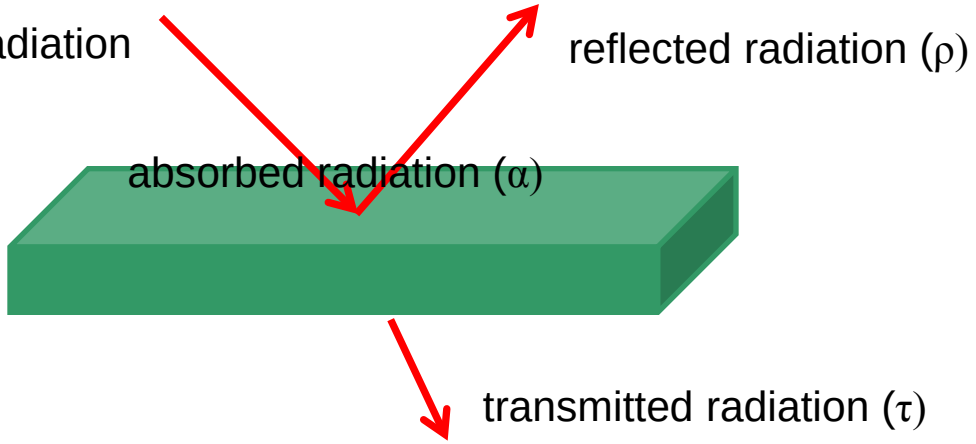

$$a_{\lambda} + r_{\lambda} + t_{\lambda} = 1$$

α, ρ, τ are **wavelength dependent** and represent **ratios** between the **absorbed**, **reflected** and **transmitted** components of the incident energy striking a terrain element and the **total energy** incident on the terrain element, respectively.

Blackbody Concept

A blackbody is a **hypothetical, ideal radiator** that totally absorbs and re-emits all energy incident upon it. The **total energy** a blackbody radiates and the spectral distribution of the emitted energy (radiation curve) **depends on the temperature** of the blackbody and can be described by:

- **Planck's radiation law**
- **Stefan-Boltzmann law**
- **Wien's displacement law**

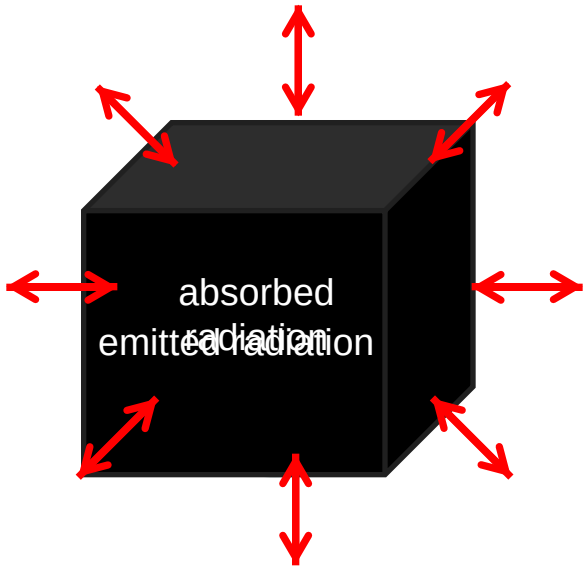

Radiation of real Materials and Emissivity

Real materials do not behave like blackbodies. They emit only a fraction of the radiation emitted by a blackbody at the equivalent temperature. This is taken into account by the EMISSIVITY, or the emissivity coefficient (ε):

$$e_l = \frac{\text{radiant exitance of an object at a given temperature}}{\text{radiant exitance of a blackbody at the same temperature}}$$

Emissivity can have values between 0 and 1. It is a measure of the ability of a material both to radiate and to absorb energy.

M = total radiant exitance [W m²]
T = absolute temperature [K
σ = Stefan-Boltzman constant]

Kirchhoff's Radiation Law

According to Kirchhoff's radiation law: $e_\lambda = a_\lambda$ (for a blackbody)

Spectral emissivity of an black body object equals its spectral absorbance:
"good absorbers are good emitters"

On the basis of Kirchhoff's radiation law α_λ can be replaced with ε_λ:

$$e_\lambda + r_\lambda + t_\lambda = 1$$

Since most objects are **opaque (do not let radiation transmit)** to thermal infrared radiation ($\tau_\lambda = 0$):

$$e_\lambda + r_\lambda = 1$$

à **The higher an object's reflectance in the thermal IR region, the lower its emissivity and vice versa.**

!!! Radiation of real Materials !!!

Provided that the emissivity of a material is known, its absolute temperature (kinetic temperature, T_{kin}) can be derived from the radiation it emits. If the emissivity is not considered, only the brightness temperature (radiant temperature, T_{rad}) of the material can be determined. Since it is valid that:

$$T_{rad} = \varepsilon T_{kin}$$

sensed touched

the **radiant temperature of a real material is always lower than its kinetic temperature**. However, **for a blackbody with ε = 1 it applies that**:

$$T_{rad} = T_{kin}$$

Radiation of real Materials

Emissivity depends on wavelength, surface temperature, and some physical properties of the surface, e.g. water content, or density.

Material	Average Emissivity over 8-14 µm
Clear water	0.98 - 0.99
Healthy green vegetation	0.96 - 0.99
Dry vegetation	0.88 - 0.94
Asphaltic concrete	0.94 - 0.97
Basaltic rock	0.92 - 0.96
Granitic rock	0.83 - 0.87
Dry mineral soil	0.92 - 0.96
Polished metals	**0.06 - 0.21**

Source: Lillesand et al. (2008)

Radiation of real Materials

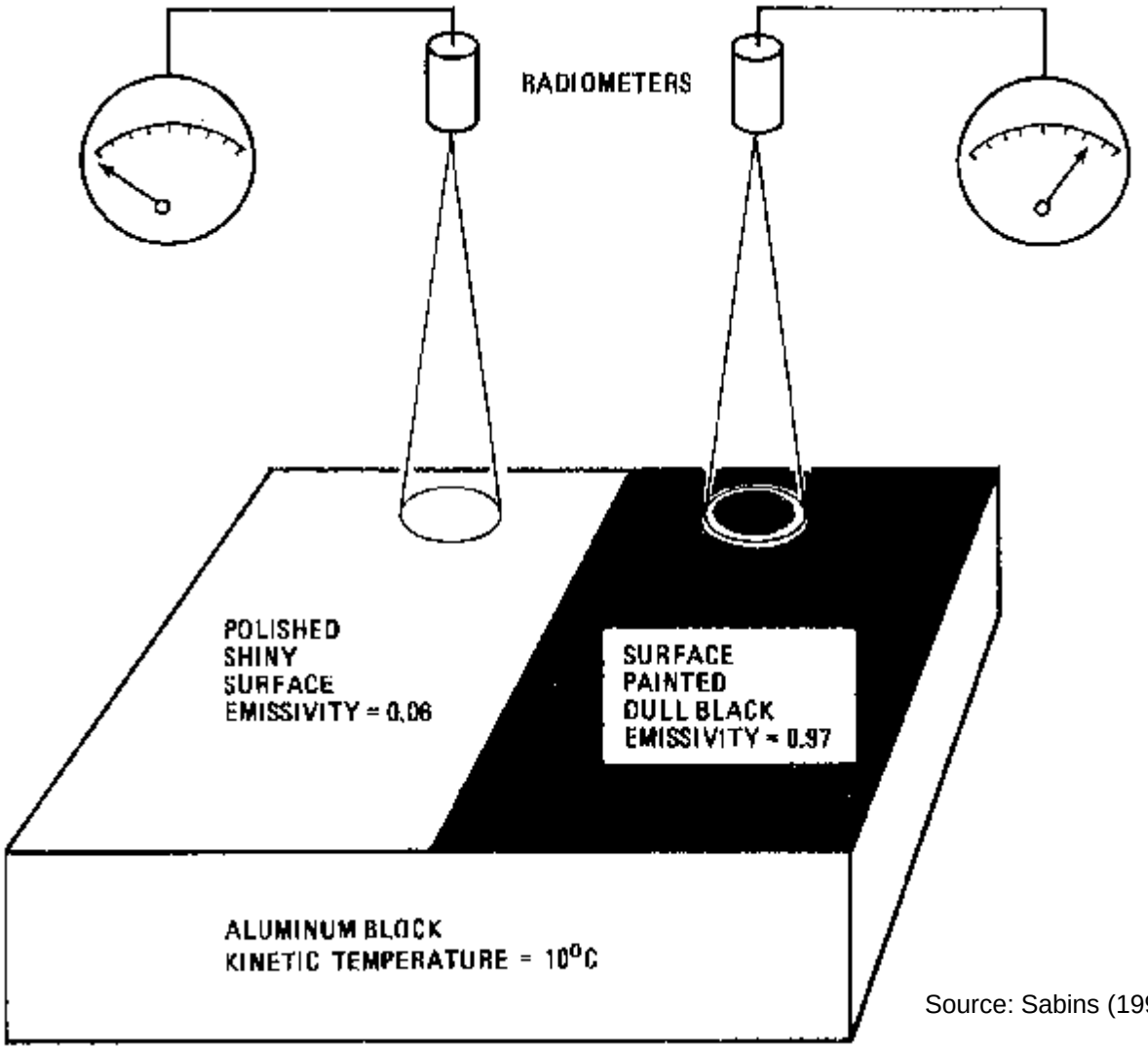

Source: Sabins (1997)

$$T_{rad} = e^{1/4} T_{kin}$$

Because of emissivity different objects can have the same kinetic temperature but differ significantly in the radiation they emit and their radiant temperatures !!!

Radiation of real Materials

visible (left) vs. thermal IR (right), Sacramento, CAL, USA

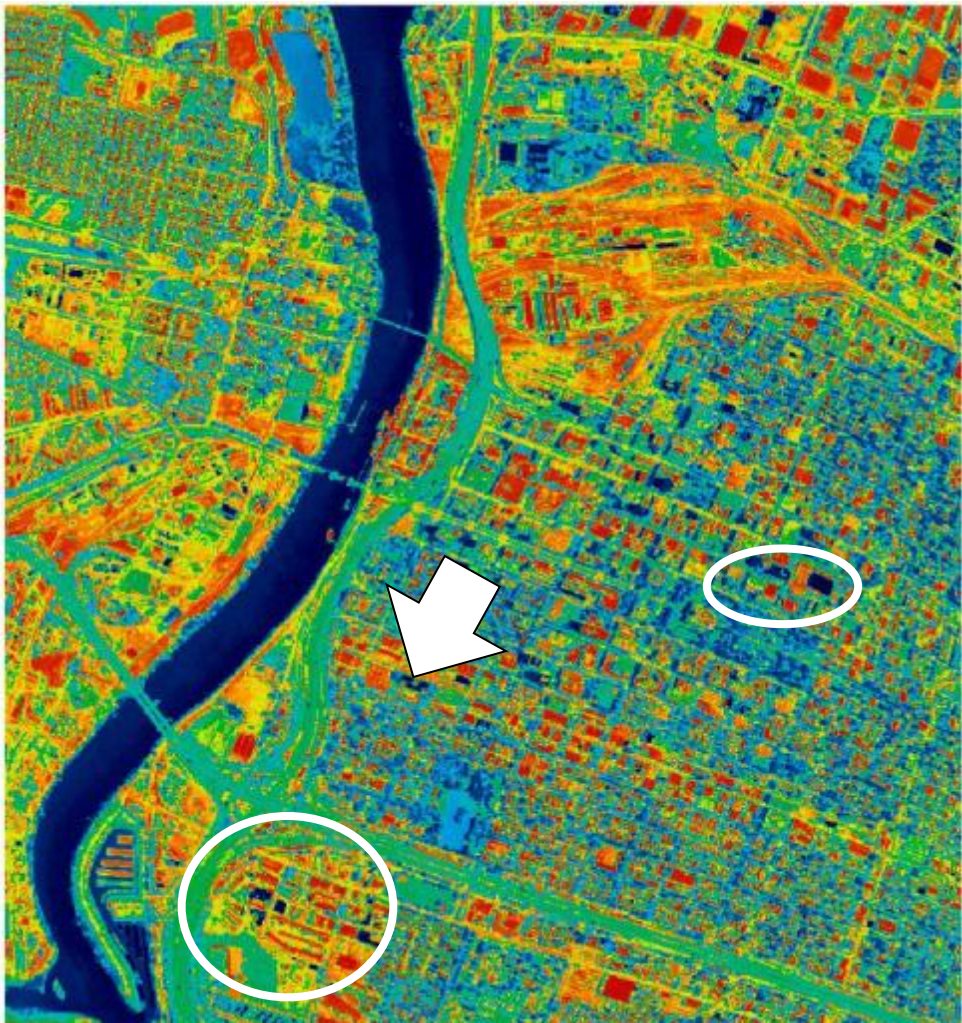

Changes in Emissivity of Surfaces .....

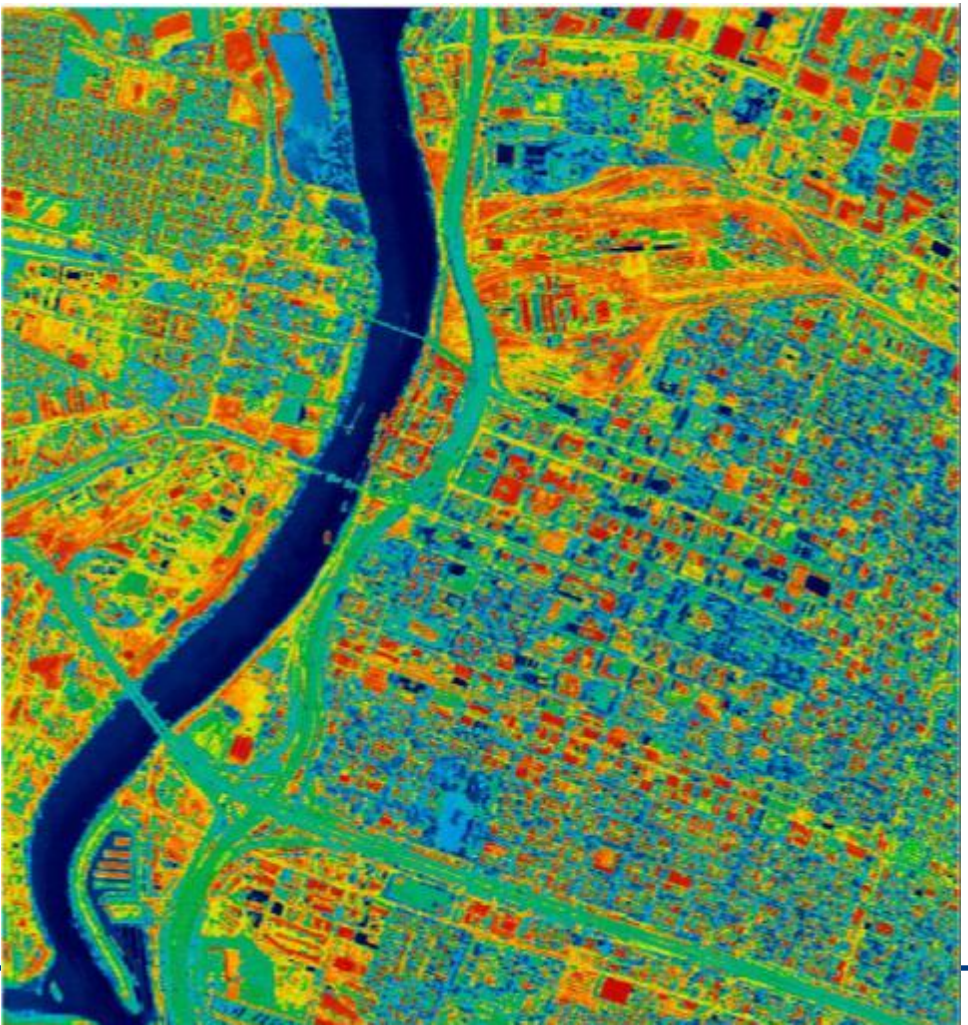

Actually should be taken into Account for any urban heat island related analyses in fast growing cities

Radiation of real Materials

Munich Downtown
with

English Garden
Main Station
Oktoberfest ‚Wiesn'

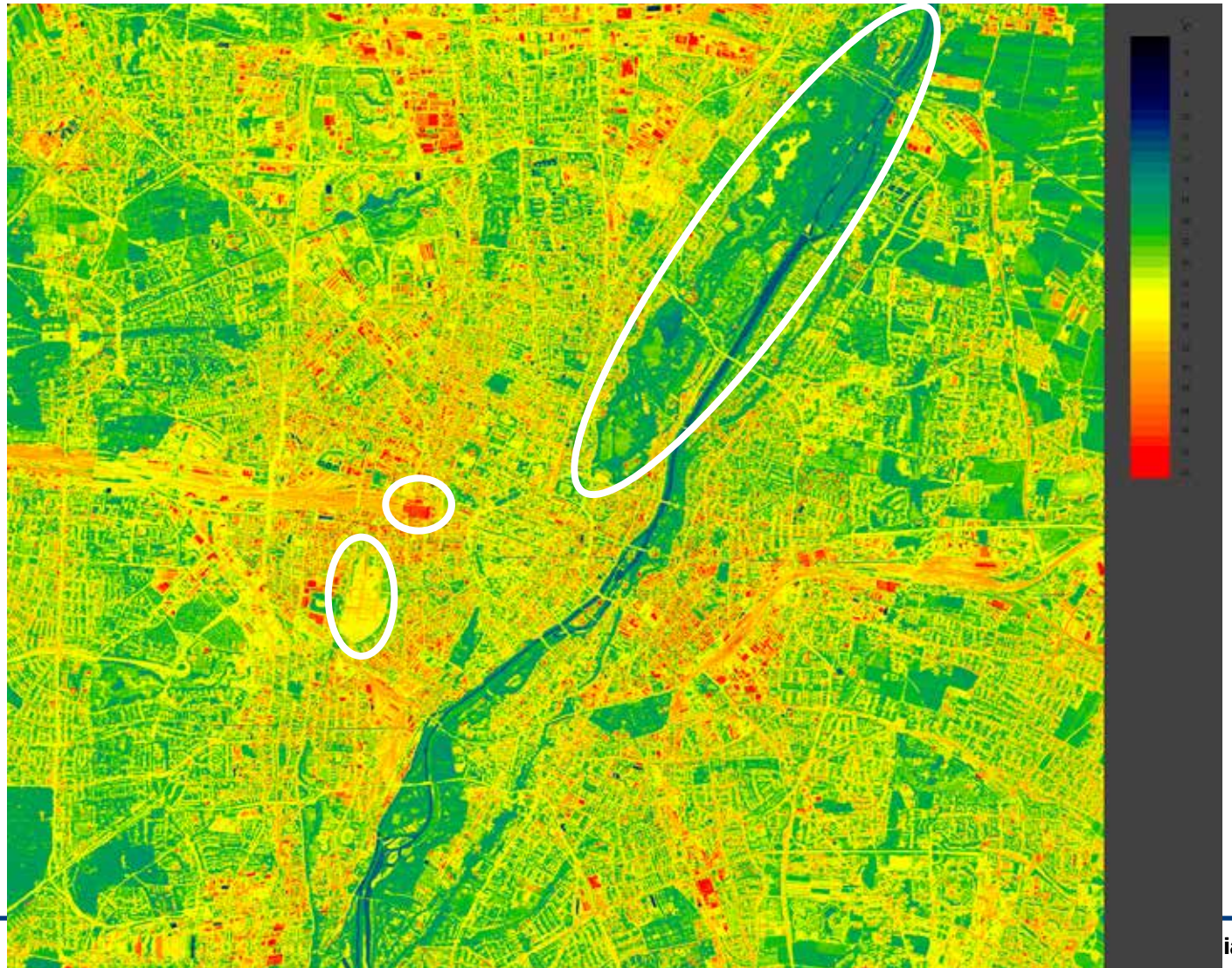

Radiation of real Materials

While the emissivity of a blackbody is always 1, real materials show a certain wavelength dependence and are referred to as selective radiator. A graybody, in turn, has an emissivity less than 1 but constant at all wavelengths.

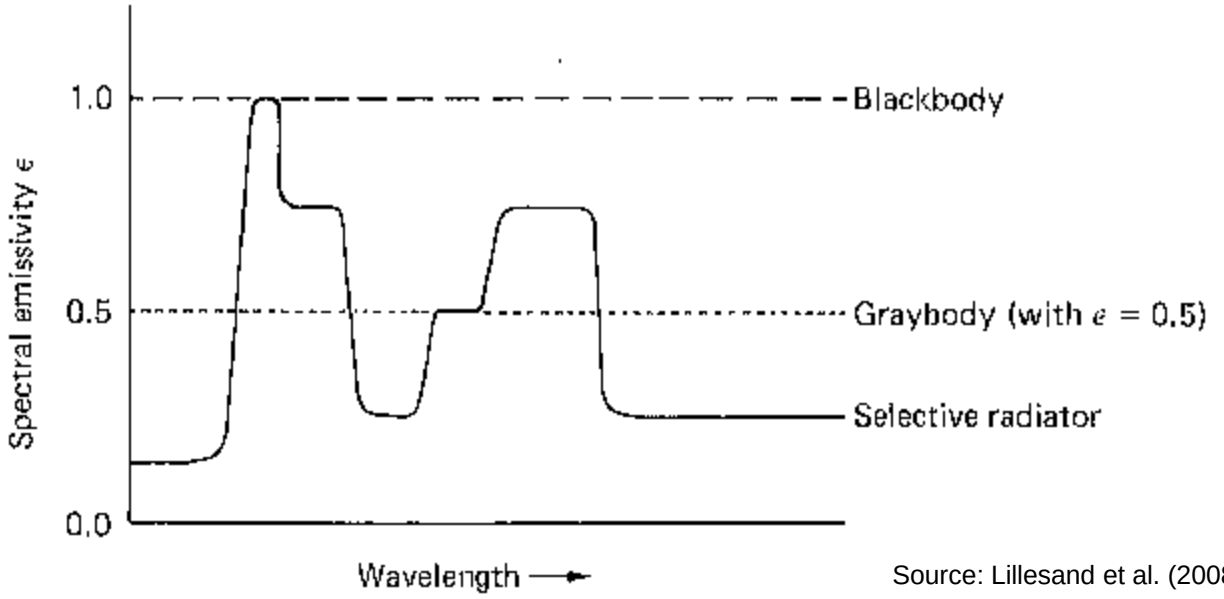

Source: Lillesand et al. (2008)

Radiation of real Materials

When broadband sensors are used emissivity for any given material type is often considered to be constant in the 8 - 14 µm range, which means these materials are treated as graybodies (but e.g. ASTER ….).

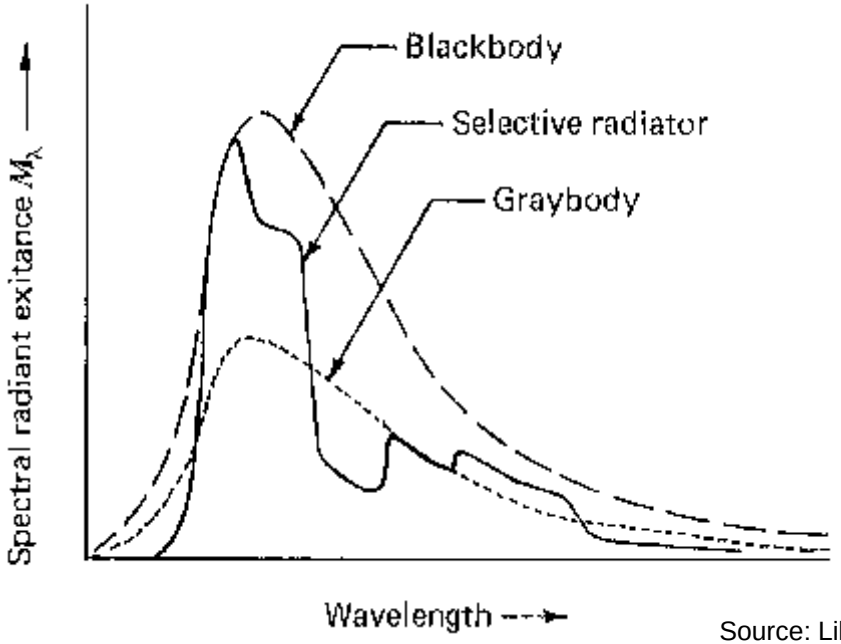

Source: Lillesand et al. (2008)

Radiation of real Materials

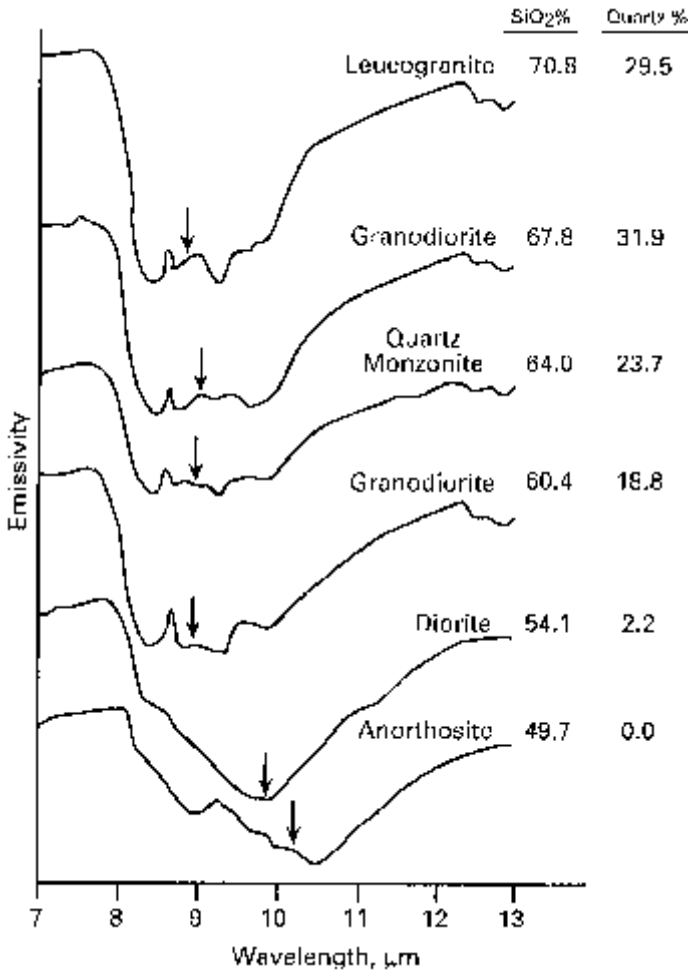

Emissivity spectra of different igneous rocks. Arrows show centers of adsorption bands. Spectra are offset vertically (Source: Sabins 1997).

Sensor Systems operating in the thermal IR Region

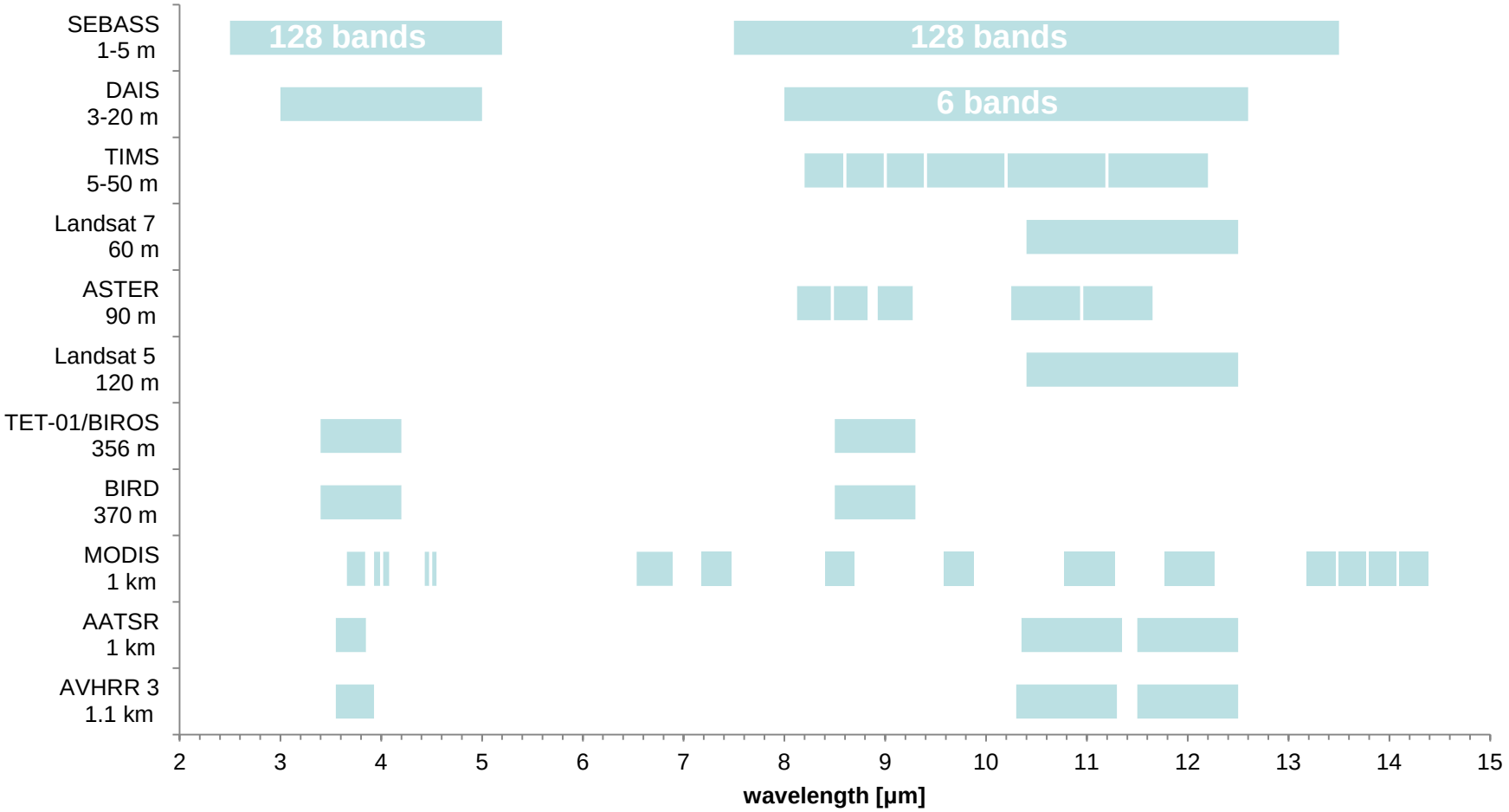

Diurnal Temperature Variation

Each terrain element shows a distinctive diurnal temperature cycle determined by the interaction between the thermal inertia of the object and the history of the incoming radiation from the sun.

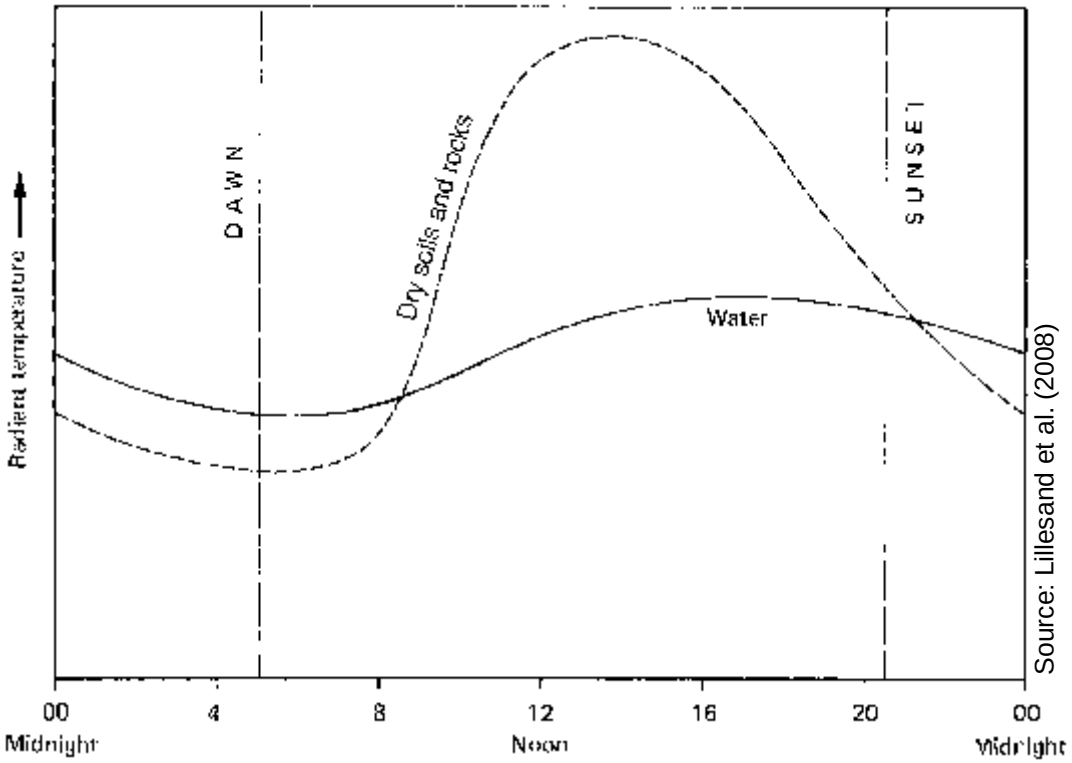

à The effects of diurnal temperature variation has to be taken into consideration by mission planning and image interpretation.

Diurnal Temperature Variation

Middleton (WI), USA

Daytime

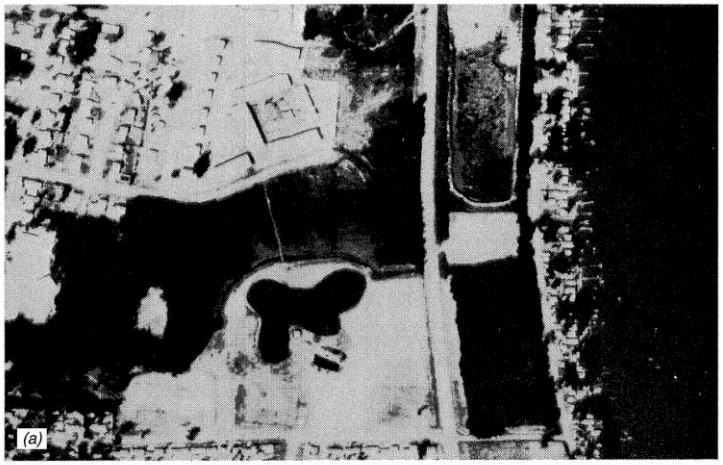

Nighttime

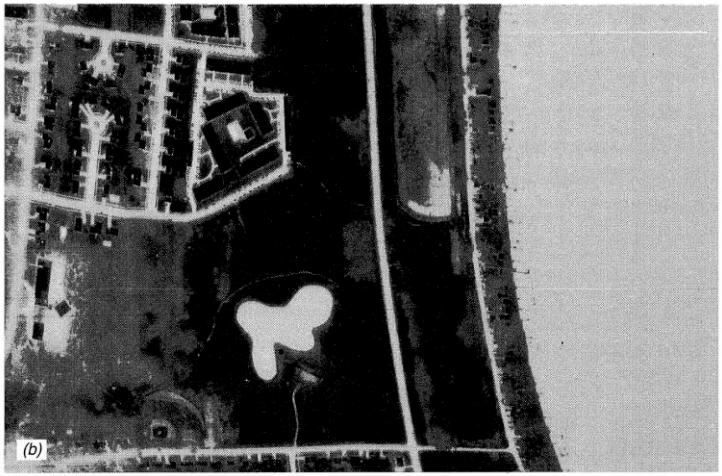

Source: Lillesand et al. (2008)

Diurnal Temperature Variation and Solar Effects Day/Night

Caliente and Temblor Ranges (CAL), USA

Daytime

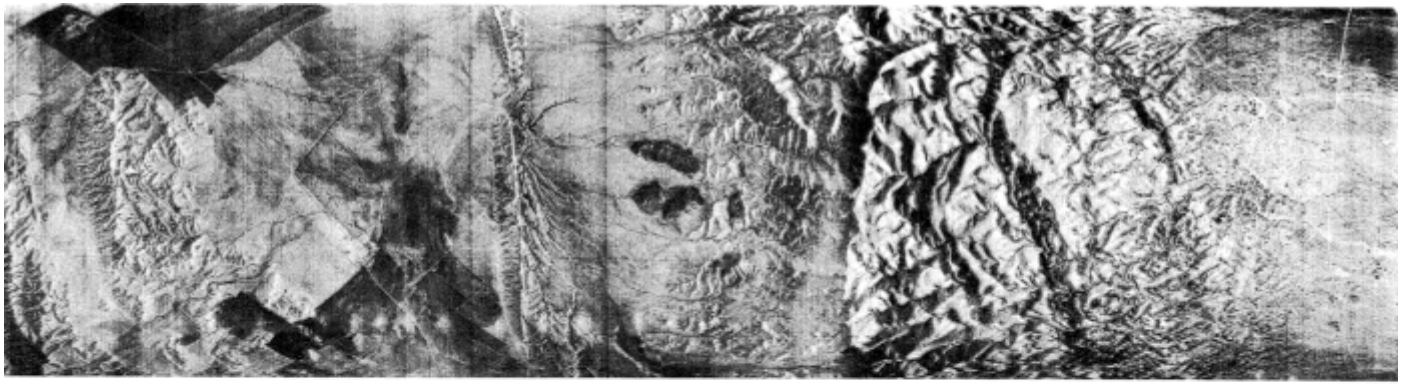

Nighttime

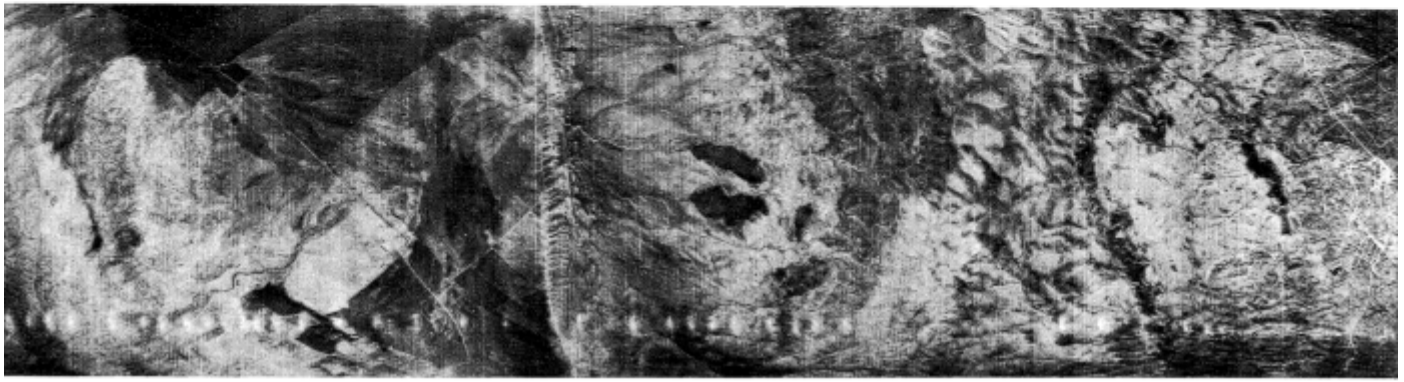

Source: Sabins (1997)

Intra-Annual Temperature Variation

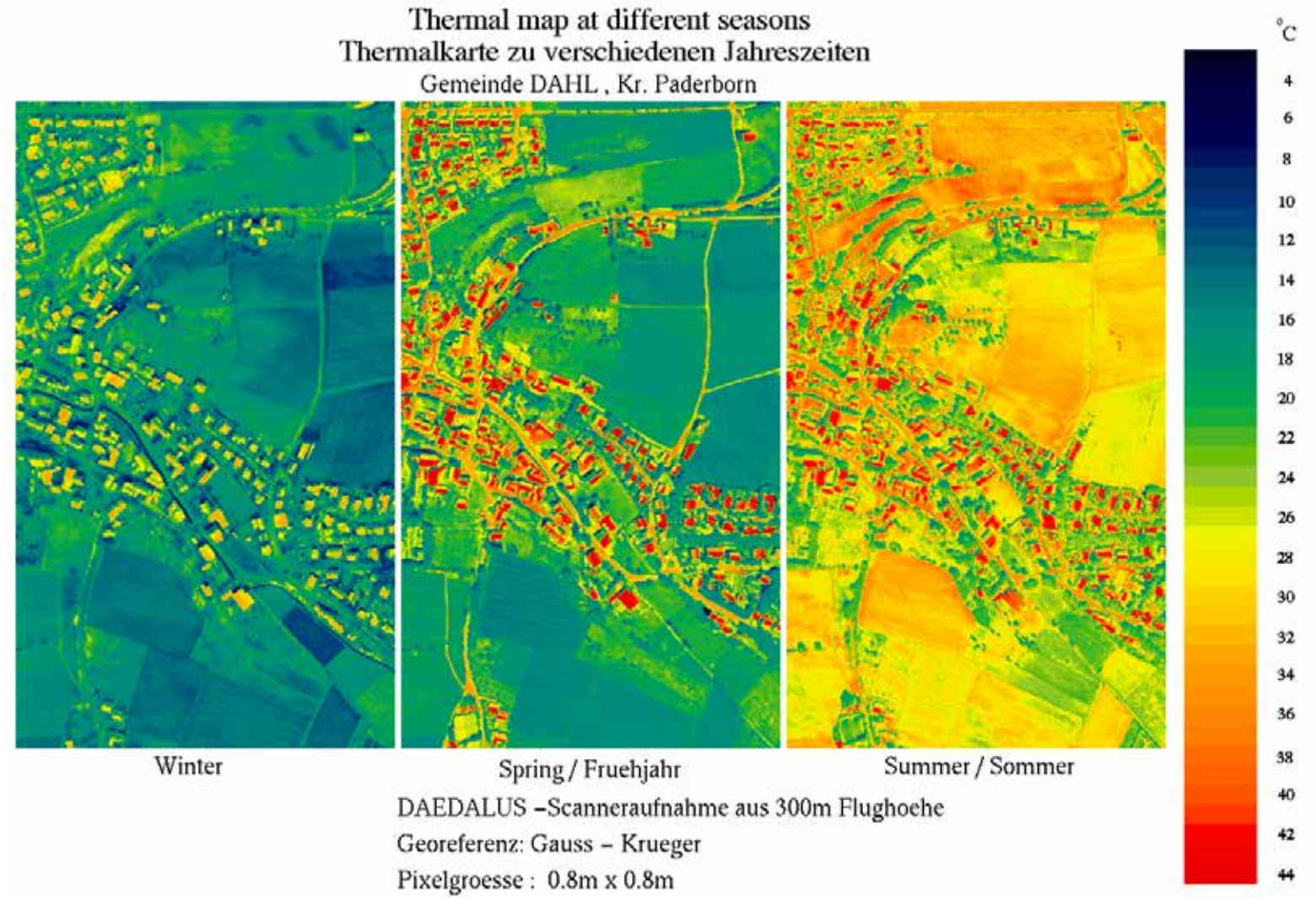

Thermal Inertia

Thermal inertia: measure of the resistance of a material to temperature changes.

In general, materials with high thermal inertia have more uniform surface temperatures throughout the day and night than material of low thermal inertia

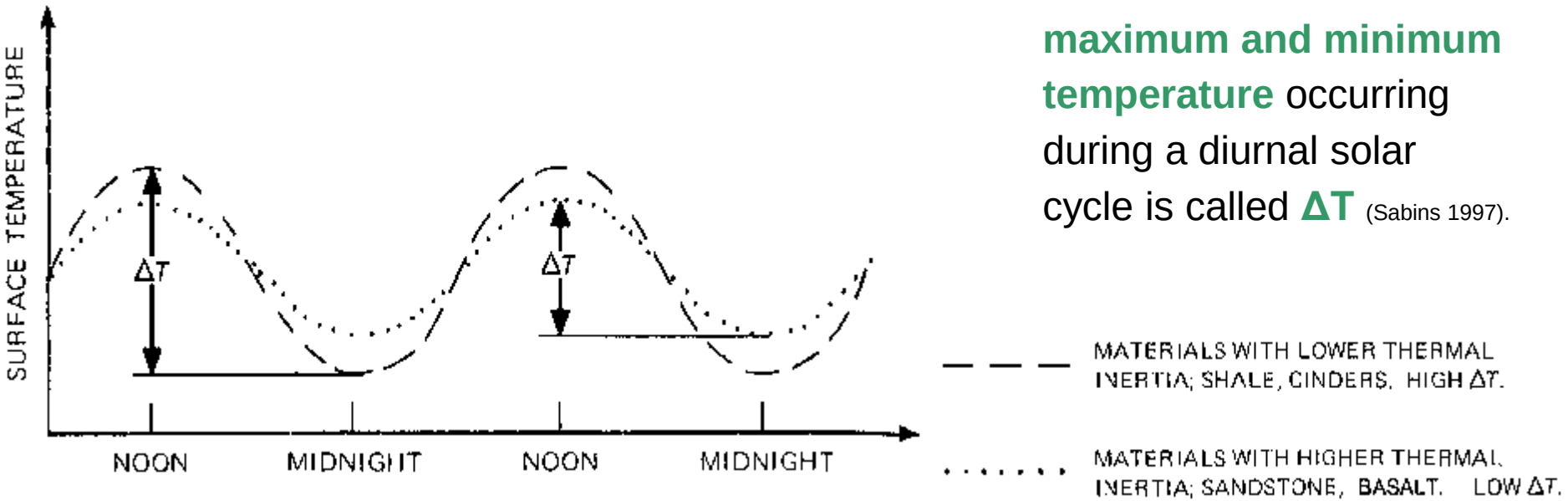

Source: Sabins (1997)

The **difference between maximum and minimum temperature** occurring during a diurnal solar cycle is called **ΔT** (Sabins 1997).

Apparent Thermal Inertia

Materials with low thermal inertia have a relatively high ΔT. The opposite is true for materials with high thermal inertia.

ΔT can be derived by subtracting the minimum nighttime temperature from the maximum daytime temperature of two images covering the same area. Then the apparent thermal inertia (ATI) can be calculated by:

$$ATI = \frac{1 - A}{\Delta T}$$

A is the albedo in the visible band and compensates for the effects that differences in absorptivity have on radiant temperature.

Influence of the Atmosphere on the thermal IR Signal

Scattering processes are negligible in the thermal IR region because of the long wavelength, but atmospheric absorption and emission by water vapor, CO_2 and O_3 are prevalent. Within atmospheric windows effects are less severe. However, signal recorded at the sensor (L) consist of the radiation emitted from the terrain element (εL_B) modified by the transmission of the atmosphere (τ), the atmospheric upwelling radiation (L_u) and the atmospheric reflected downwelling radiation (L_d).

Atmospheric correction methods:

- **- Empirical line method (ELM)**
- **- Radiative transfer model (RTM)**
- **……**

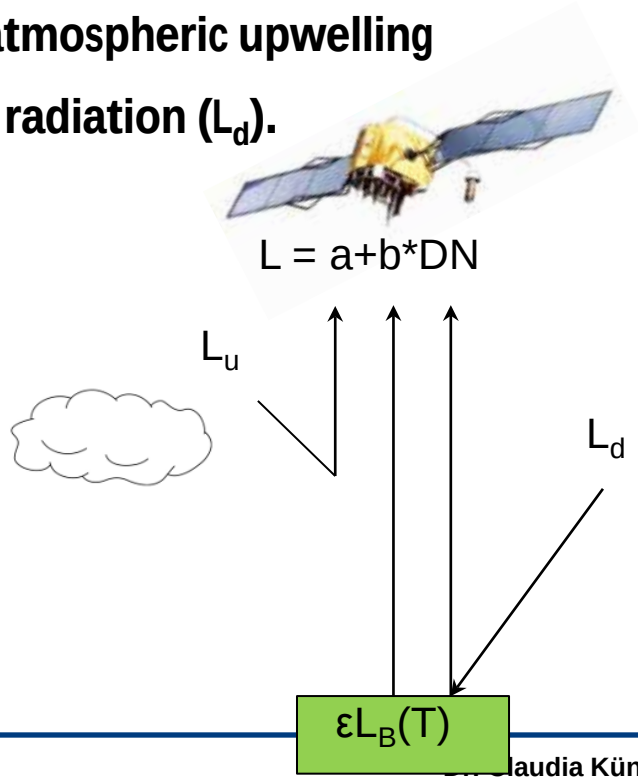

Empirical Line Method (ELM)

ELM applies a linear regression to each band by plotting DN or at-satellite reflectance (L_λ) values against in-situ temperature measurements recorded simultaneous with satellite overpass. The resulting coefficients a (offset) and b (gain) are used to transform each pixel value in the scene to its kinetic temperature (T_k).

$$T_k = a + b * DN$$

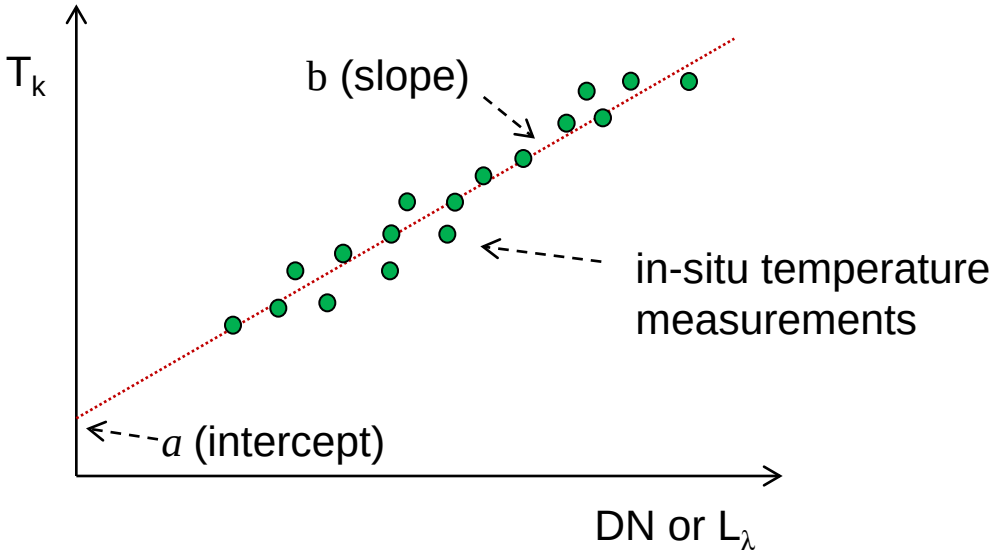

Drawback:

- **in-situ measurements are cost intensive, time-consuming and not available for remote areas or images from the past**

Radiative Transfer Model (RTM)

Based on a radiative transfer equation the path of the radiation through the atmosphere can be simulated by:

$$\underbrace{L(\lambda)}_{\text{at-satellite radiance}} = \underbrace{\varepsilon(\lambda) L_B(\lambda, T) t(\lambda)}_{\text{emitted surface radiance}} + \underbrace{L_u(\lambda)}_{\text{upwelling radiance}} + \underbrace{\frac{(1 - \varepsilon(\lambda)) L_d(\lambda) t(\lambda)}{\pi}}_{\text{downwelling radiance reflected at the surface}}$$

RTM (e.g. MODTRAN) is used to solve this equation by **modeling the atmospheric conditions during image acquisition**. Highly variable parameters (aerosol and water vapor content) have to be estimated carefully if no in-situ data are available. In the thermal IR region the atmospheric **water vapor** is the dominating parameter.

Summary of Theory

Thermal remote sensing data needs to be treated differently from other remote sensing data, most important are the laws of Planck, Boltzmann, Kirchhoff and Wien

Proper preprocessing: Data must first be atmospherically corrected

Derived temperatures need to be corrected for the emissivity effect, this is usually done with the support of precise landcover classificatiosn data

When comparing multi date imagery diurnal effects must be considered, thermal pixel values cannot be compared as easily as multispectral values

Materials with a high thermal inertia have a less accentuated diurnal cycle, materials with a low thermal inertia show a much larger variability (e.g. water, metal), synthetic ATI images can help in the differentiation of materials with similar spectral properties

Operational AVHRR LST Composites for Europe

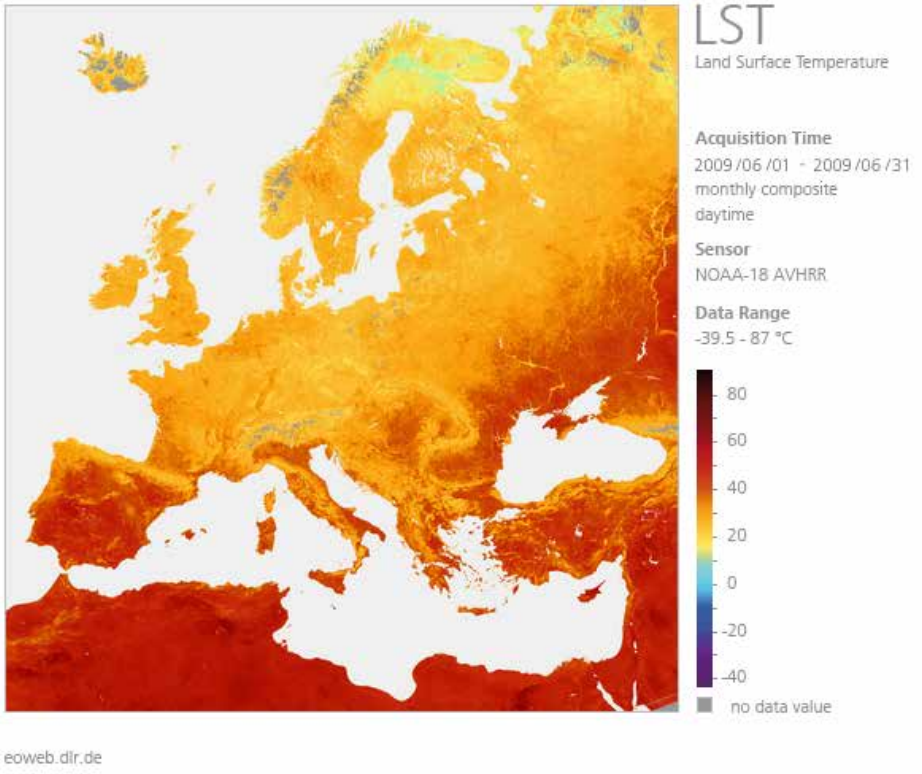

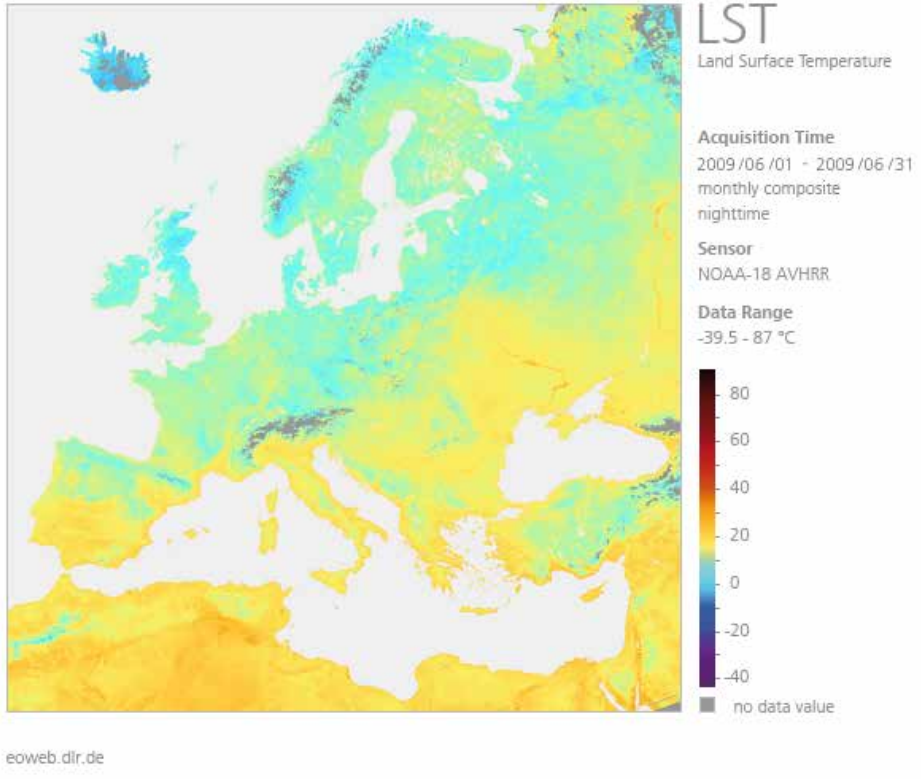

Publication: Frey C.M., Kuenzer C., Dech S. (2012): Quantitative comparison of the operational NOAA AVHRR LST product of DLR and the MODIS LST product V005. International Journal of Remote Sensing. Vol. 33, No. 22, 7165-7183

Diurnal Temperature Variations

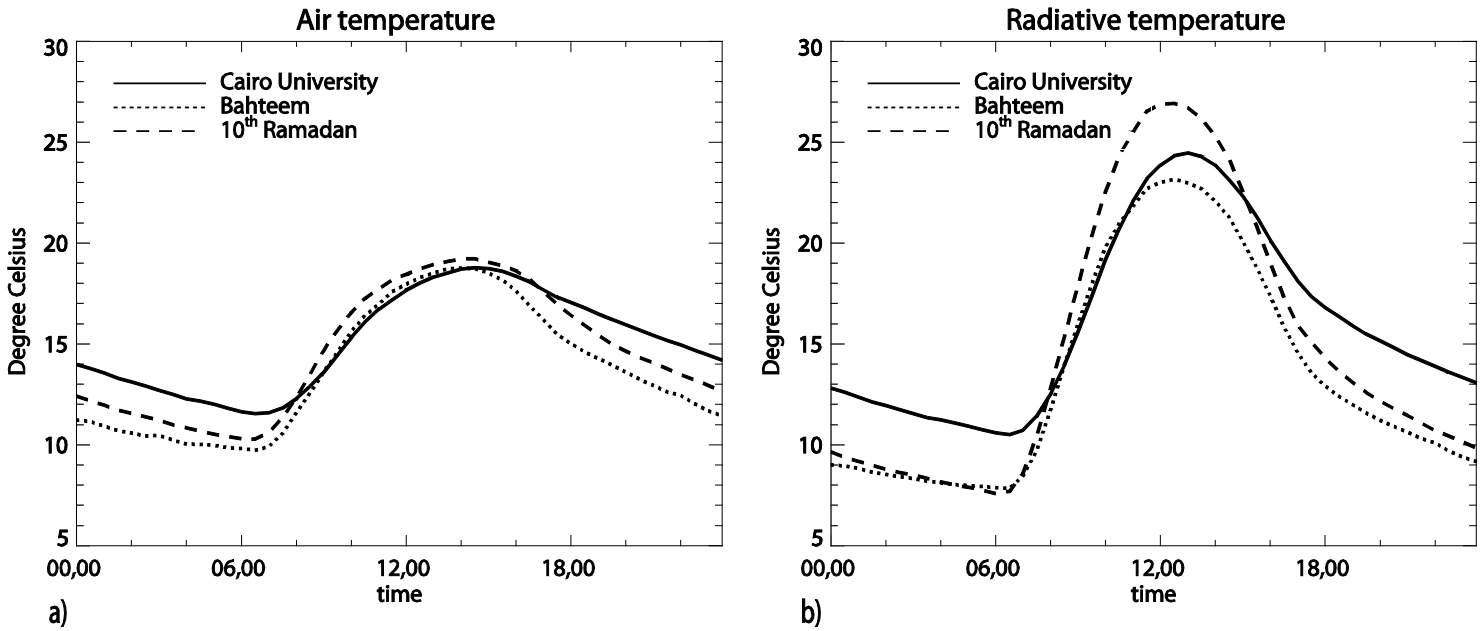

- à LST shows an extremely high diurnal variation
- à The variation of LST is higher than the variation of air temperatures
- à Figure: up to 4 K difference in LST per hour (mean values of three month)

Diurnal Temperature Variations

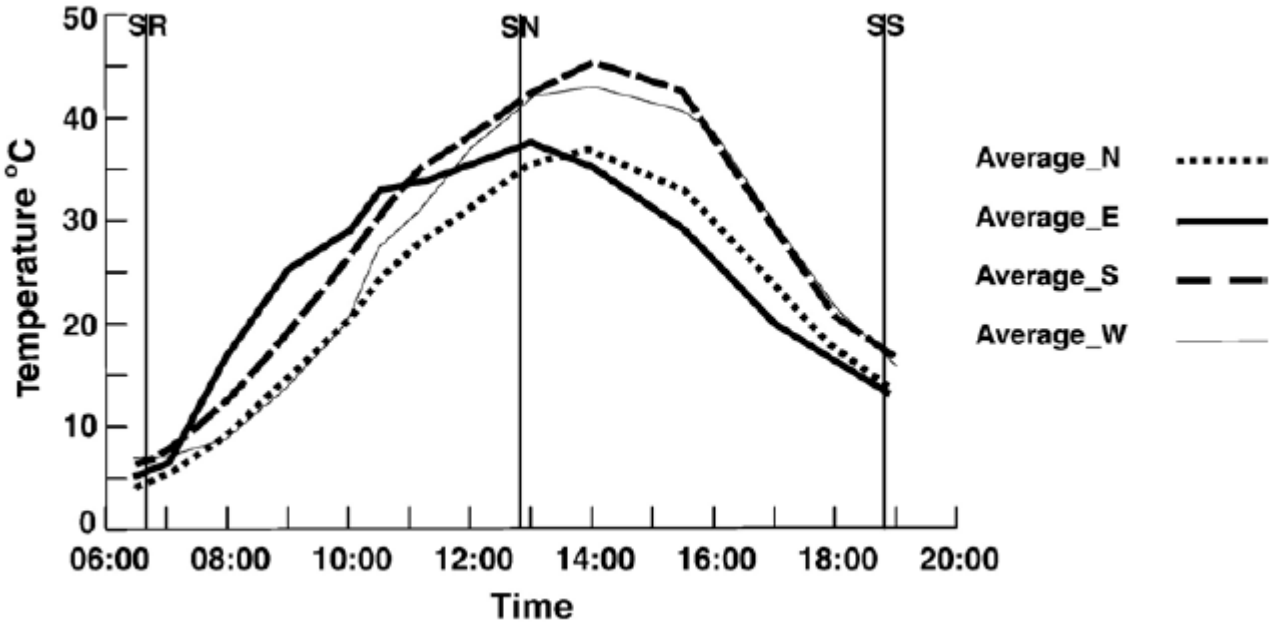

à in extreme and sloped terrain even up to > 10 ° C
à LST differences depend on aspect

The NOAA-AVHRR-LST Product: a Composite

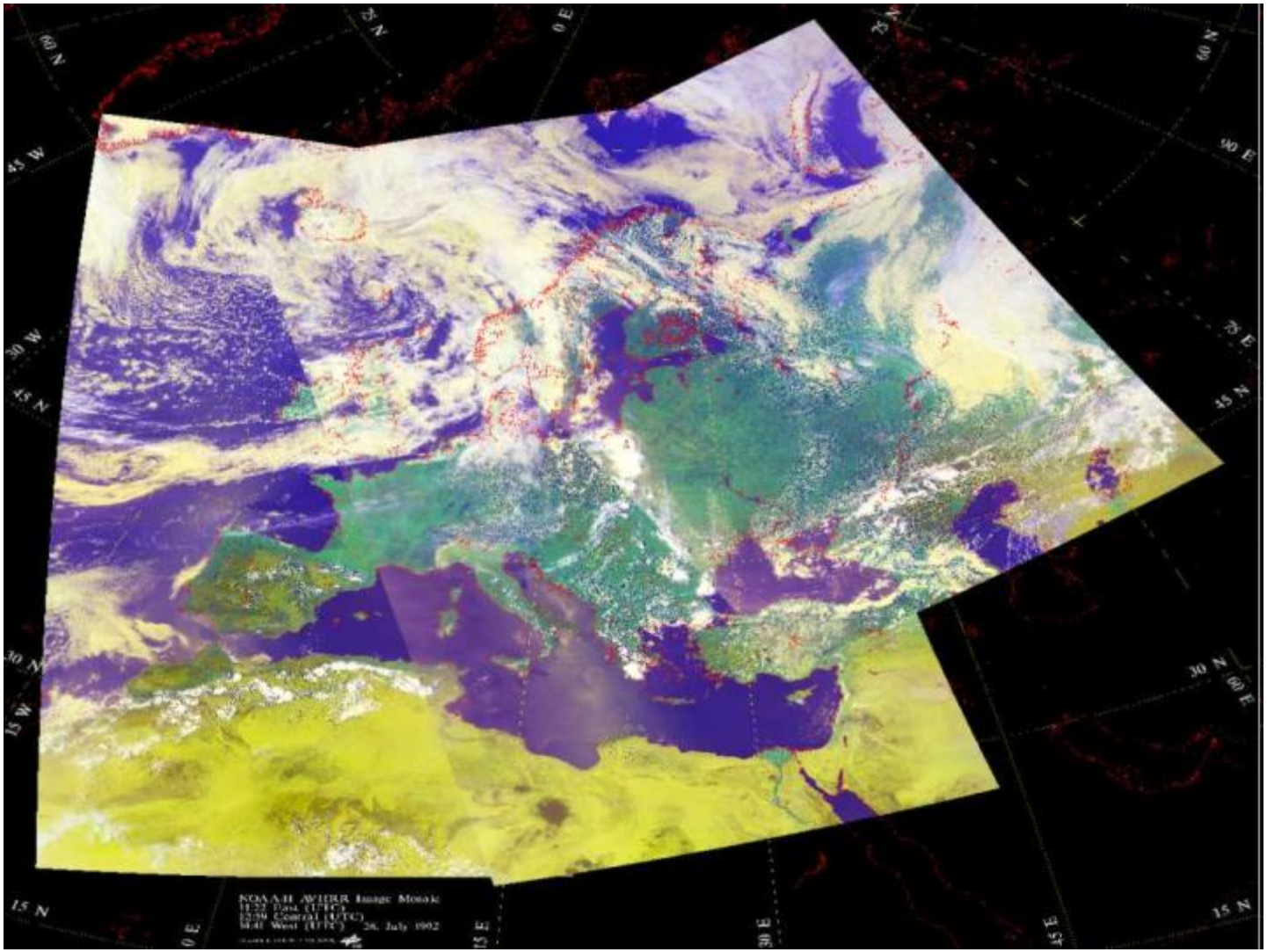

Geographical coverage for AVHRR data reception from Oberpfaffenhofen, Germany (www.eoweb.de)

Compositing Effects (30.03.03, night)

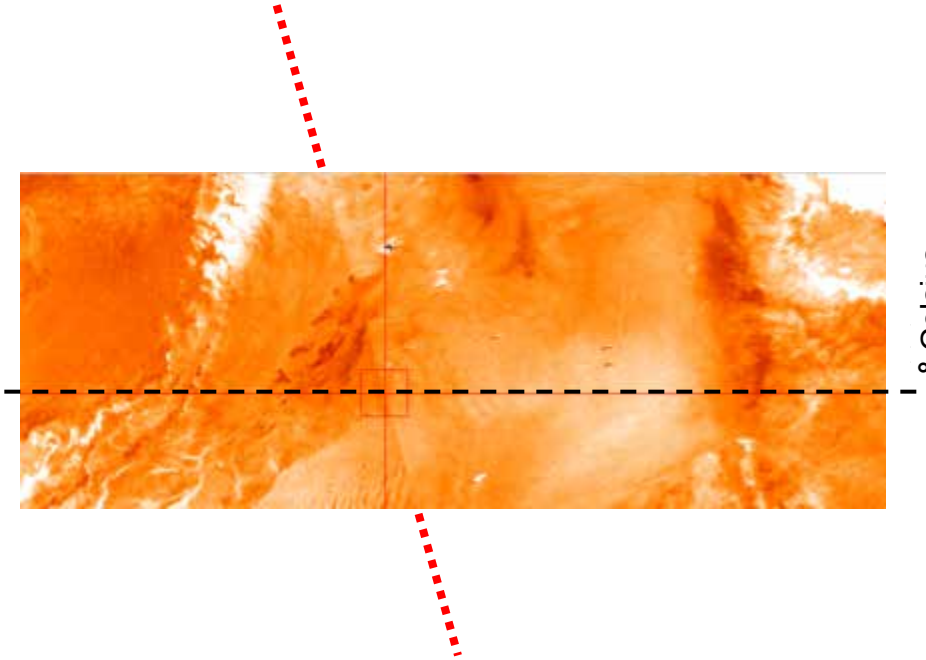

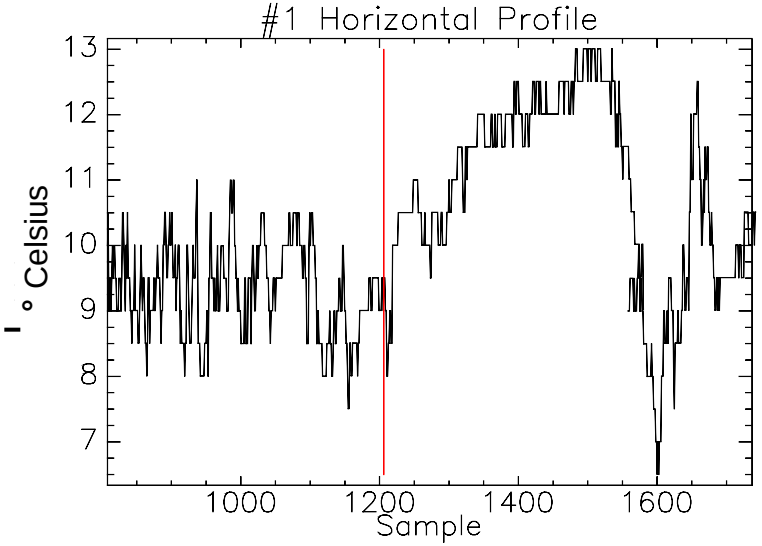

à At the borders of the single scenes: leaps in LST

NOAA-AVHRR LST often miss Metadata

Pixelwise time of acquisition

Only the day of acquisition is given in the metadata. However, due to the compositing techniques and the wide swath width, local times of single pixels may differ considerably

Pixelwise acquisition angle

Usually, no information about the acquisition angle is given. The acquisition angle however is important due to thermal anisotropy (BRDF)

Quality information

No information about the quality of the acquisitions for a given pixel is provided

Emissivity

The emissivity is calculated via the NDVI and not delivered as a separate layer. This missing data complicates the interpretation and validation of the data.

NOAA-AVHRR LST often miss Metadata

Consequences:

- **The missing metadata (time of acquisition, acquisition angle, quality information, emissivity) complicates the interpretation of the data considerably.**

  - The data – as it is – cannot be used as model input, e.g. for climate models

  - There is a need to investigate the product concerning its accuracy.

Cross-Comparison AVHRR-LST / MODIS-LST

Cross comparison of AVHRR LST and MODIS LST c5 daily (day and night scenes)

- **Comparison pixelwise for selected pixels**
- **Acquisition time difference: daytime 5 minutes, nighttime 30 minutes allowed**
- **Acquisition time is not available for AVHRR, therefore this had to be reconstructed**
- **Only ‚spatial homogeneous' pixels were chosen.**

- Four years, each containing only data of one NOAA satellite:
  - 2003 à only NOAA-16 scenes
  - 2005 à only NOAA-17 scenes
  - 2008 à only NOAA-18 scenes
  - 2010 à only NOAA-19 scenes
  - Data generated by other NOAA-Satellites were eliminated

The NOAA-AVHRR-LST Product: a Composite

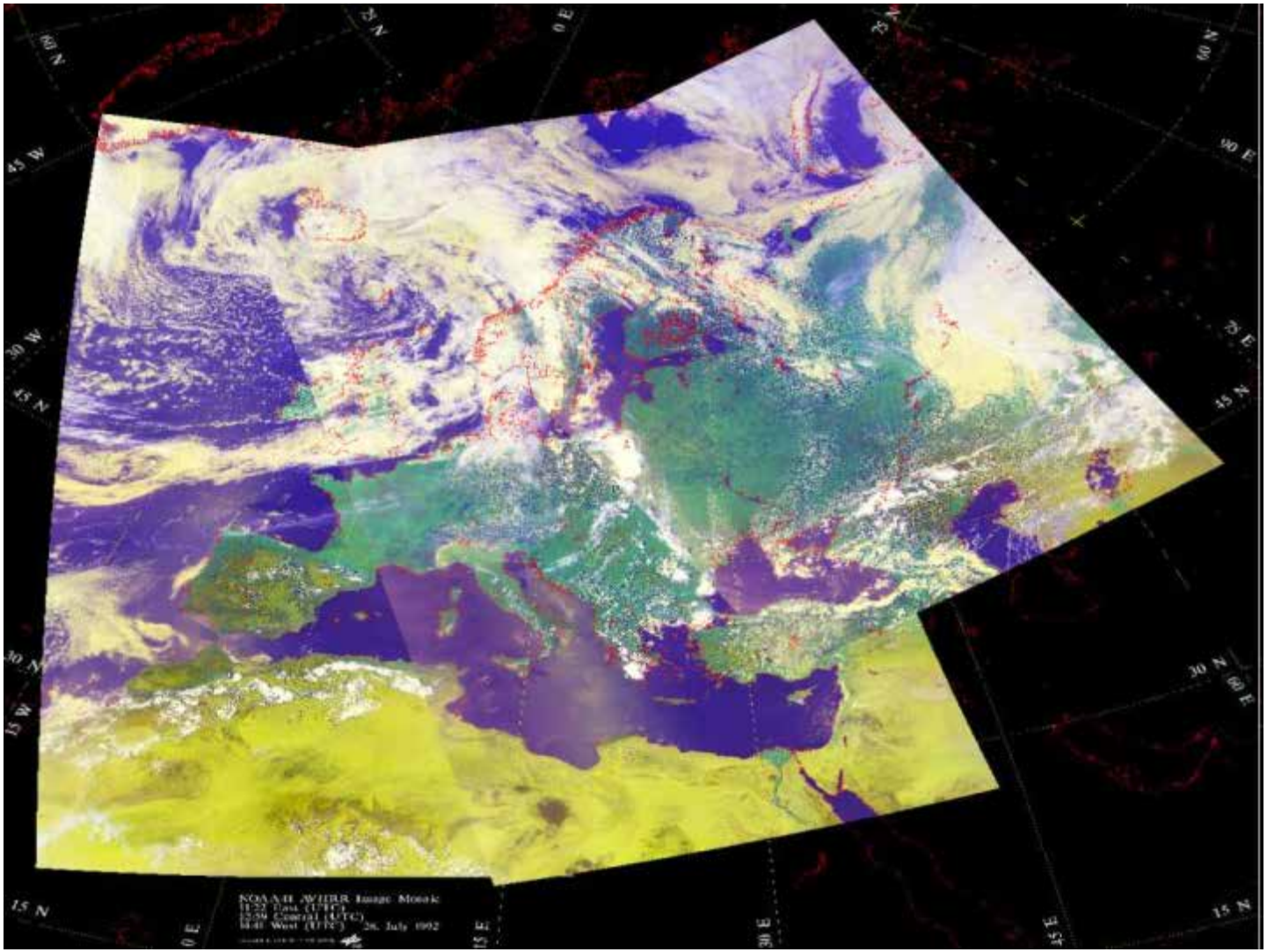

Geographical coverage for AVHRR data reception from Oberpfaffenhofen, Germany (www.eoweb.de)

Calculation of pixelwise Acquisition Time

à Input data: Generated positions of the raw scenes
à Output: Layer giving the acquisition time pixelwise (local time)

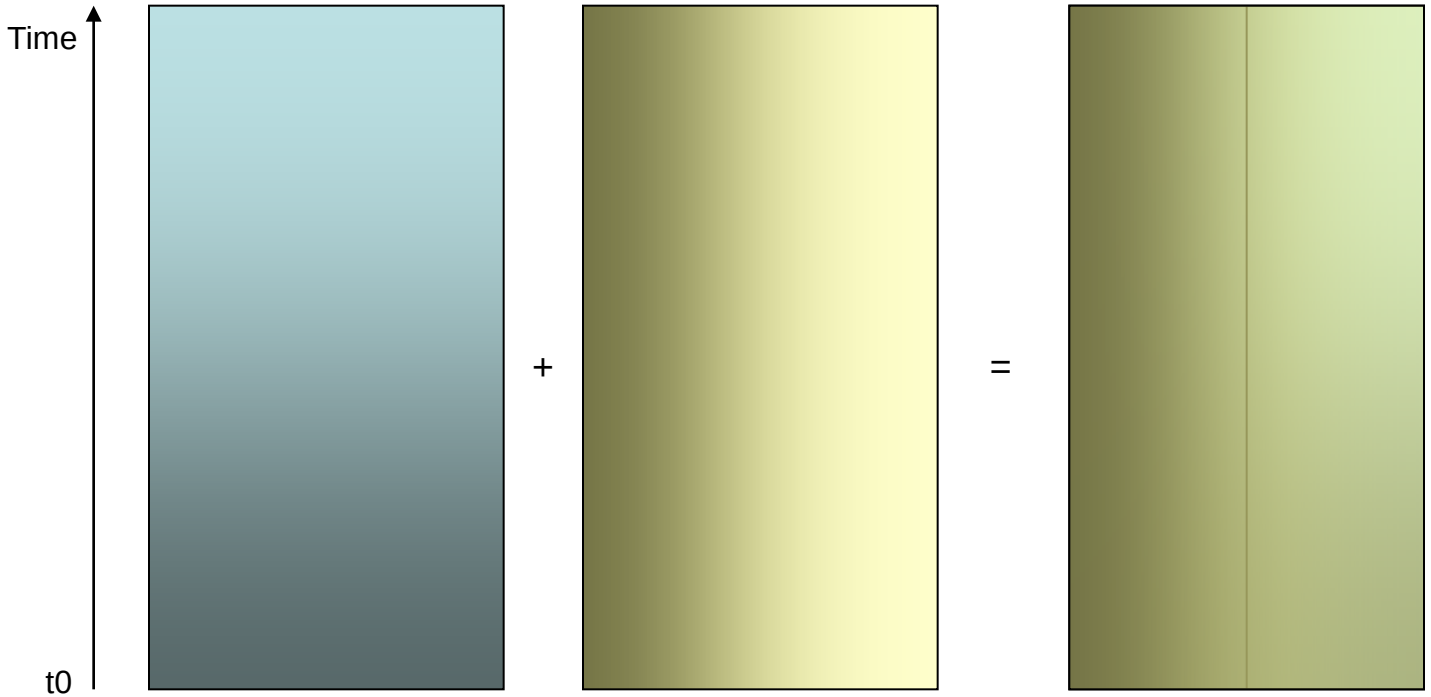

Local time of the subsatellite track, calculated from the starting time t0 and the acquisition velocity of AVHRR

Longitudinal variation

Local time

AVHRR LST – Homogeneous Pixels

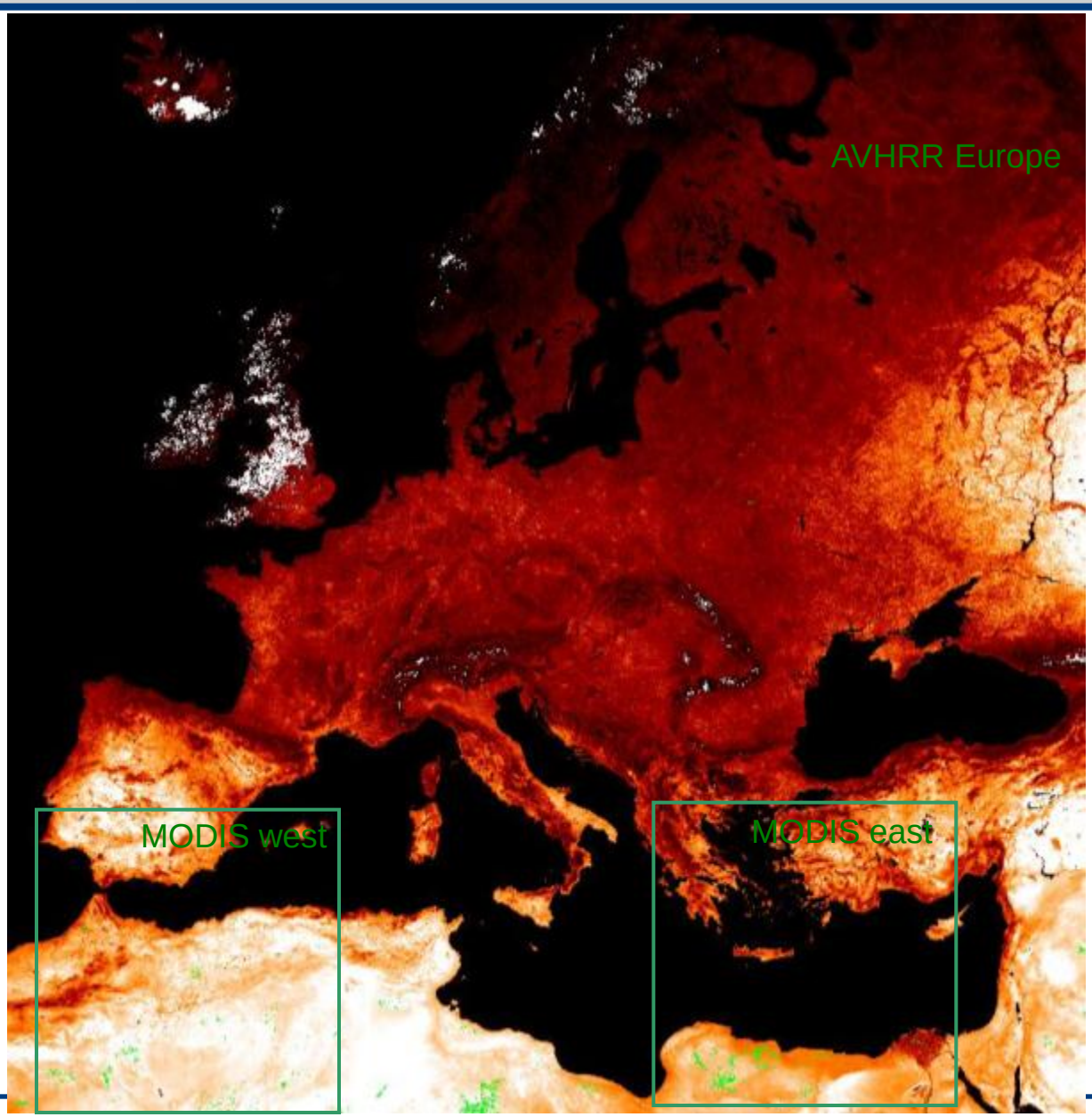

Filter:

1. **Pixels in areas without path overlaps**
2. **Low variability of NDVI and LST inside a 5x5 pixel environment**
3. **250m SRTM DEM slope is < 2 °**

à Homogeneous pixels are mostly found in North Africa

Comparing AVHRR & MODIS LST

Scatterplot AVHRR versus MODIS LST for 2003, daytime

à Maximum time difference: 5 minutes
à Filter mask: 5 Pixel - 2 degree slope, MODIS view zenith angle (VZA) <30 °

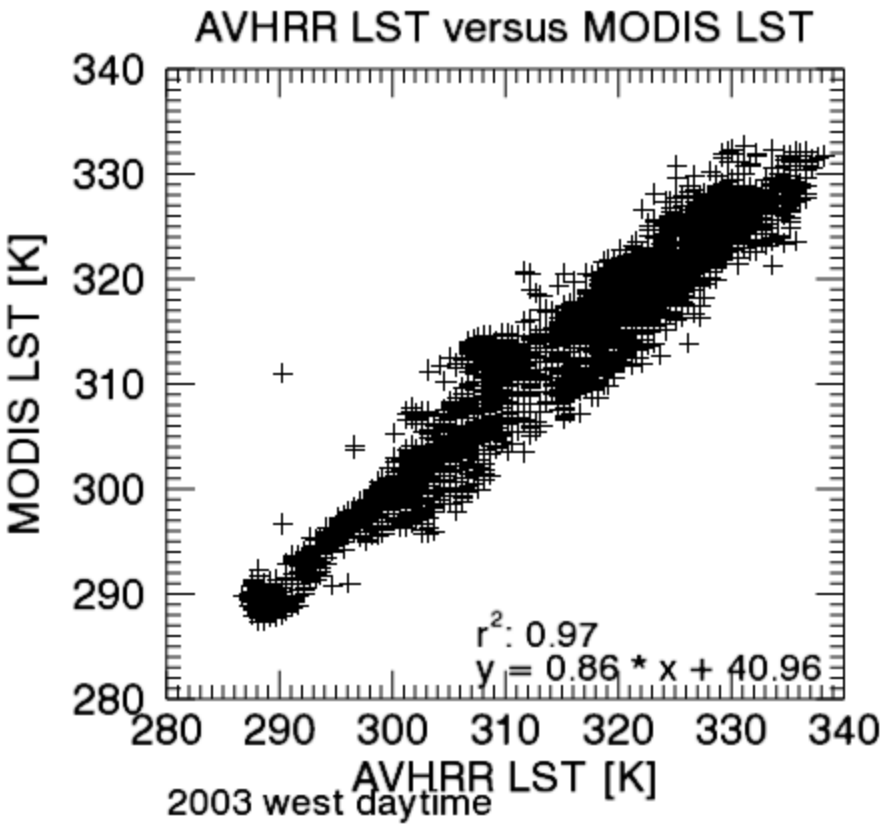

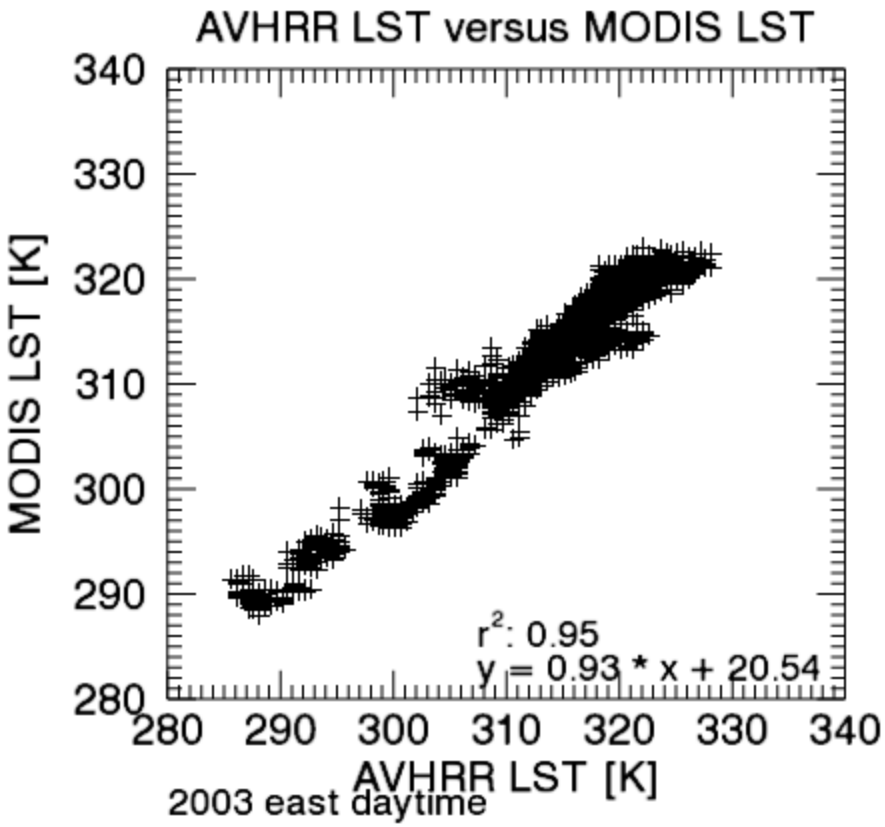

Comparing AVHRR & MODIS LST

Scatterplot AVHRR versus MODIS LST for all Years and all Scenes

à Maximum time difference: 5 minutes for daytime, 30 for nighttime scenes
à Filter mask: 5 Pixel - 2 degree slope, MODIS view zenith angle (VZA) <30 °

Daytime

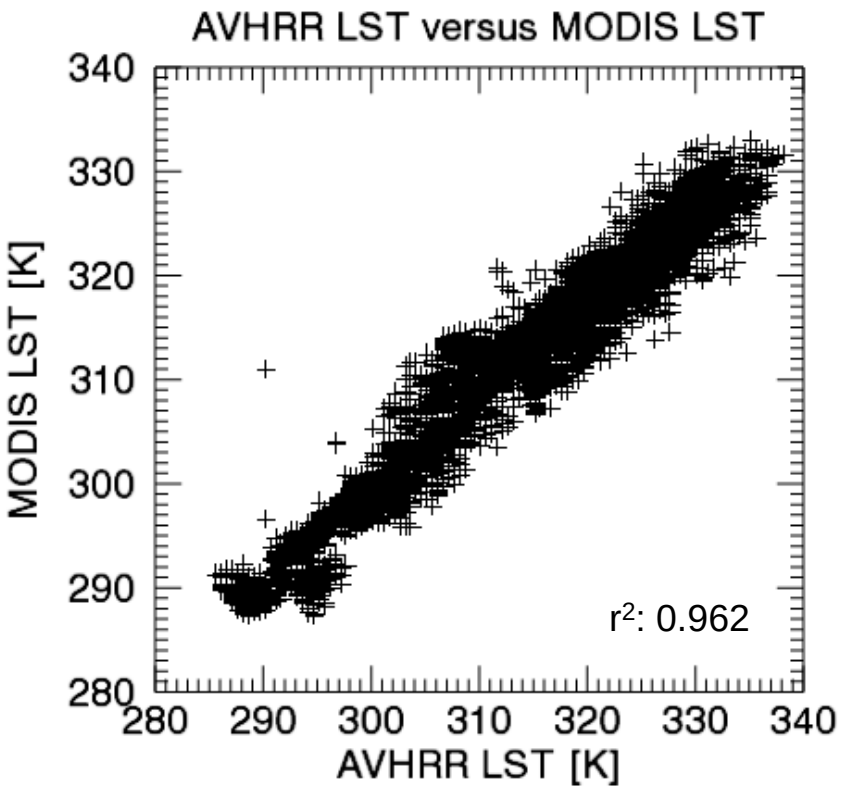

Nighttime

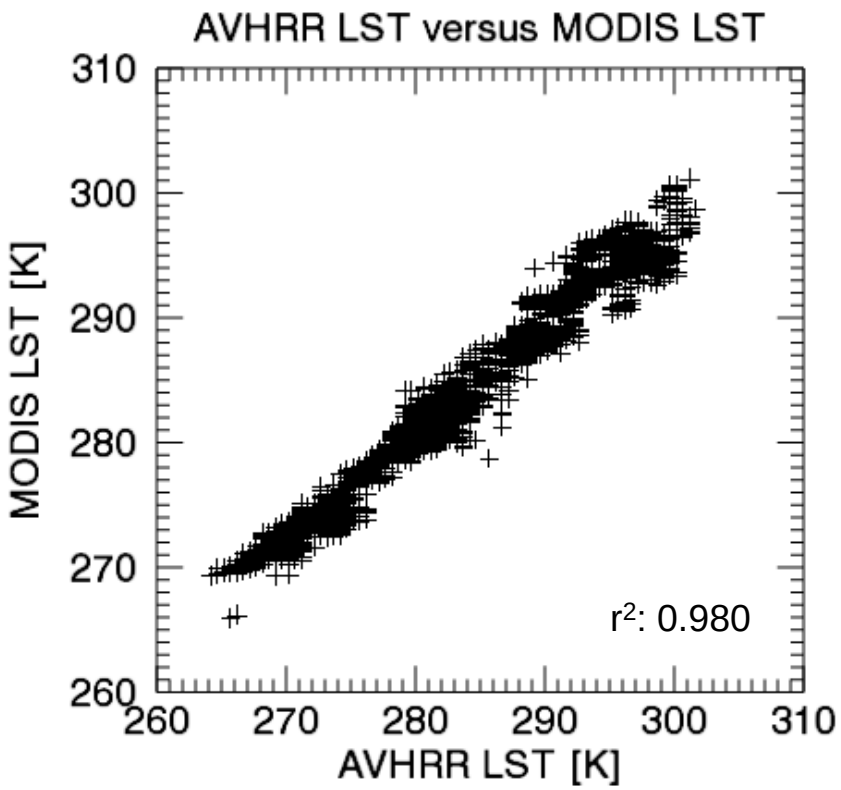

Scatterplot Differences AVHRR versus MODIS LST and Homogenity of Area (2003, 2010)

à **Impact of homogenity criteria**

à Filtermask: 2 degree slope à MODIS VZA<30 ° , varying homogeneous areas

Kein Filter

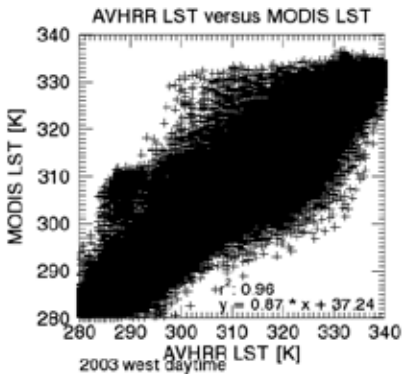

MAD: 3.17

3 pixel 3 degree

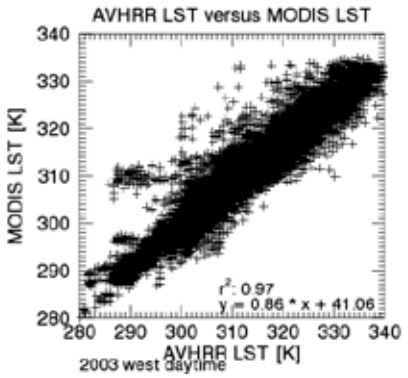

MAD: 2.49

5 pixel 2 degree

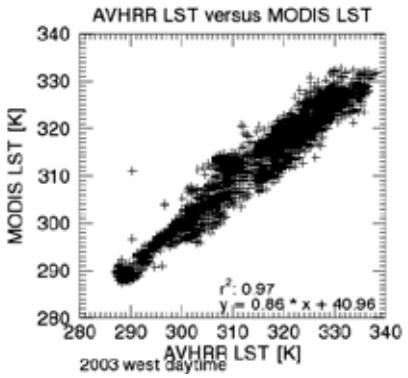

MAD: 2.46

7 pixel 2 degree

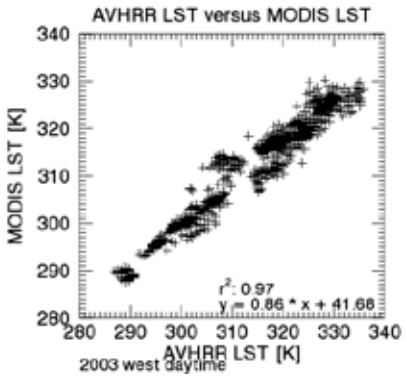

MAD: 2.43

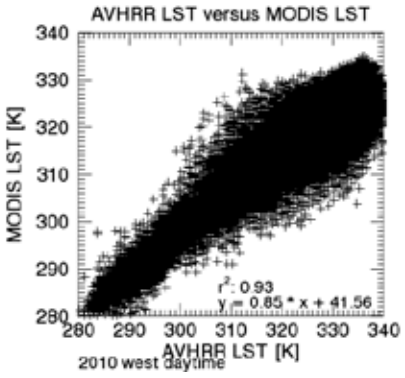

MAD: 5.22

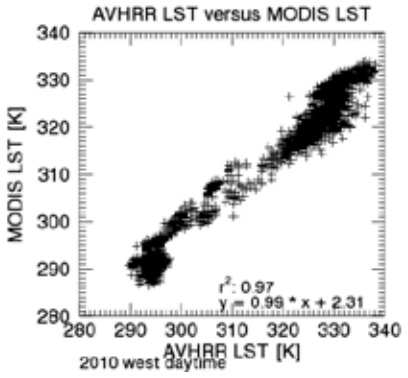

MAD: 2.70

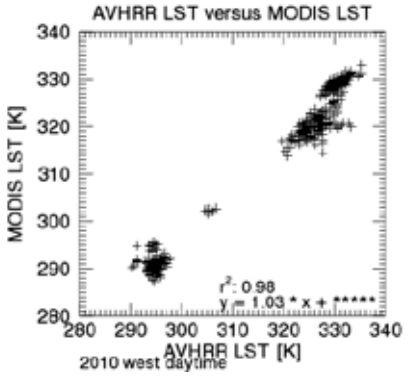

MAD: 3.22

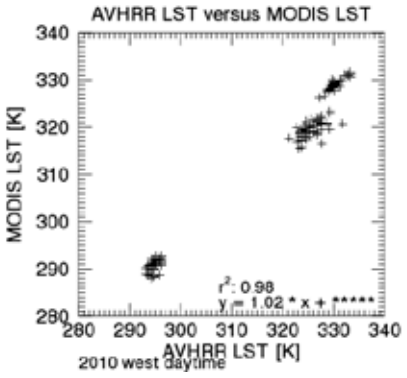

MAD: 3.83

Comparing AVHRR & MODIS LST

Scatterplot Difference AVHRR versus MODIS LST depending on MODIS VZA

- à **Influence of the VZA of MODIS**
- à (only every 10th pixel plotted)
- à Filtermask: 5 Pixel - 2 degree slope

MODIS VZA <50 °

<40 °

<30 °

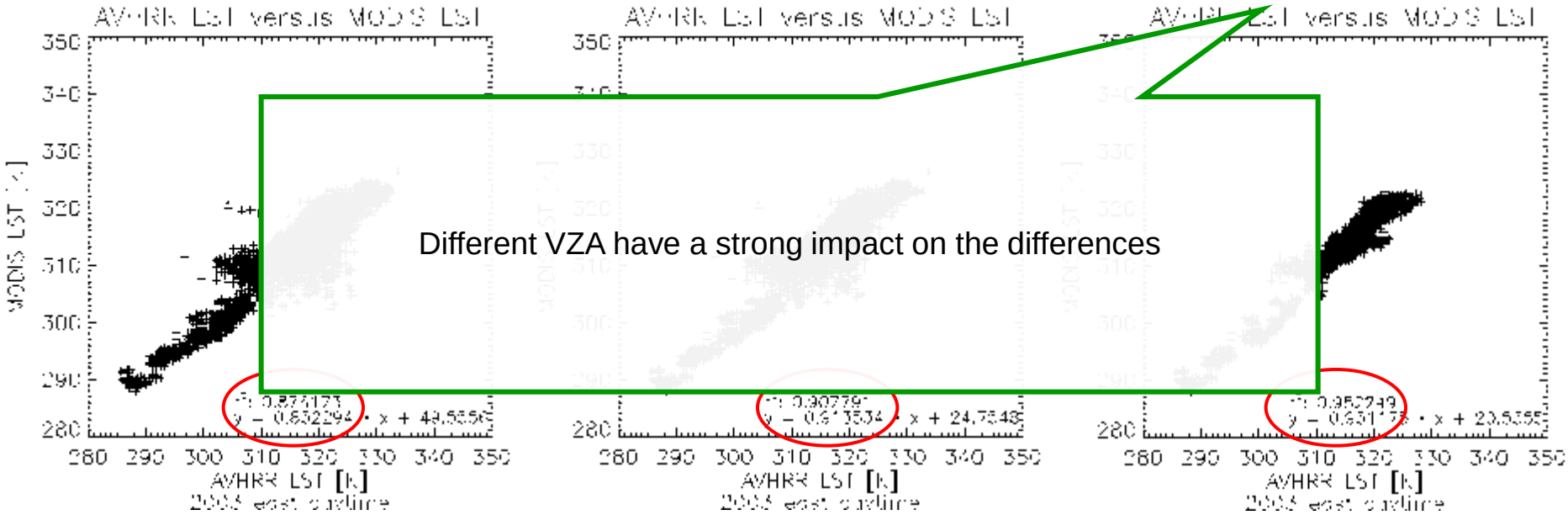

Different VZA have a strong impact on the differences

Scatterplot AVHRR versus MODIS LST for the Year 2010, nighttime

à Maximum time difference: 30 Minutes

à Filtermask: 5 Pixel – 2 degree slope, MODIS VZA<30 °

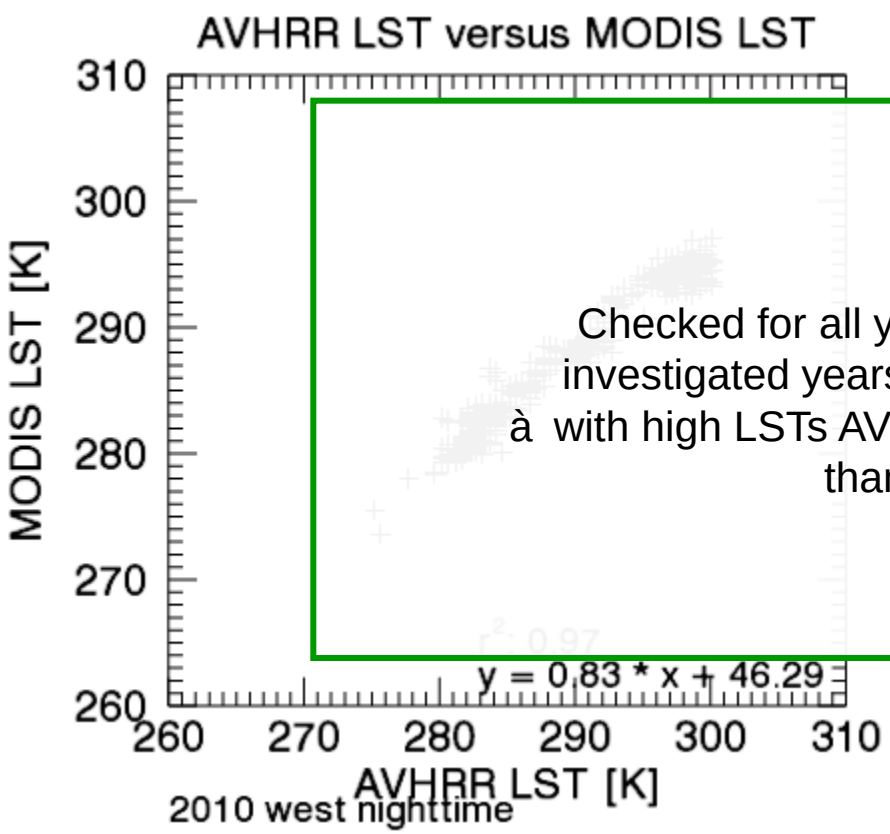

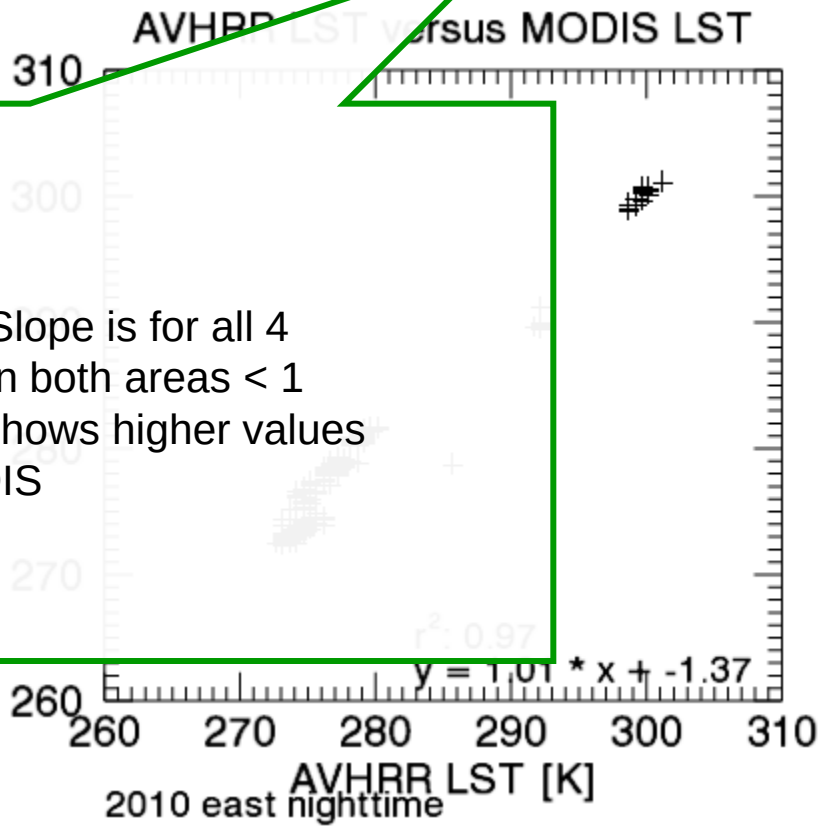

Checked for all years: Slope is for all 4 investigated years and in both areas < 1

à with high LSTs AVHRR shows higher values than MODIS

Comparing AVHRR & MODIS LST

Cross-Comparison of NOAA-AVHRR LST and MODIS LST

Day and night with and without homogenity critera

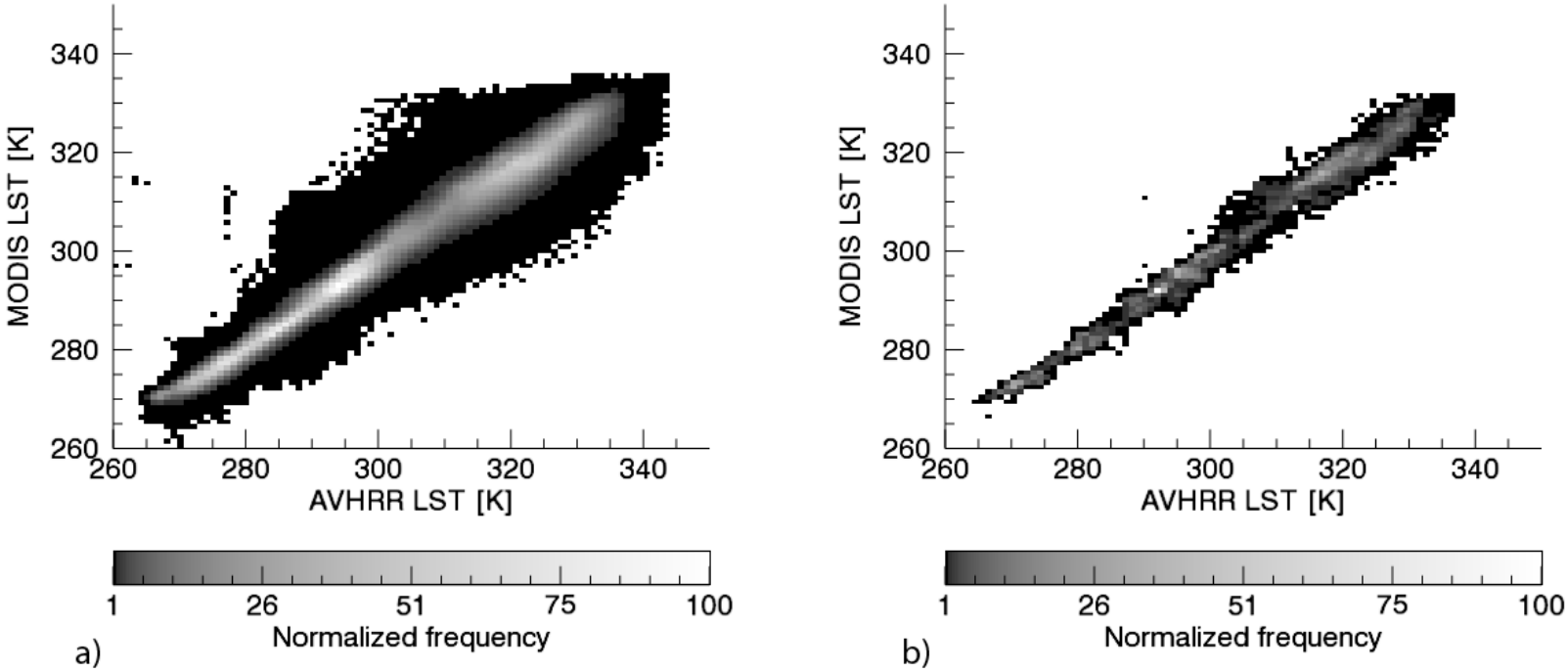

2D histograms of AVHRR and MODIS LST for all four years, both MODIS tiles, **day- and nighttimes**. Only pixels with viewing angles lower than 30 ° were used and the maximal time difference was 5 min for the daytime scenes, 30 min for the nighttime scenes. **a) with no homogeneity filter applied b) with the homogeneity filter applied.**

Diurnal Mean absolute Difference (MAD) per Day and Tile between AVHRR and MODIS LST

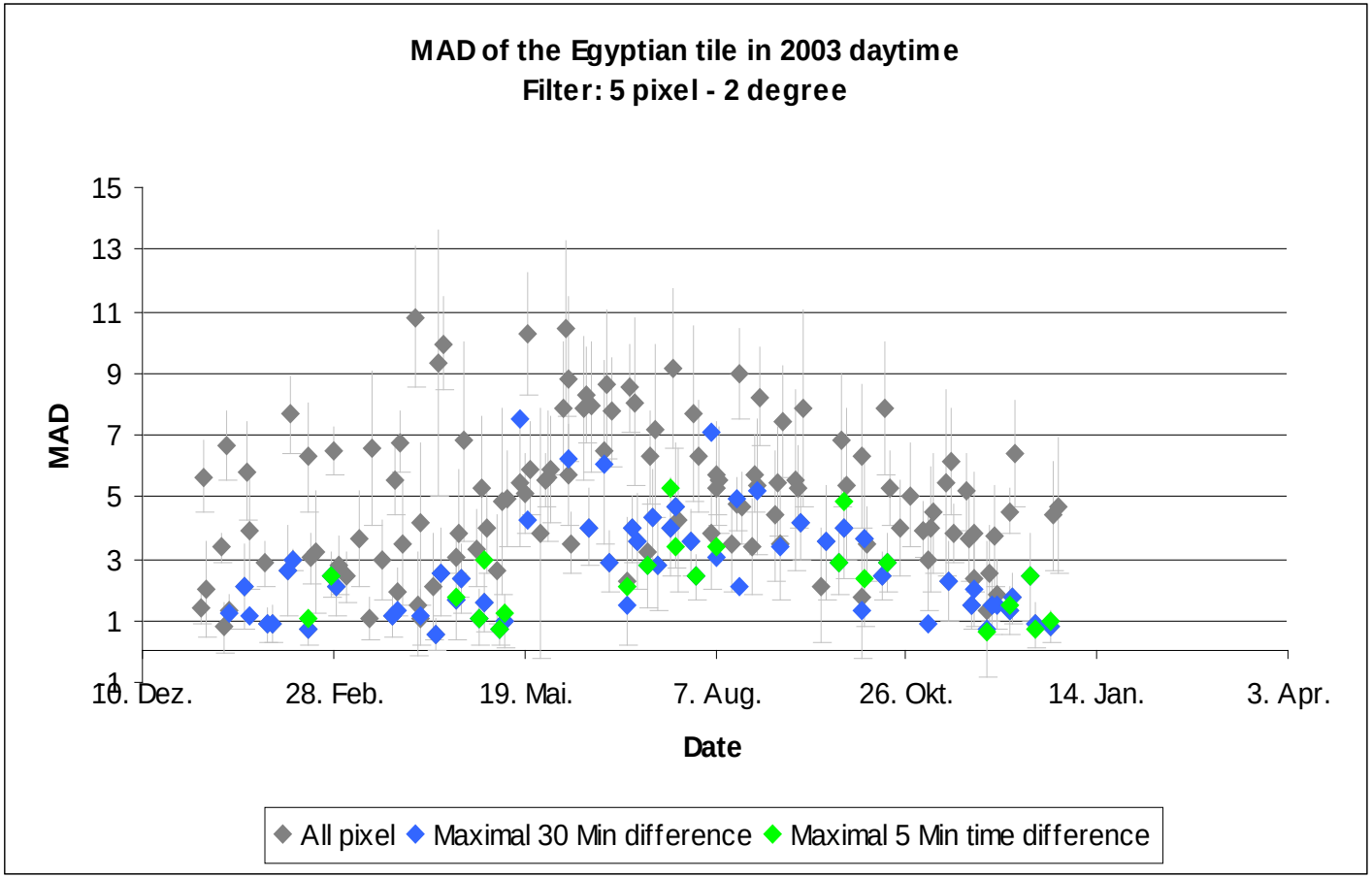

Daytime - MODIS VZA<30 °

Diurnal Mean absolute Difference (MAD) per Day and Tile between AVHRR and MODIS LST

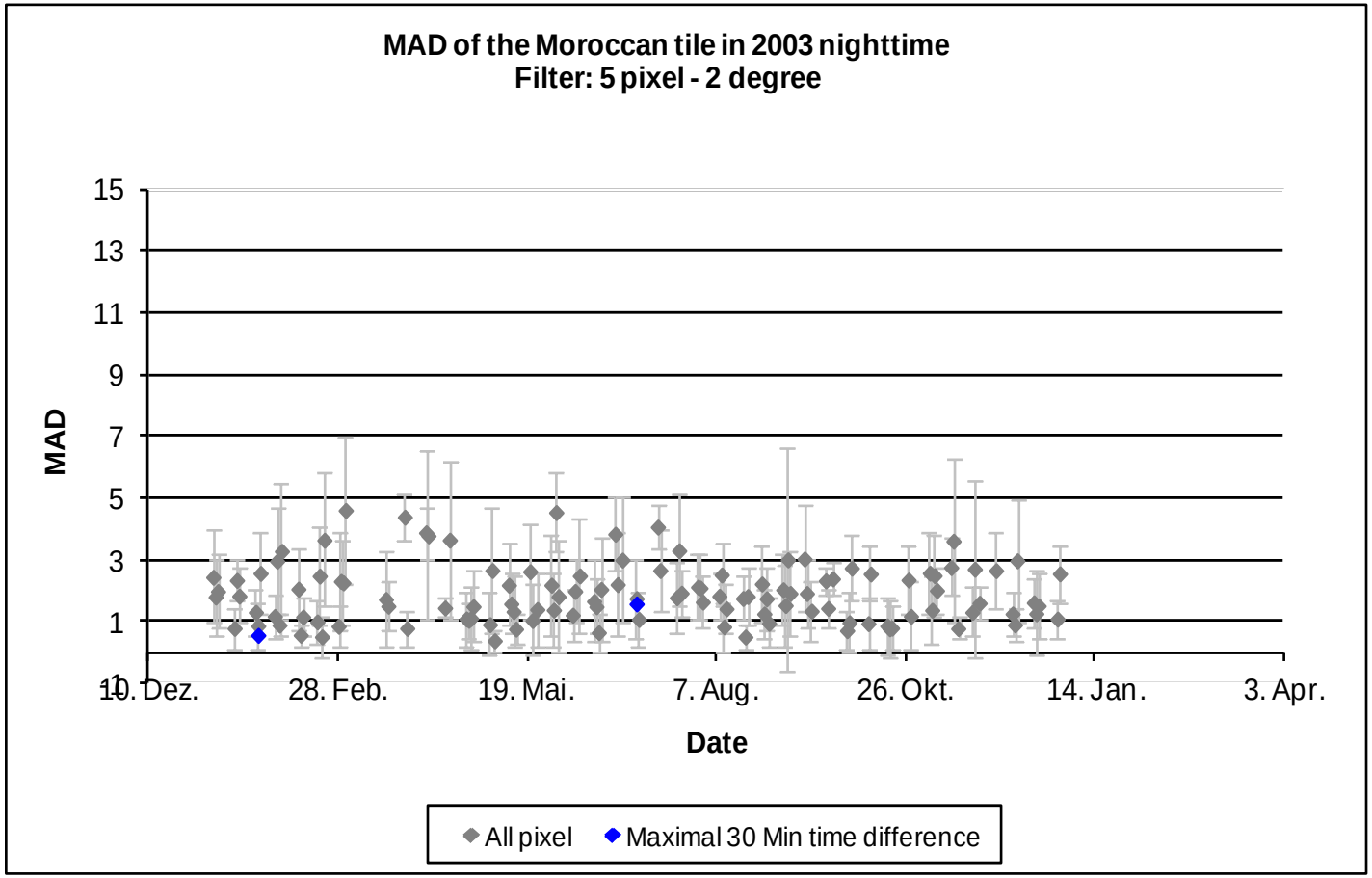

Nighttime - MODIS VZA<50 °

Daytime Differences (AVHRR LST – MODIS LST)

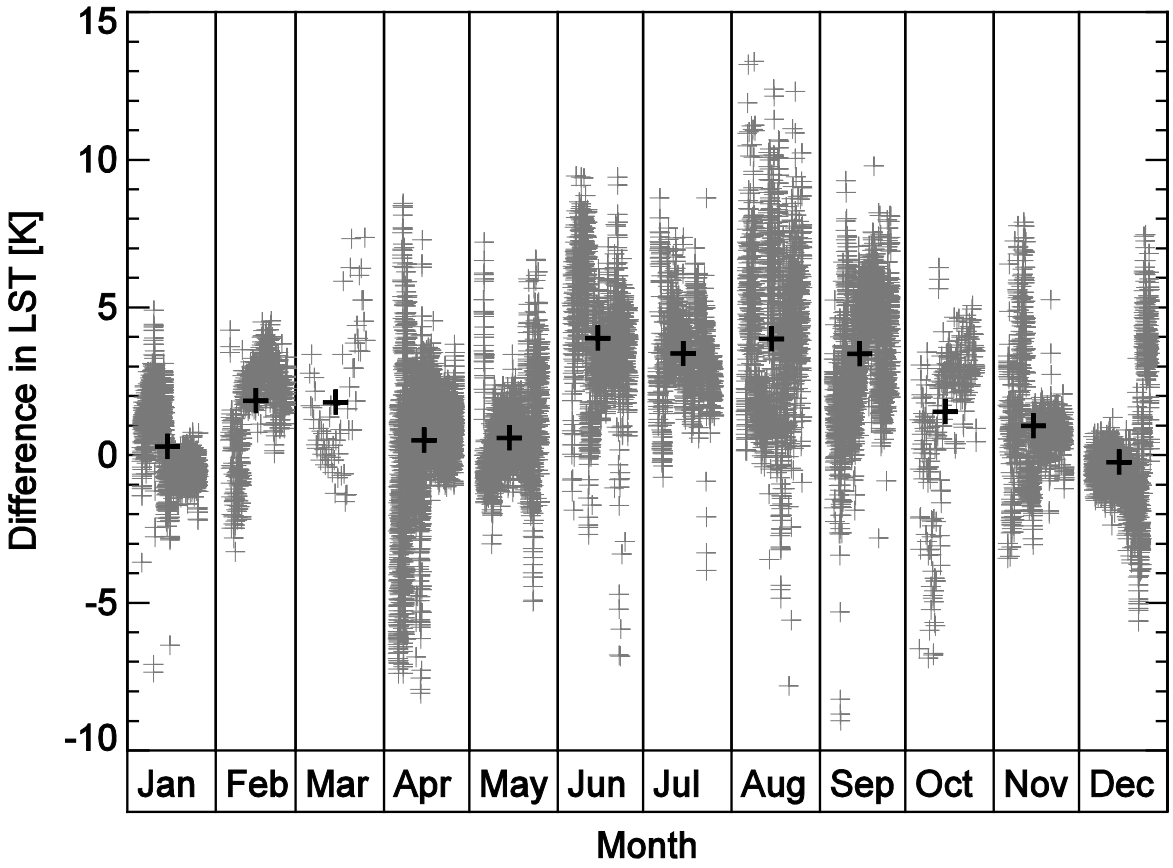

Nighttime Differences (AVHRR – MODIS)

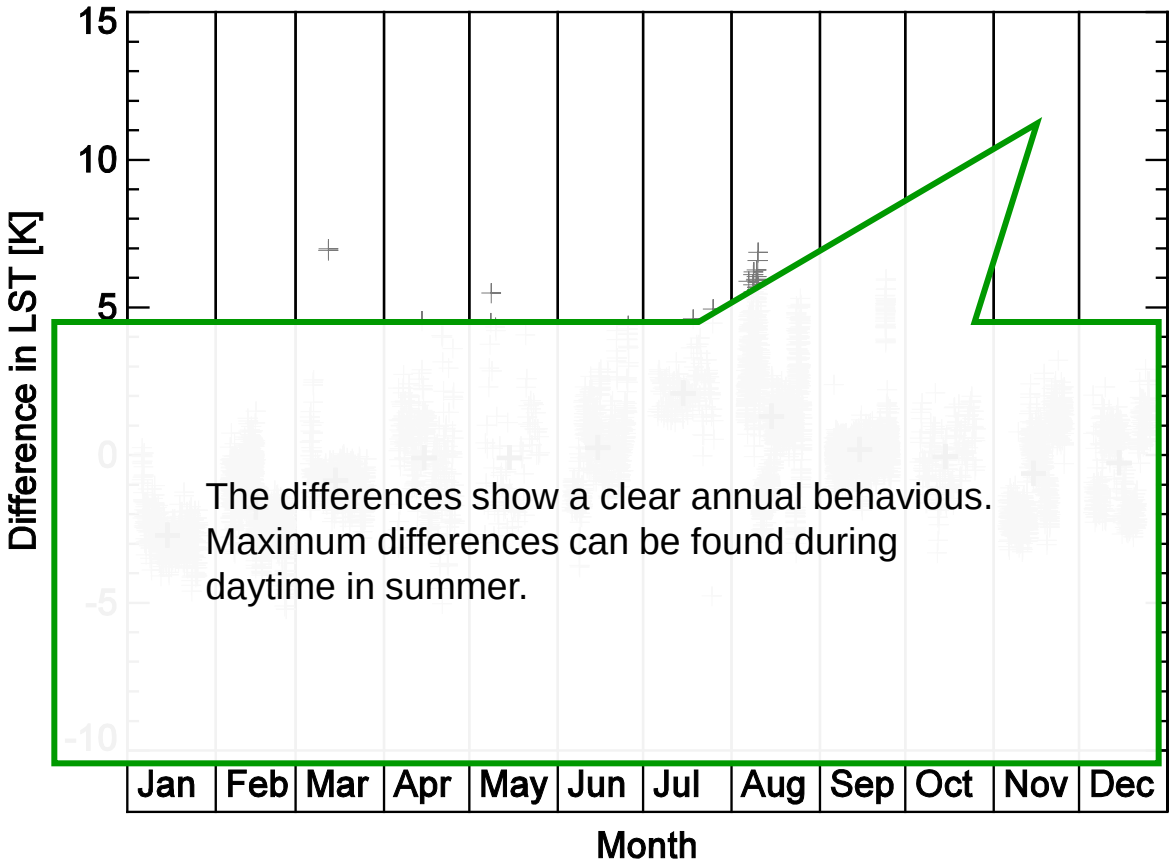

Comparing AVHRR & MODIS LST

Statistics of the data after elimination of acquisition angles > 30deg., time differences higher than 5 minutes (daytime scenes) / 30 minutes (nighttime scenes) and inhomogeneous pixels

	MAD [K]	Slope	Correlation coeffizient r^2
Daytime	2.2	0.89	0.96
Nighttime	1.4	0.88	0.98

à Good agreement between the two datasets!

Frey C.M., Kuenzer C., Dech S. (2012):
Quantitative comparison of the operational NOAA AVHRR LST product of DLR and the MODIS LST product V005. International Journal of Remote Sensing. 33:22, 7165-7183

Comparing AVHRR & MODIS LST

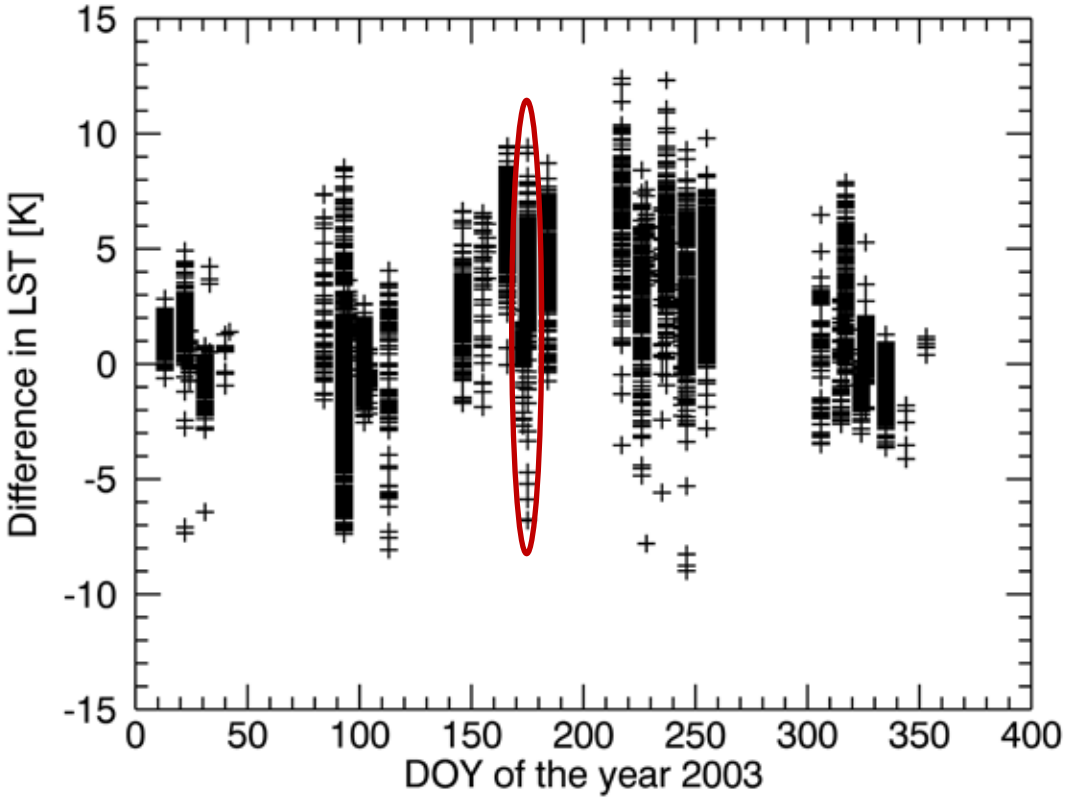

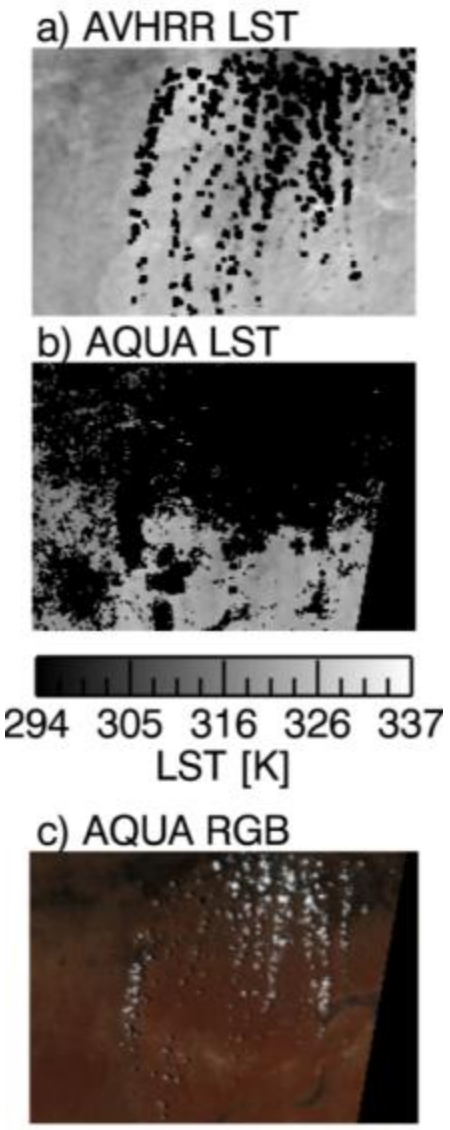

Summary: Results of the scientific Comparison

à Only a strict selection of pixels allowing only certain acquisition time differences, homogeneity of the pixels and view zenith angle enables an optimal comparison between AVHRR LST and MODIS LST

à Mean aboslute difference MAD per scene and year ranges from **1.4 to 3.2 K** (daytime scenes) and from **0.9 to 2.2 K** (nighttime scenes)**.**

à A distinct annual course was found in the daytime data. Highest differences are found in summer, which may considerably exceed mean annual MADs.

à A weak annual course is found in the nighttime data.

Application: Remote Sensing of Coal Fire Environments

Coal Fires in China: Introduction

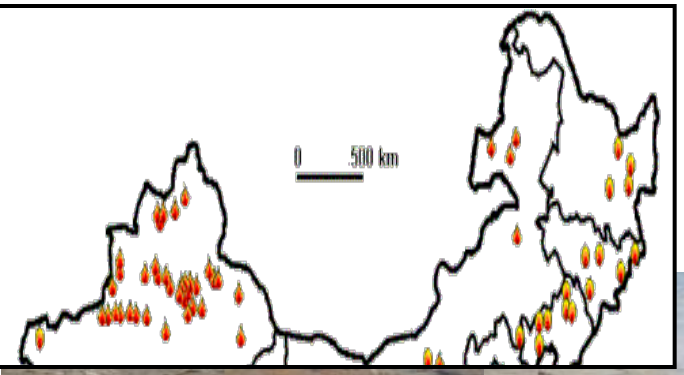

Spontaneous combustion:

C + O2 >> CO2 + 394 KJ/mol
2C + O2 >> 2CO + 170 KJ/mol

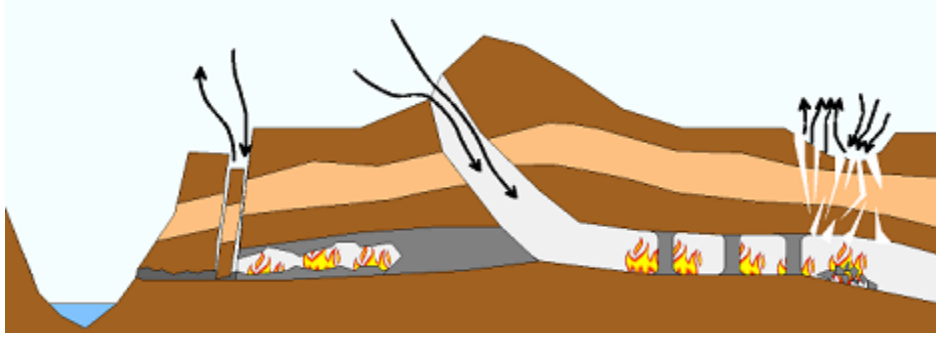

Coal Fires: An International Problem

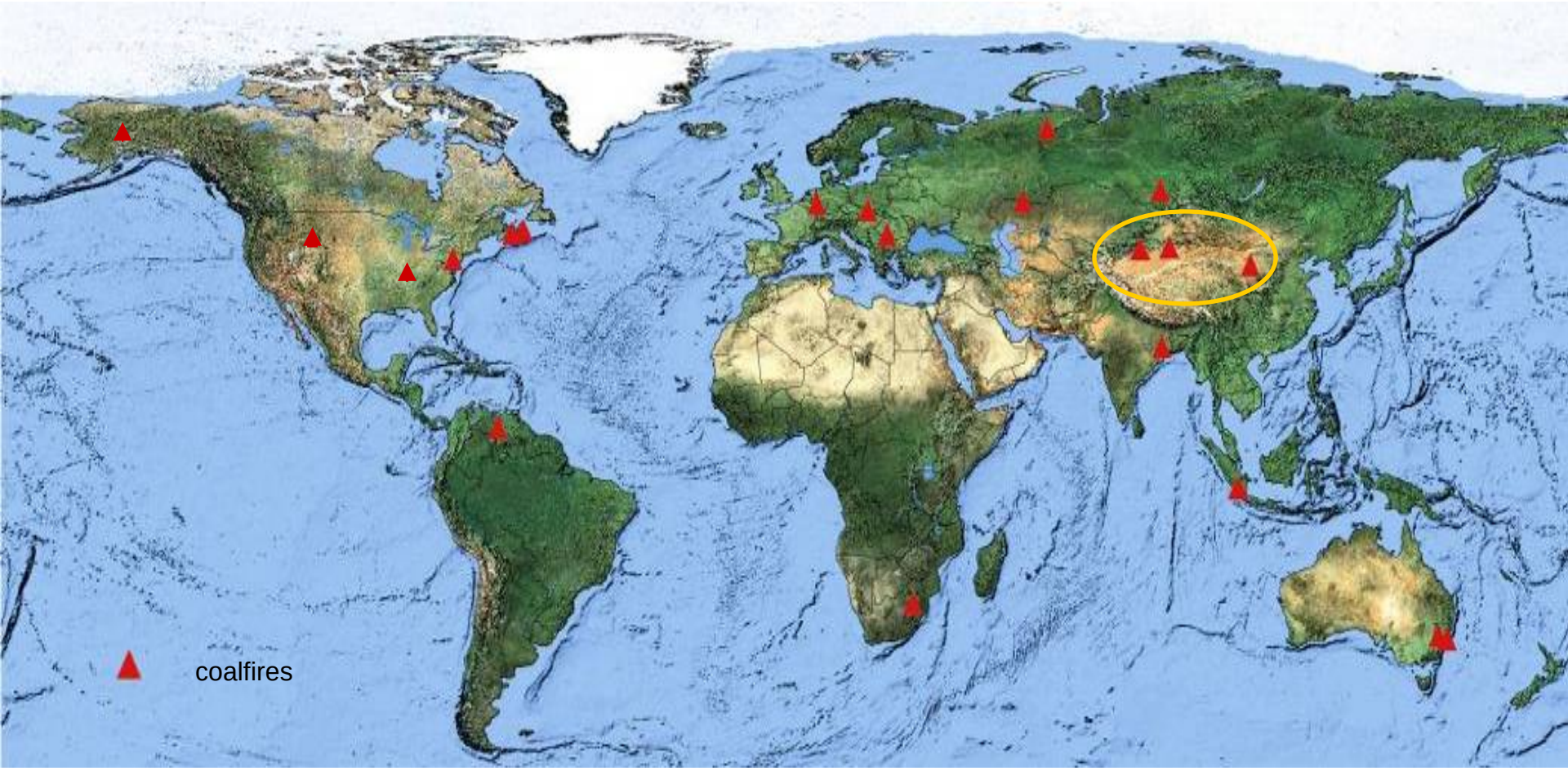

Coal Fires: An International Problem

- **Environmental Problems**
  - Gas Emissions (CO2, CH4, others)
  - Land subsidence and cracks
  - Threat to human health
  - Regional landscape degradation
- **Economic Problems**
  - In China: 20 Mio. t coal loss / year
  - Coal fire research needs funding
  - Deserted mining towns; migrations






Greenhouse-Relevant and Toxic Gases

Emitted:

- Carbon dioxide (CO2)
- Carbon monoxide (CO)
- Water vapor (H2O)
- Methane (CH4)
- Nitrous oxides (NOx)
- Sulfur oxides (SOx)
- (N2O)
- and other partially toxic gases

Economic Loss of Valuable Resource

- 70% chinese energy covered by coal
- 2 billion t/a mined
- 20-30 million tons burning
- the 10-fold becomes inaccessible
- discrepancy: energy demand / production

Coal Fire Fighting – Challenges

Methods:

- Digging out and isolating the fires

- Water injections for cooling

- Covering of fires

Location of Study Areas in Ningxia and Inner Mongolia

Orientation Map: Chinese Provinces

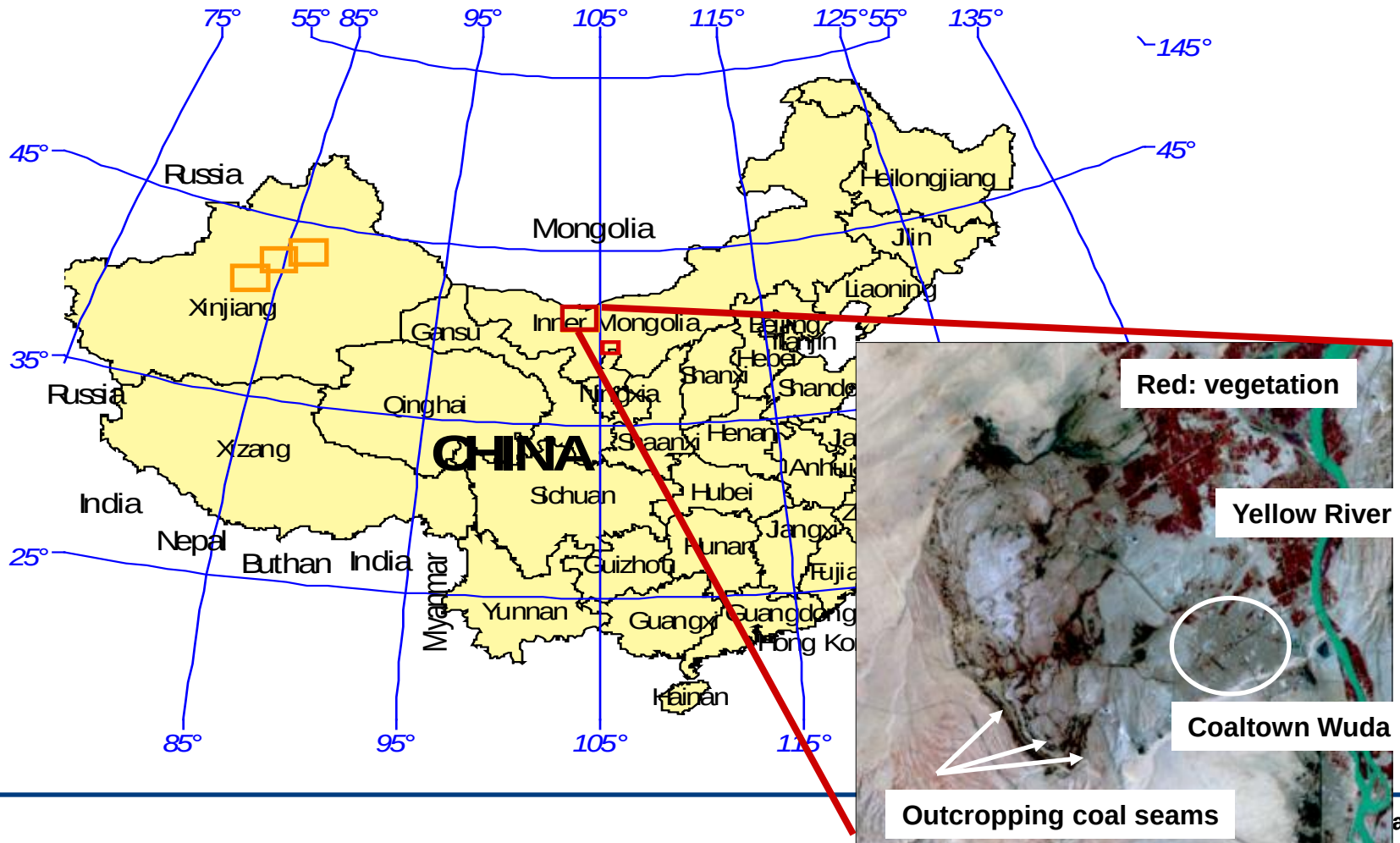

Chinese mining Town Ruqigou in Ningxia

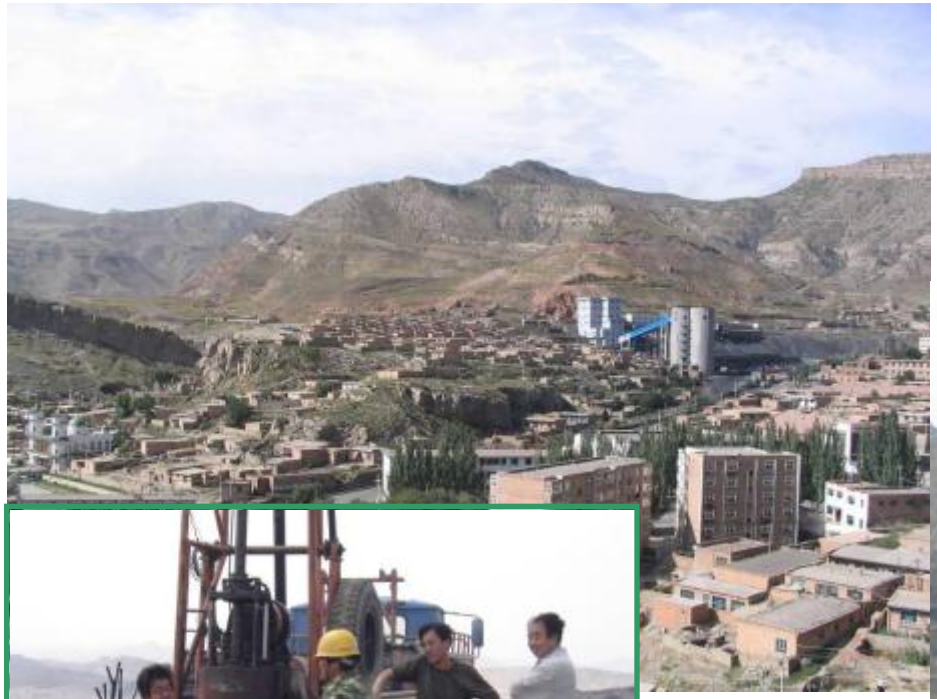

Some Impressions ...

Data Analyzed over the Course of the Project

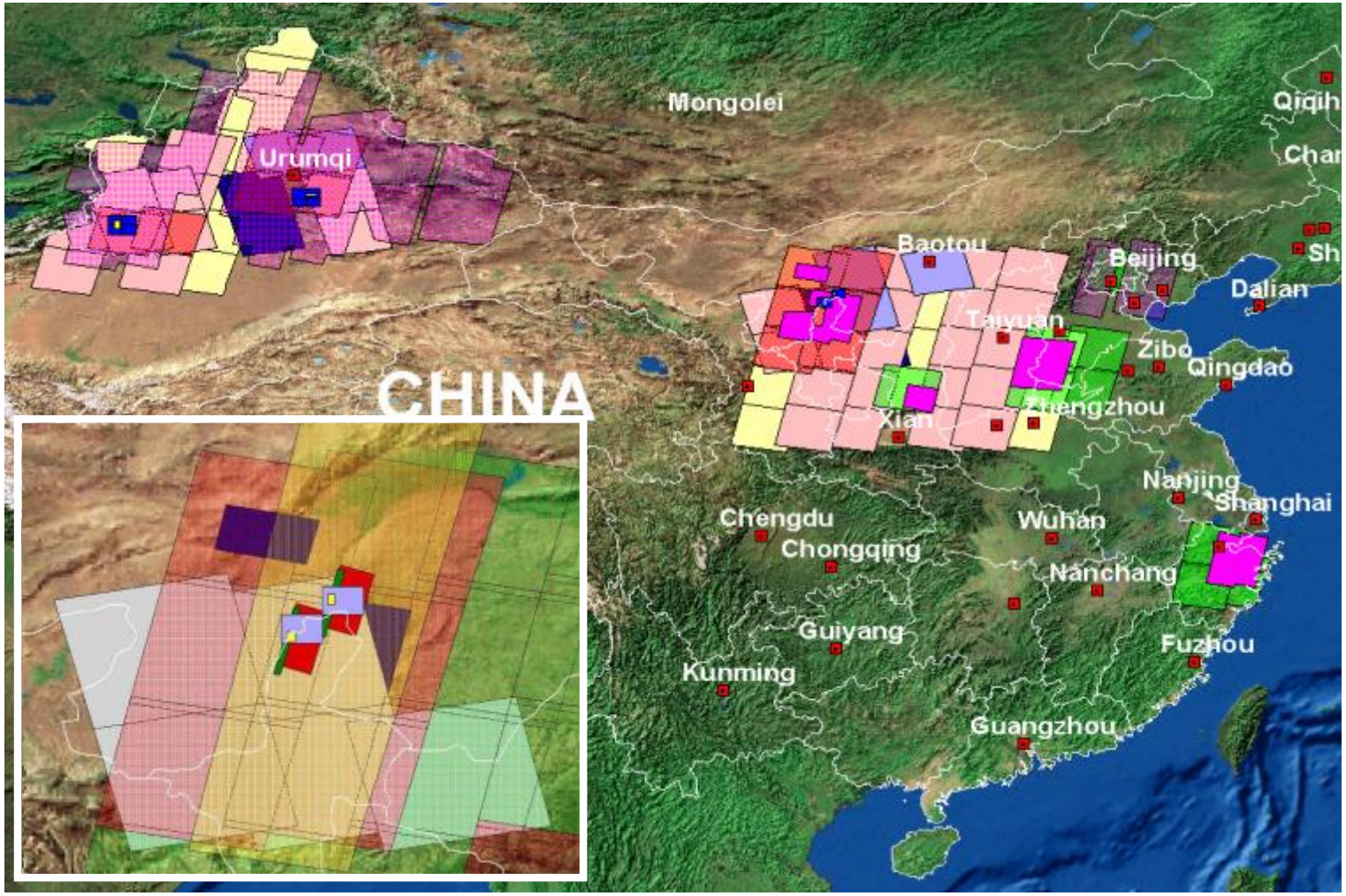

Thermal Expression of Coal Fires in EO Data

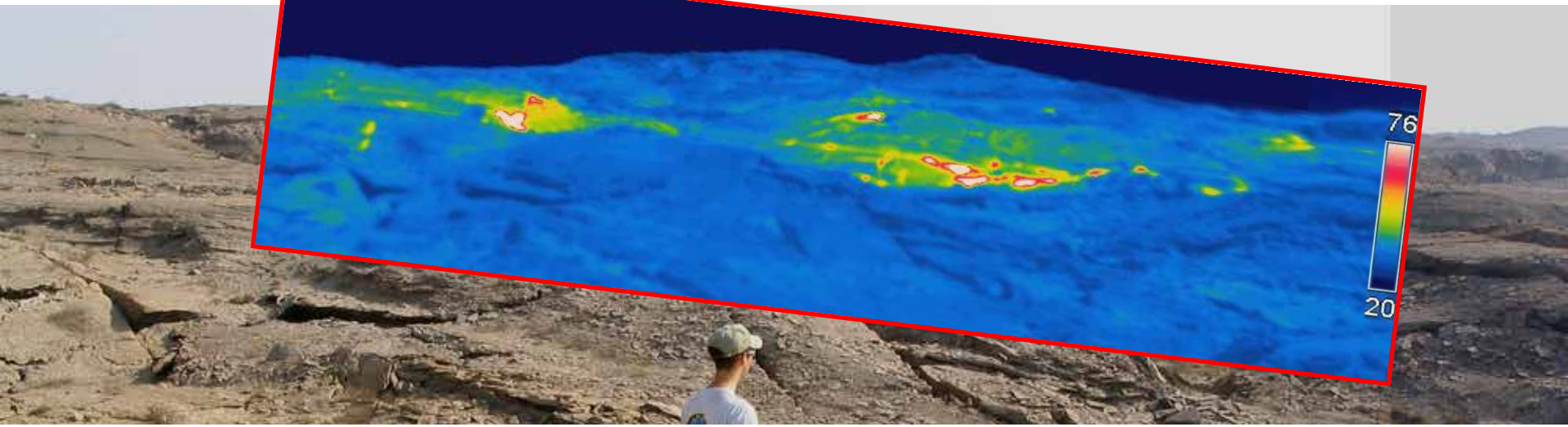

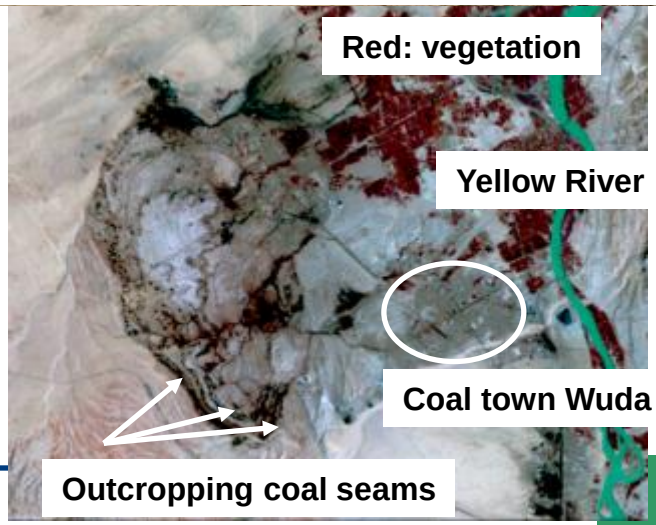

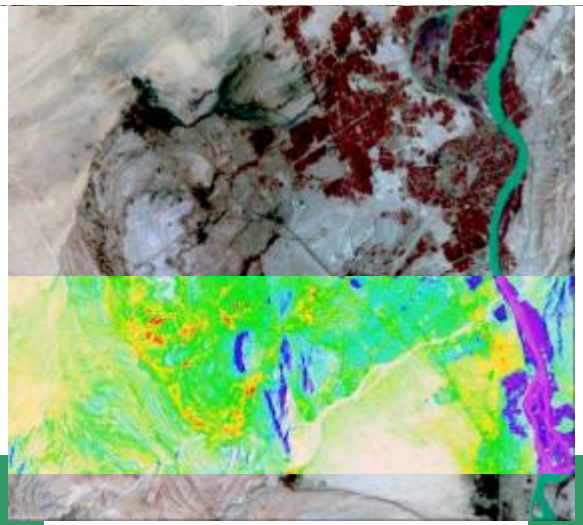

Thermal Expression of Coal Fires In-Situ

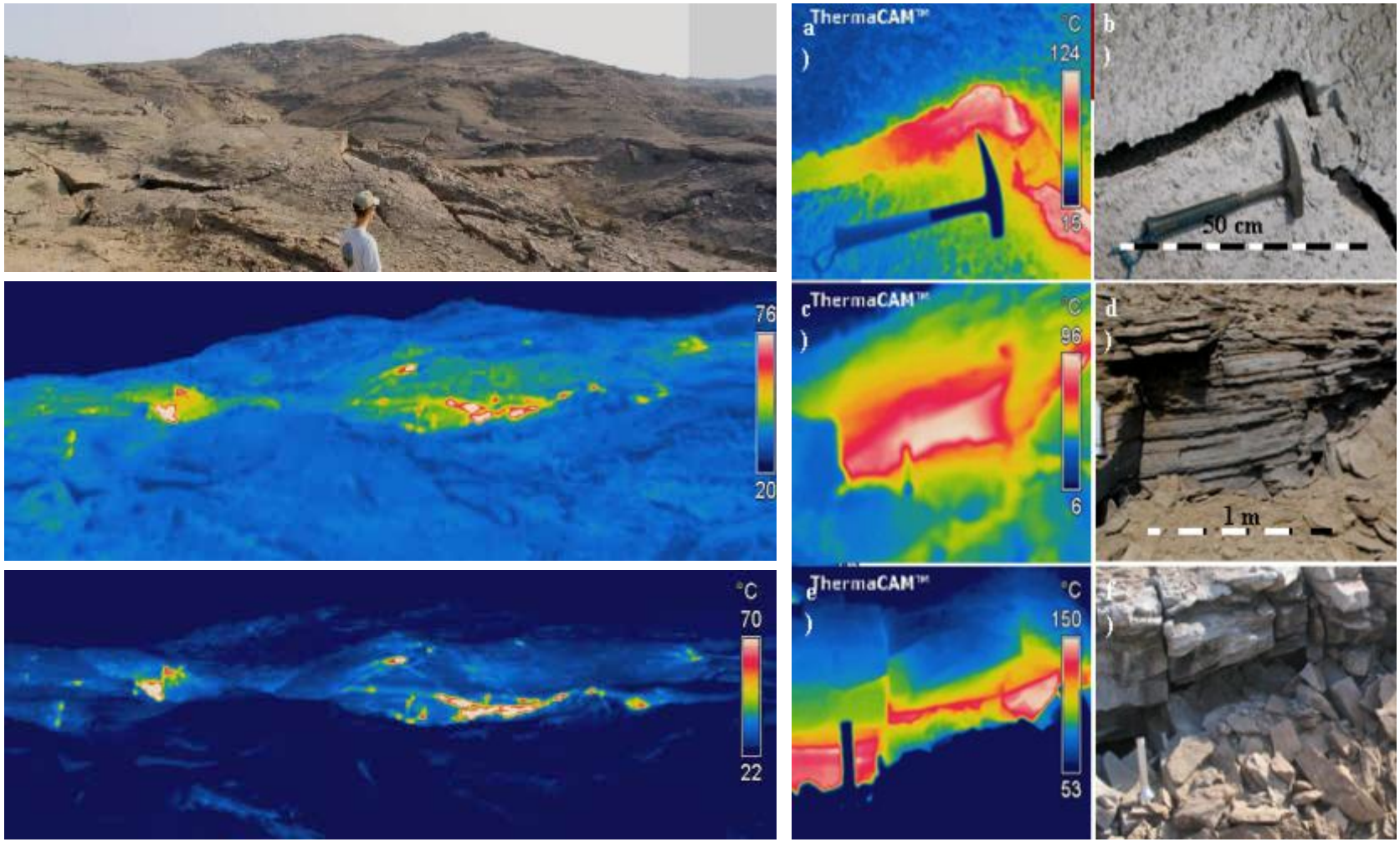

Thermal Characteristics of Coal Fires: WEAK Anomalies

(much different from e.g. forest fires !)

Real subsurface coal fire

Simulated surface coal fire

Statistical fire properties:

- Fire temparatures strongly varying
- Coal fire areas in satellite imagery: high variability
- Coal fire areas do not exceed a certain size
- Contrast in night time data higher
- Contrast in winter data better than in summer data
- Solar influence least pre dawn
- Surface coal fires give stronger expression

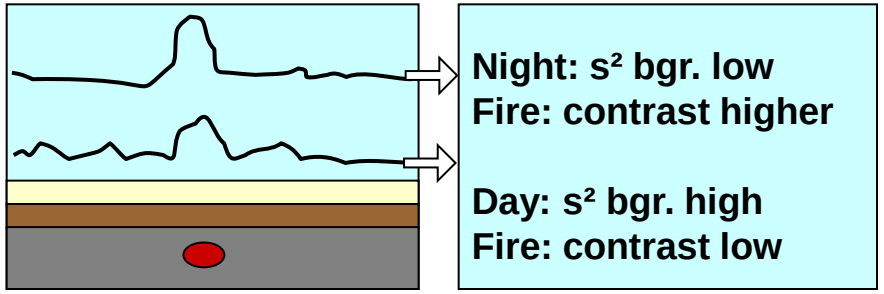

Thermal on Site Experiments with different Fires

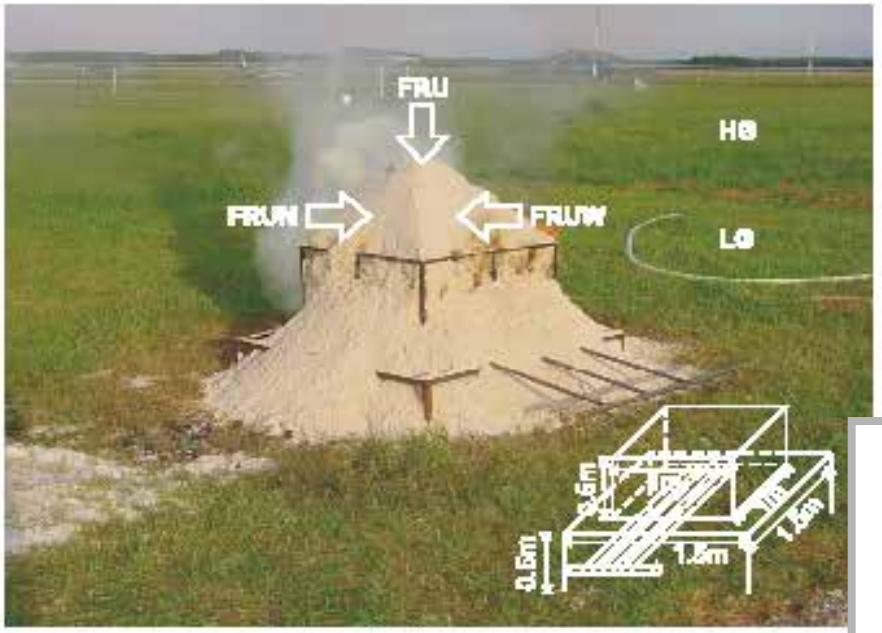

ZHANG, J. and **KUENZER, C**., 2007: Thermal surface characteristics of coal fires 1: Results of in-situ measurements. Journal of Applied Geophysics, DOI:10.1016/j.jappgeo.2007.08.002, Vol. 63, pp. 117-134

ZHANG, J., **KUENZER, C**., TETZLAFF, A., OERTL, D., ZHUKOV, B. and WAGNER, W., 2007: Thermal characteristics of coal fires 2: Results of measurements on simulated coal fires. Journal of Applied Geophysics, DOI:10.1016/j.jappgeo.2007.08.003, Vol. 63, pp. 135-147

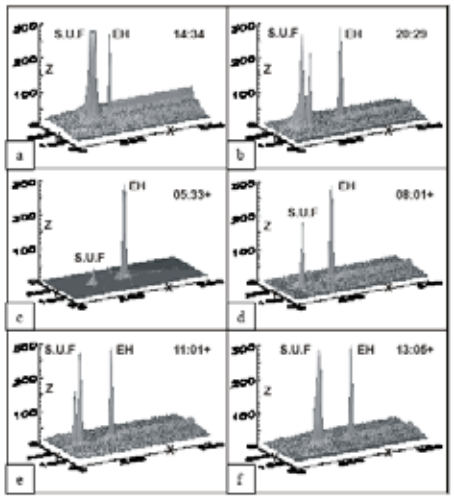

Figure 9: MP 50 line scanner Images. X: Rows; Y: Columns; Z: Temperature (°C); S.U.F.: Simulated underground coal fire, EH: Electric heater. The coal fire with a dimension of 1m*1m forms an outstanding thermal anomalous cluster in MP 50 line scanner images, whose spatial resolution is 5cm.

Regional Thermal Anomaly Detection Algorithm

Based on statistical analysis of image subwindows and texture parameters

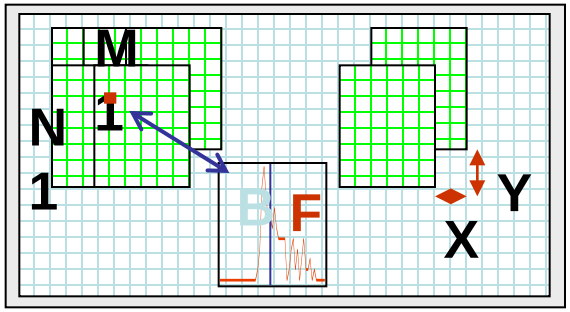

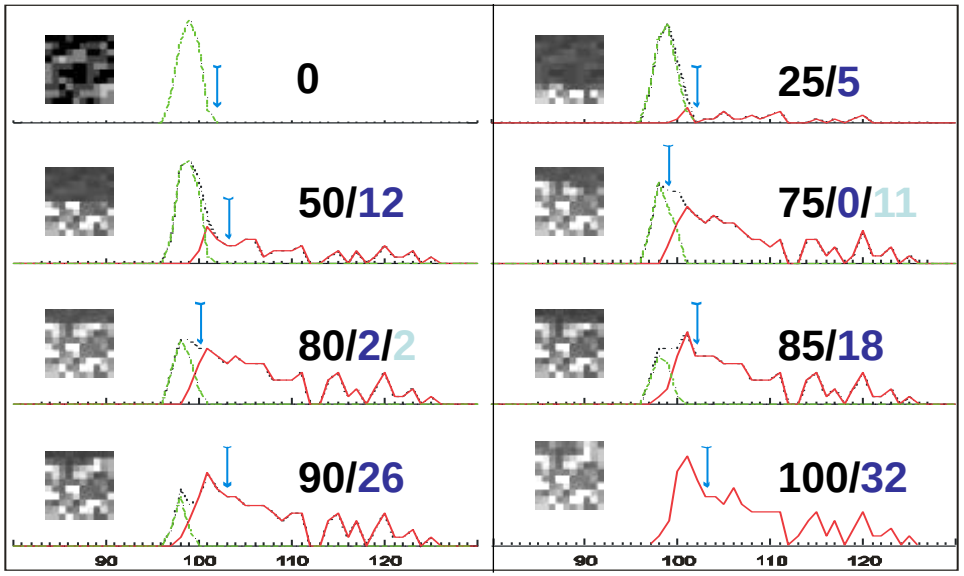

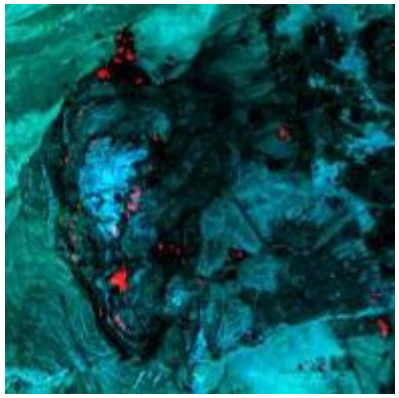

11x11 to 35x35

Only if pixel counted 70% of times

(121 to 1225 times) = thermal anomaly

70%-85%: probability 1

>85%: probability 2

KUENZER, C., ZHANG, J., LI, J., VOIGT, S., MEHL, H. and WAGNER, W., 2007: Detection of unknown coal fires: synergy of coal fire risk area delineation and improved thermal anomaly extraction. In: International Journal of Remote Sensing, DOI: 10.1080/01431160701250432, Vol. 28, pp. 4561-4585

Thermal Anomaly Extraction from EO Data

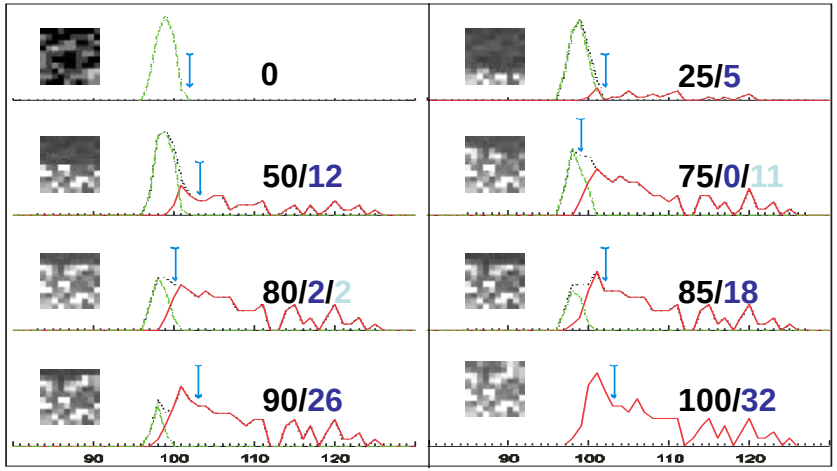

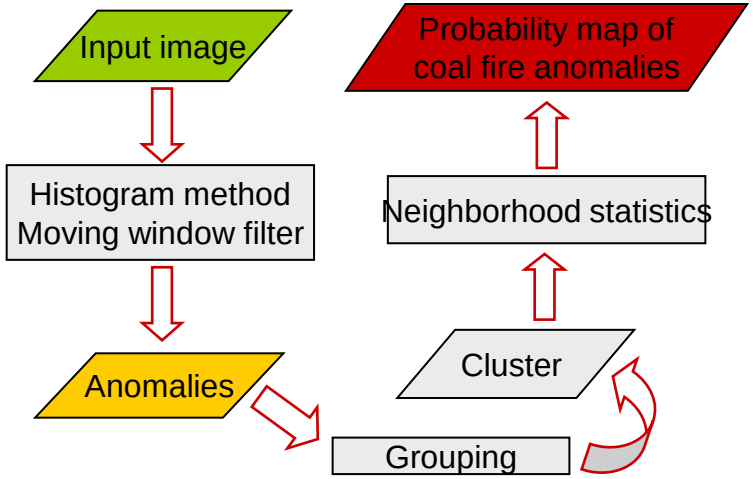

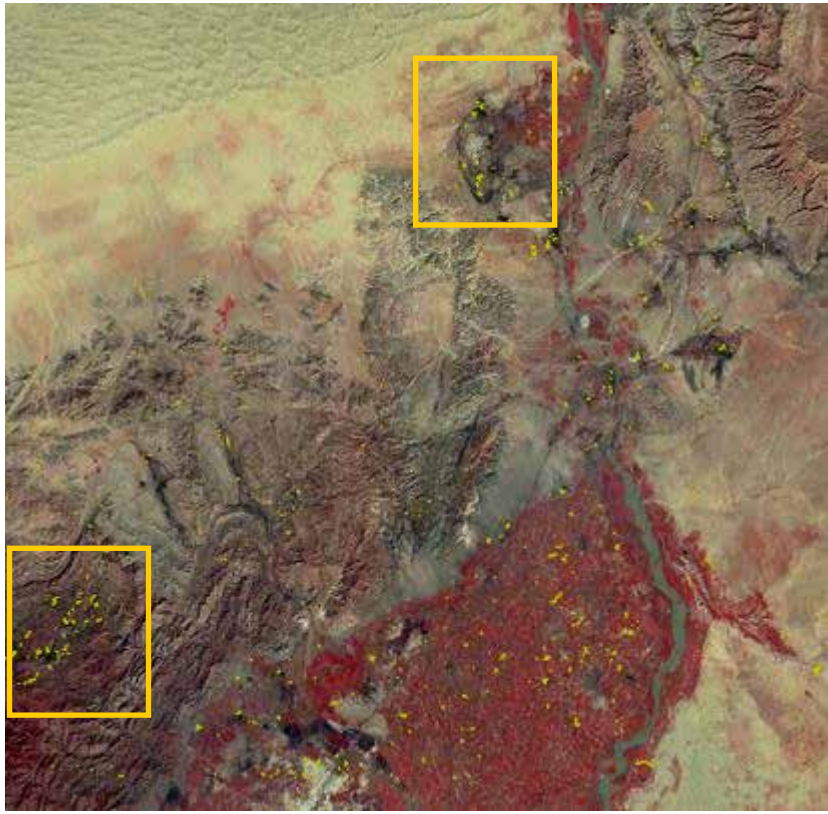

Coal Fire Area Demarcation: Present Areas and Risk Areas

Detection of Unknown Fires in 2004

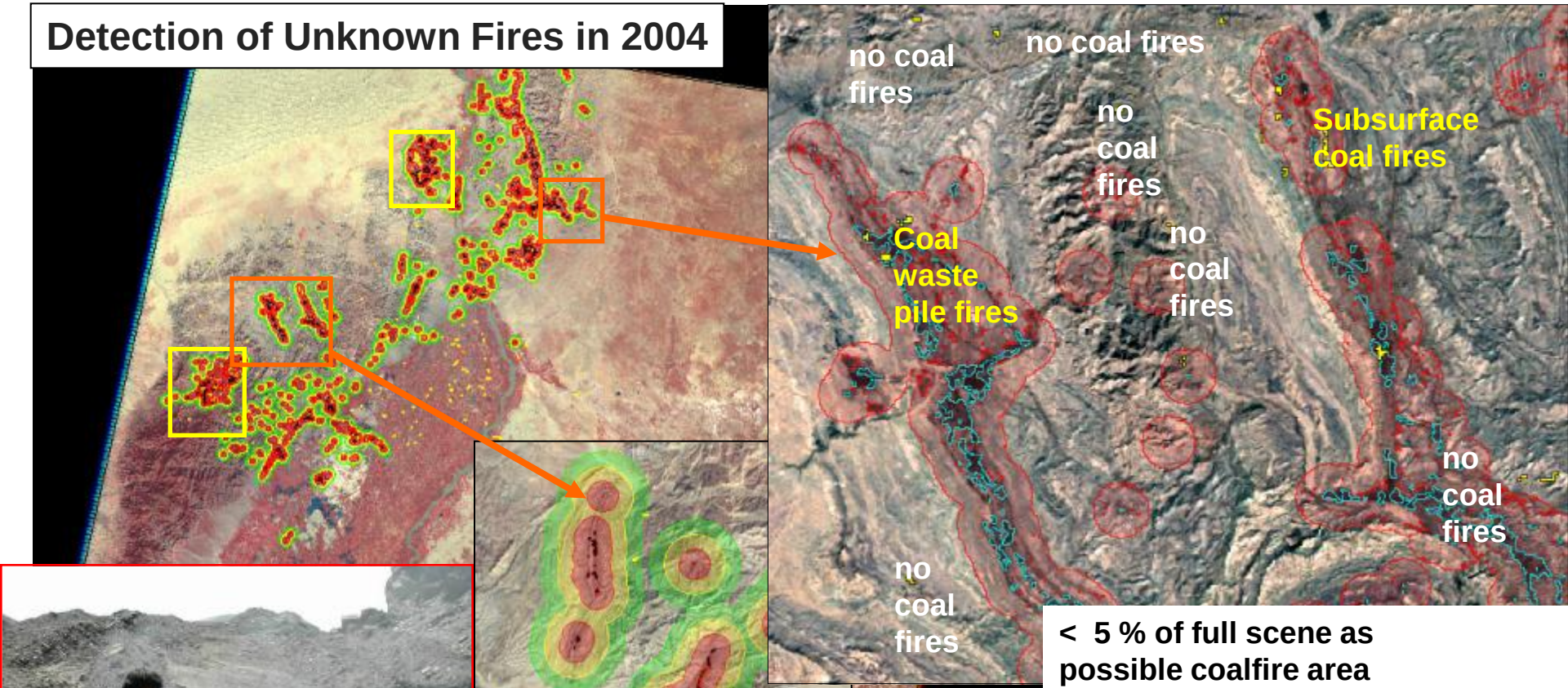

< 5 % of full scene as possible coalfire area

new fires detected
4 underground
2 coal waste piles

risk areas

Thermal Anomaly Quantification

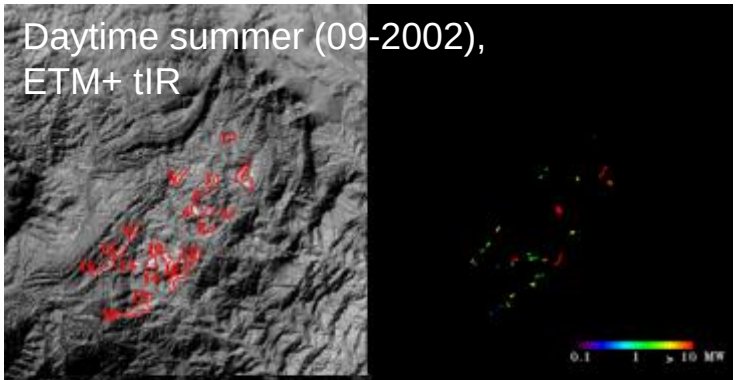

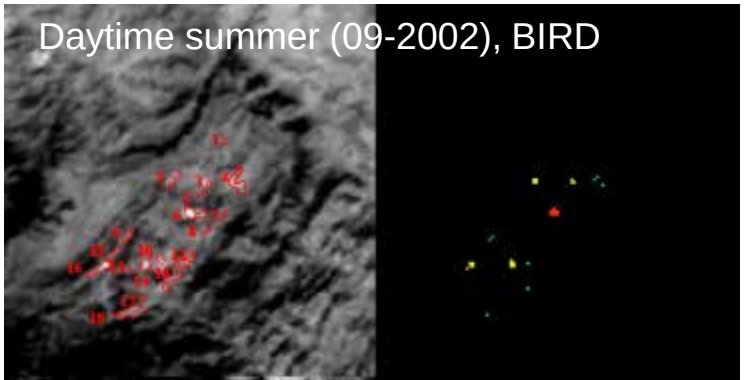

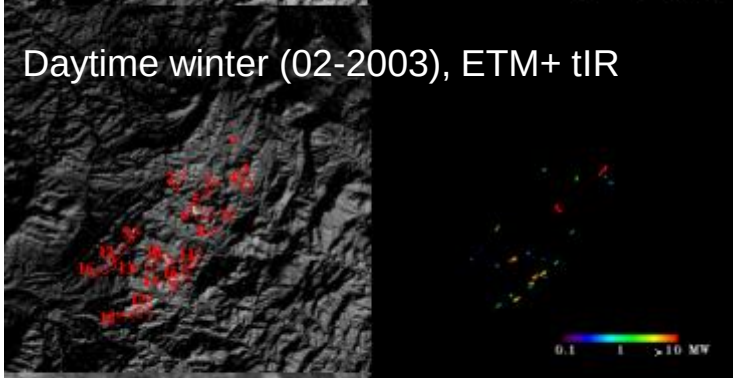

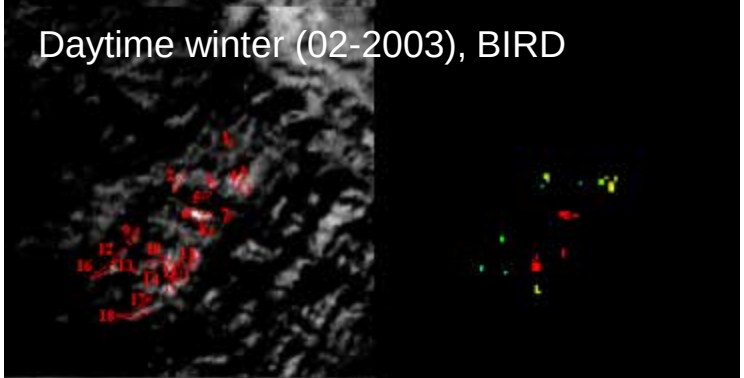

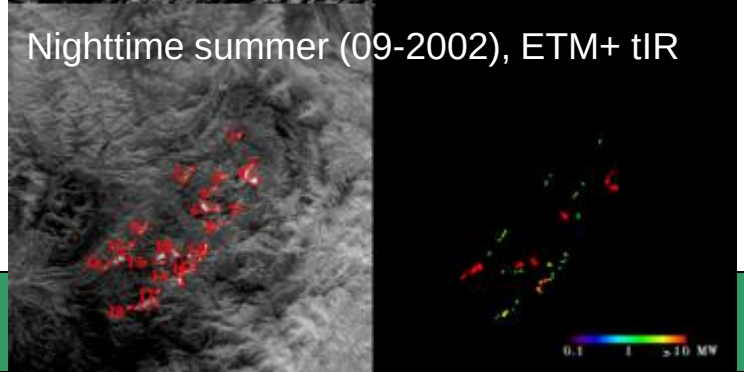

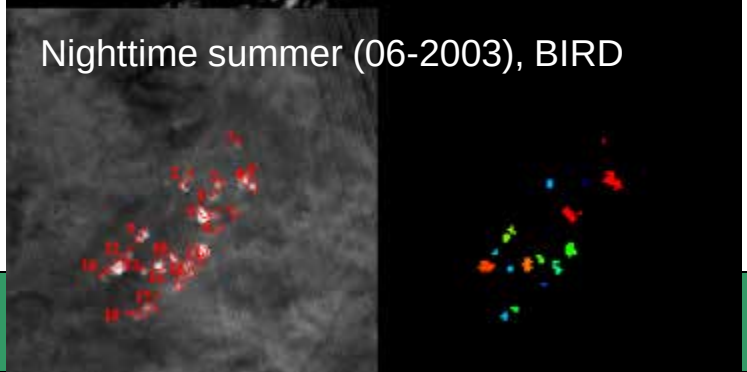

(Post-) Kyoto Relevance

Simplified Model of the Origin of Greenhouse Gases during Complete and Incomplete Combustion

Complete combustion

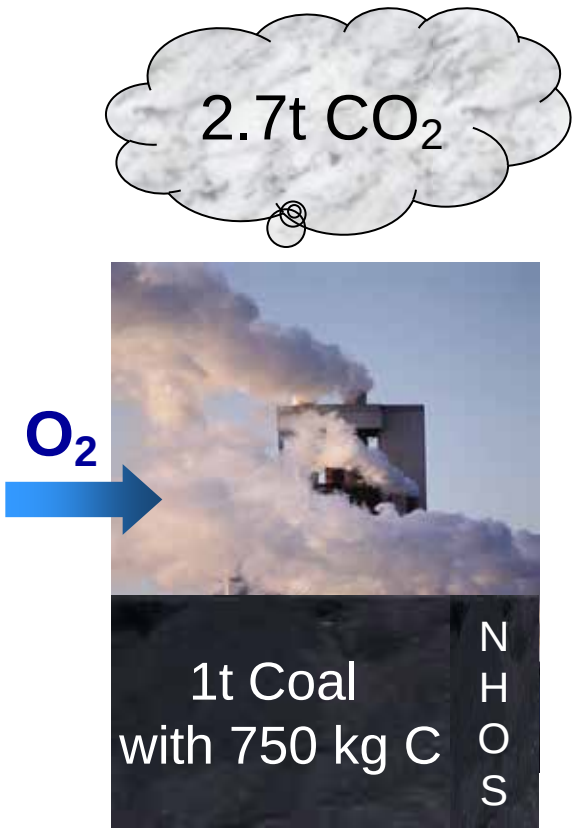

Incomplete combustion (coal fire)

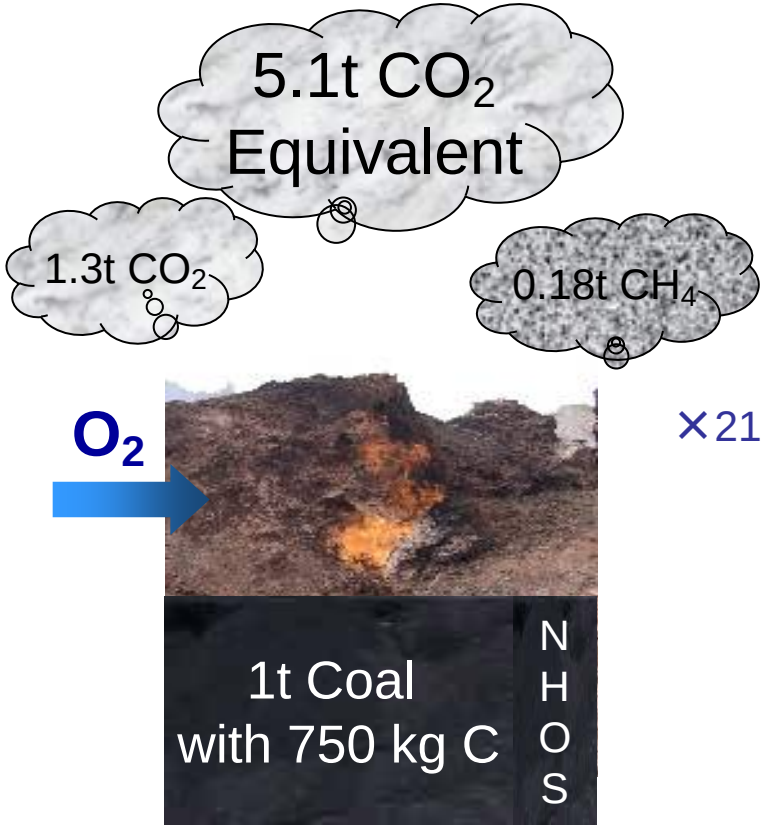

Gas Temporal Variability – Ventilation Pathways

Gas Variability

CO [ppm]

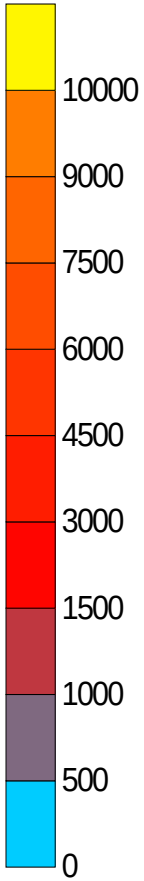

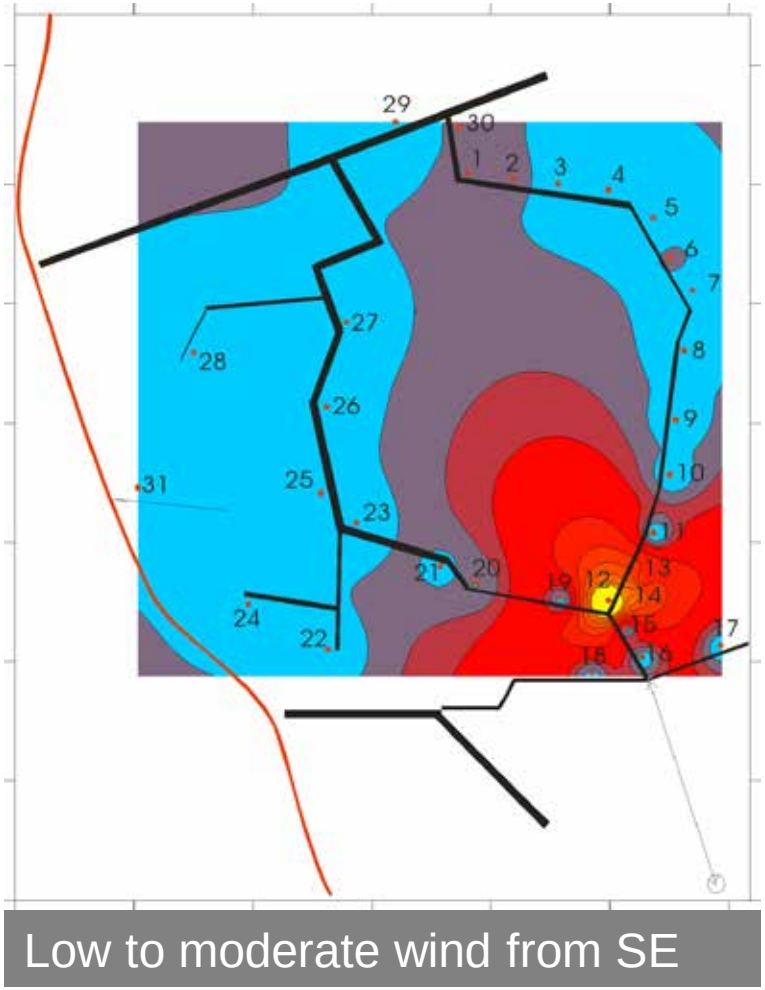

Low to moderate wind from SE

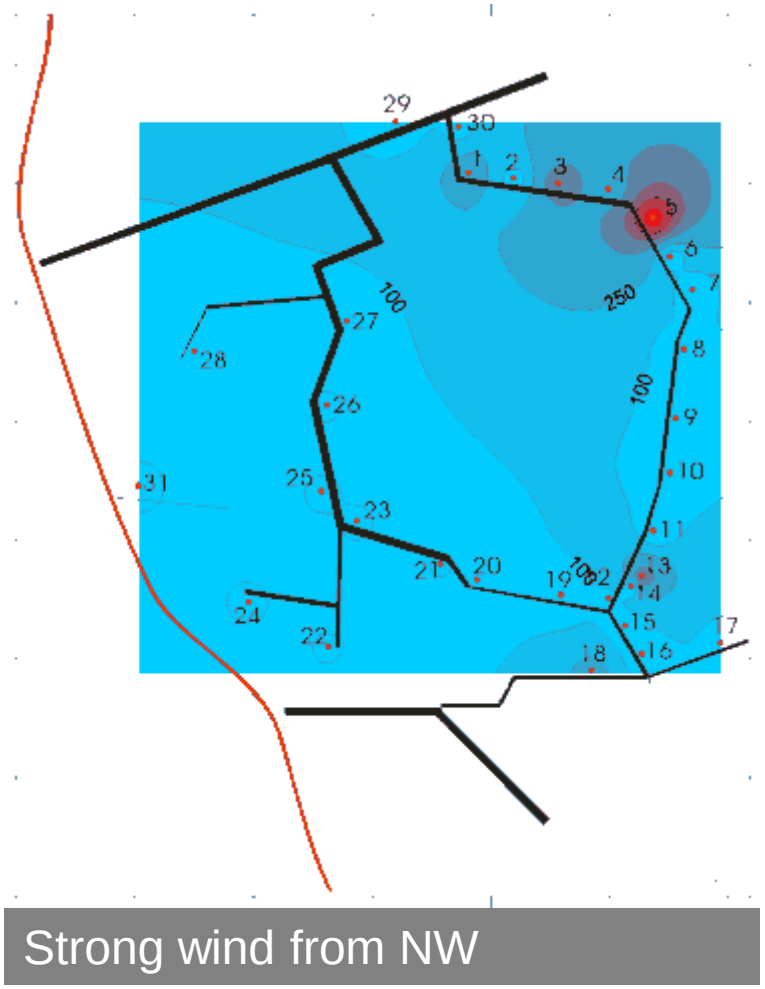

Strong wind from NW

Coal Fire Mapping in-situ (2000-2005, 2008)

- Every year over 600 to 1000 thermal point measurements
- For each fire point maximum, minimum and average temperature
- Differentiation in colder and hotter areas
- Polygons yearly updated and provided to partners, mines, minng authorities

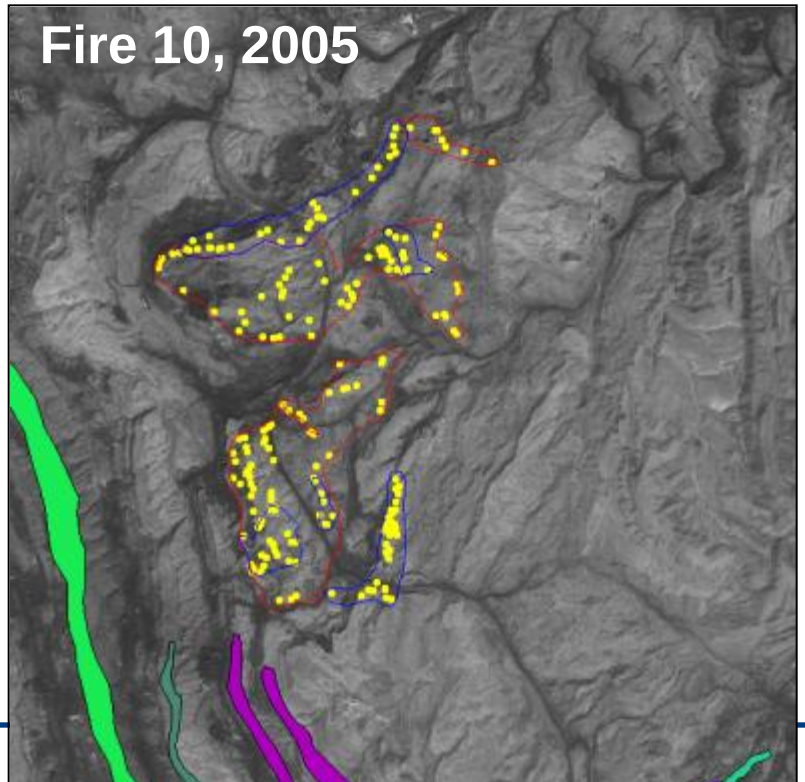

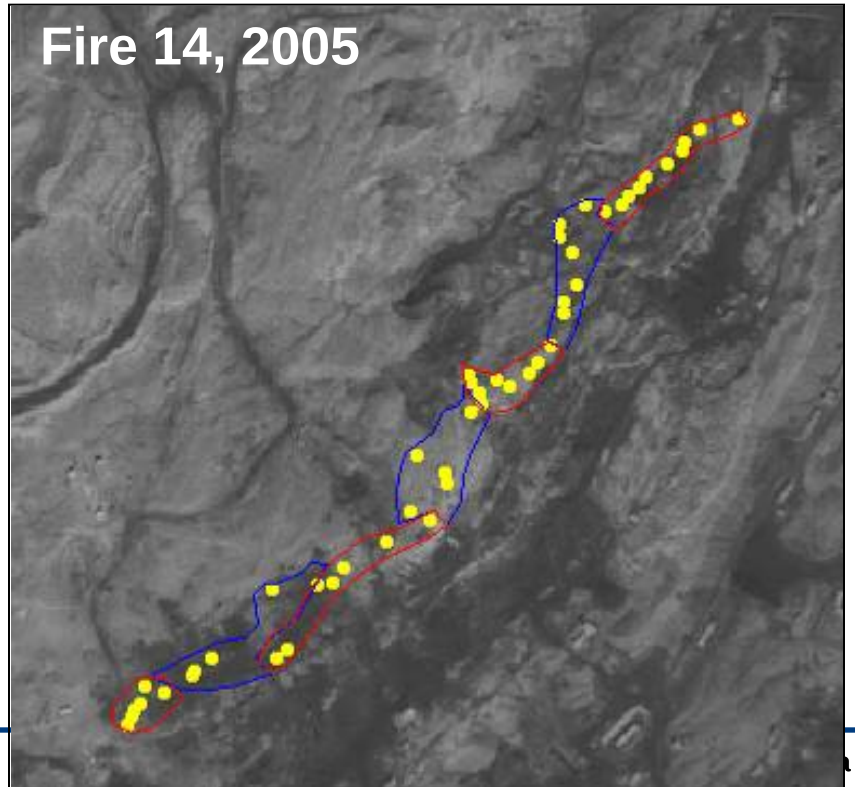

Field Mapping versus Remote Sensing

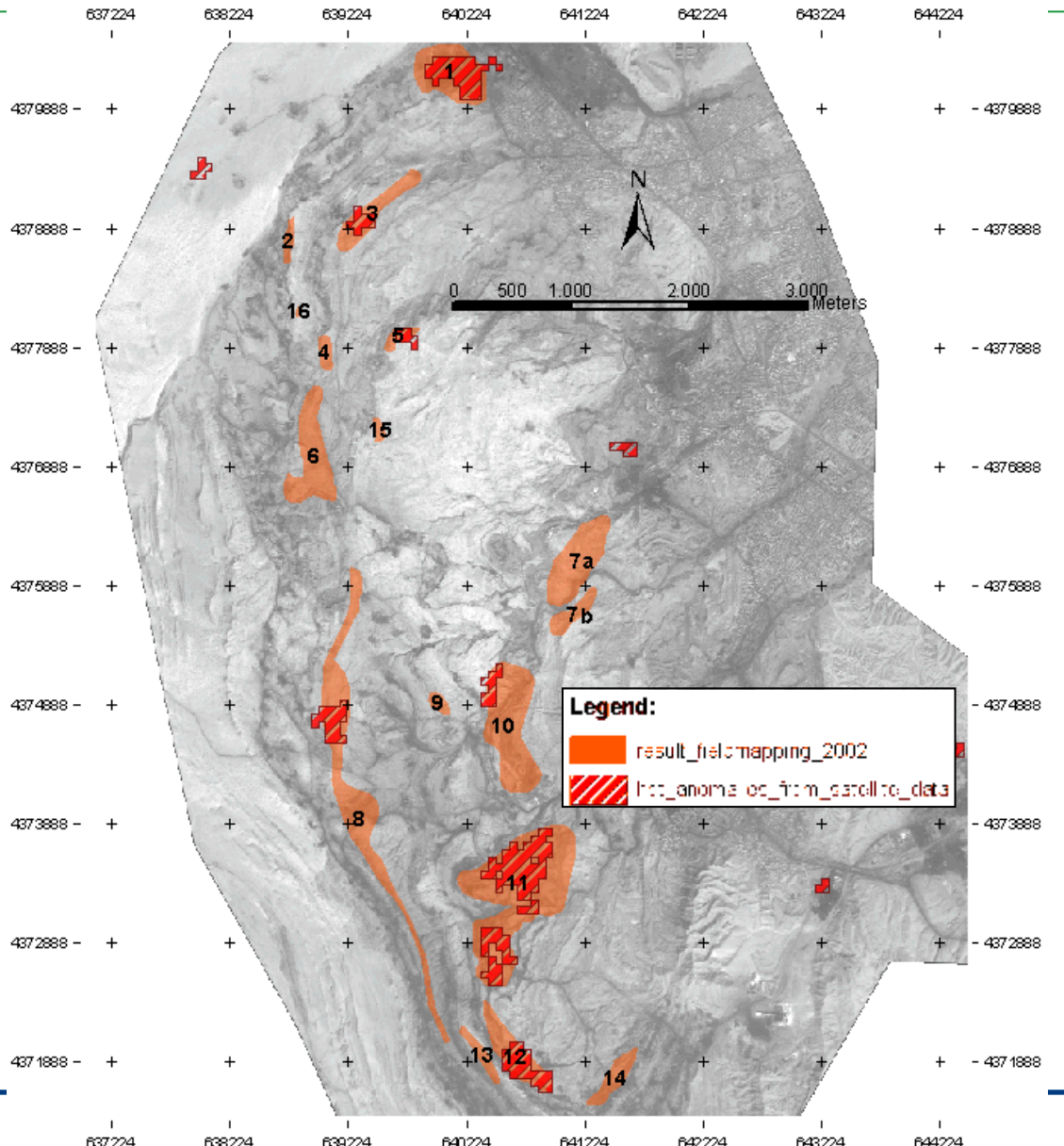

Changes in Extent within one Year (2004-2005)

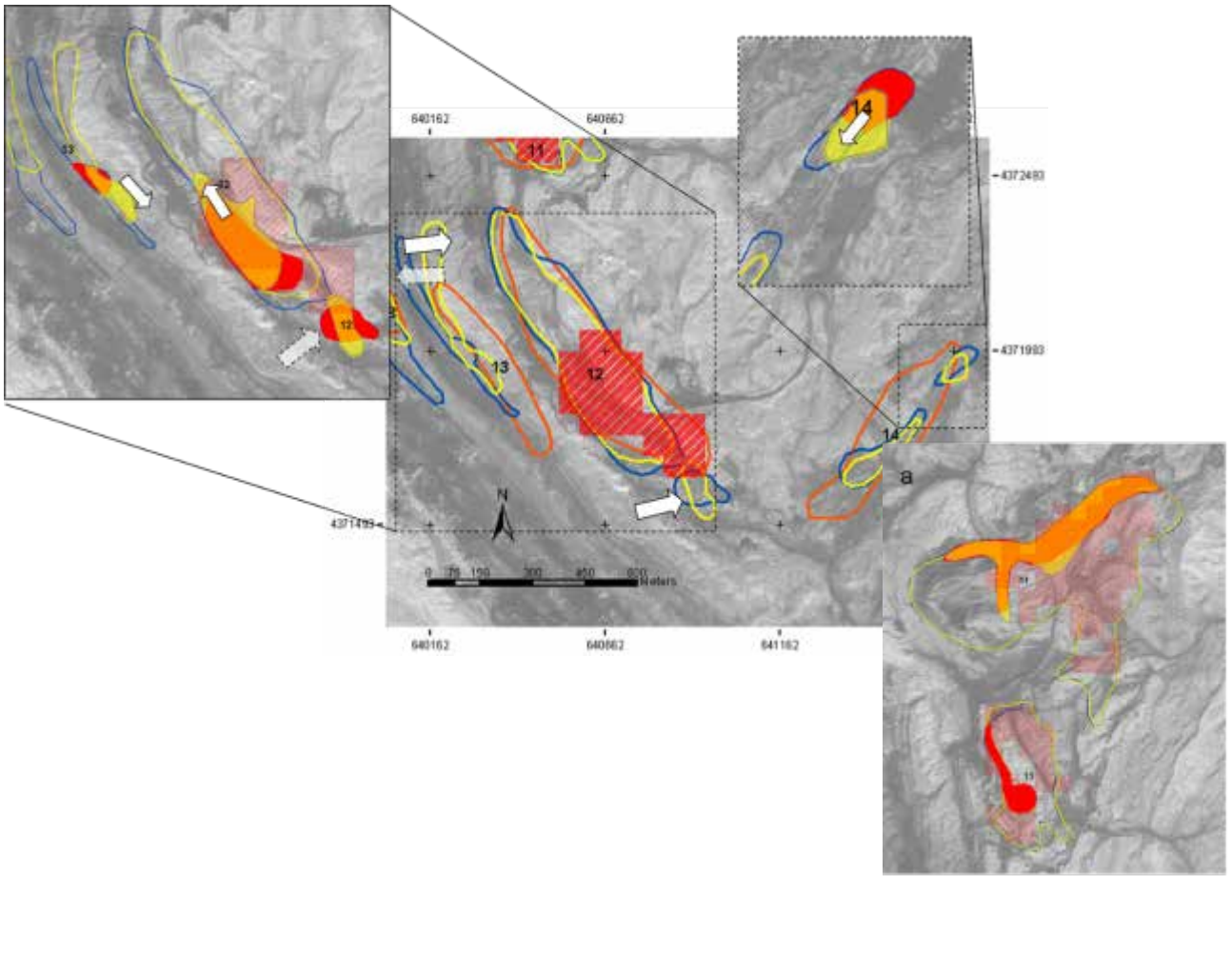

Changes in Extent within one year (2004-2005)

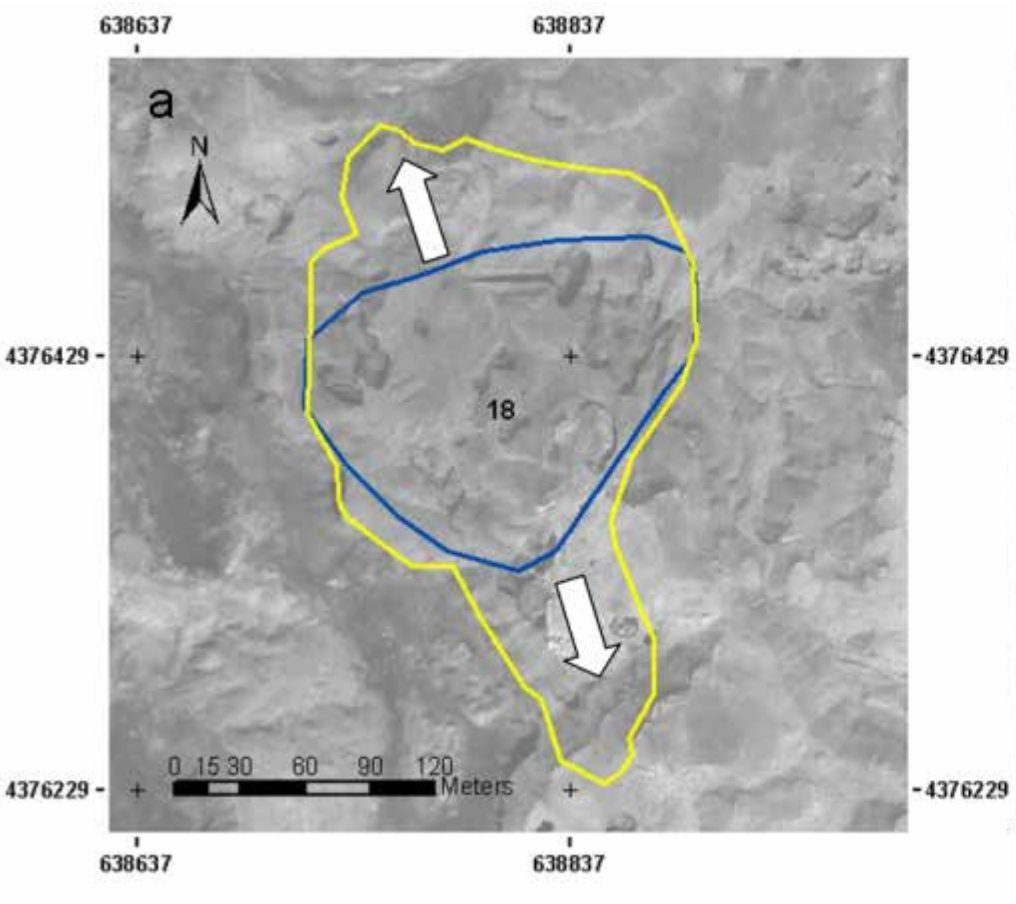

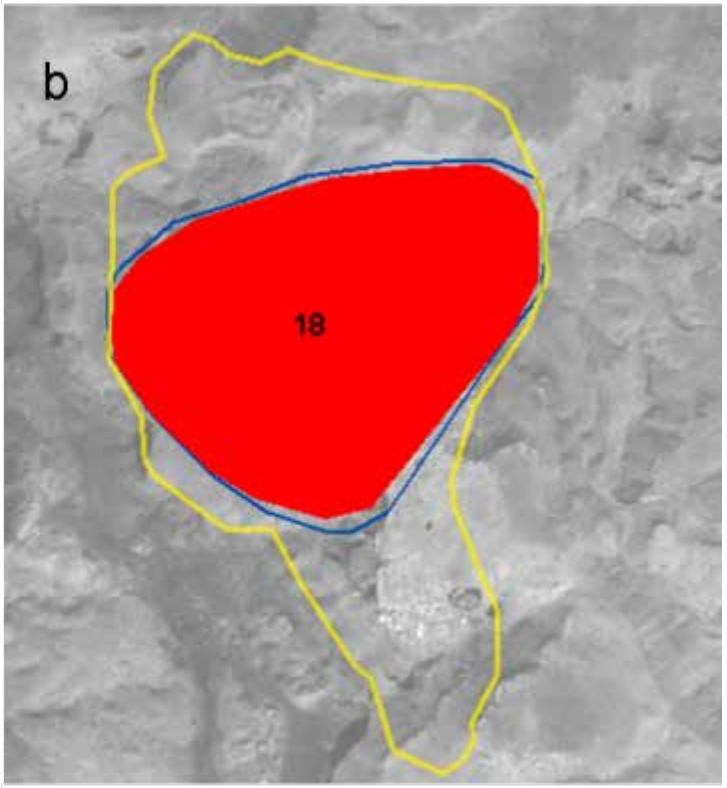

Multi-Sensor Transfer from Landsat to MODIS:

- ASTER à often: ‘occupied’, data not always available
- LANDSAT à ETM+ erroneous, new mission soon
- NOAA, AATSR etc, only one thermal band

à **Suitability of low resolution MODIS data to monitor subtle coal fire related thermal anomalies ?**

The MODIS Sensor: Coverage of the Thermal Domain

- **36 bands**, bands 8-36 1km res., Relevant for LST analyses: bands 20-23 (3,66 – 4,08µm) and 31, 32 (10,78 – 12,27µm)
- **TERRA ('99), AQUA ('02)** à 4-5 times within 24 hour cycle (diurnal cycle), if large scan angles accepted (overlap frames)
- **4-5 days if nadir** (climate rel. bgr. variations over 4 days < than diurnal var.)
- Favorable for **hotspot detection** within 24 hour cycle: Night. Best: predawn (solar effects least accentuated); Seasonal: early spring or late autumn (or if no-snow-area even winter)
- **Data free of charge**, some preprocessing needed: bowtie correction, geocorrection with geolocation files, radiance to temp. conversion

Adapted to low resolution MODIS Data

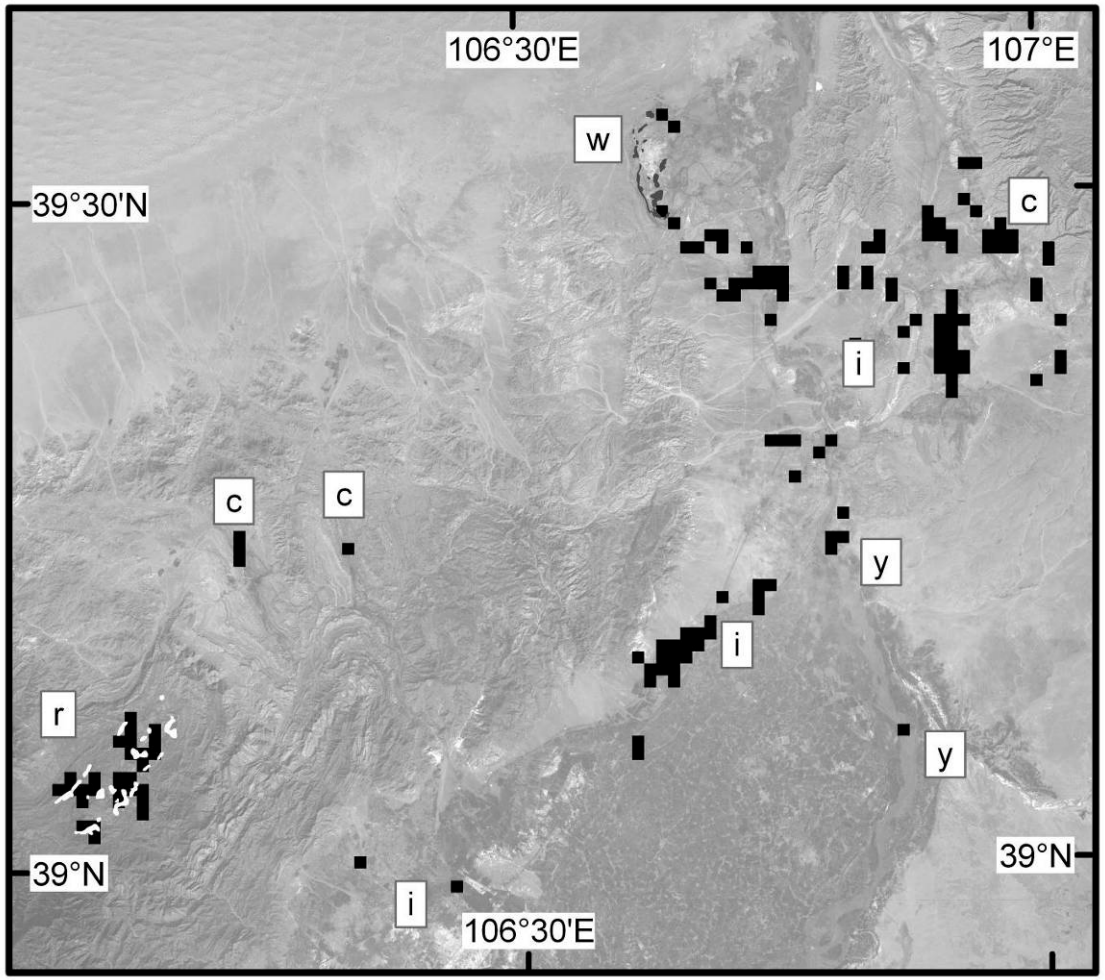

Automatic detection in MODIS pre-dawn data (China)

- Coalfires
- Industry

Study Area, Data, Research Setup

- Jharia coalfield, largest coalfire globally, 50-100 fires, 1916 first

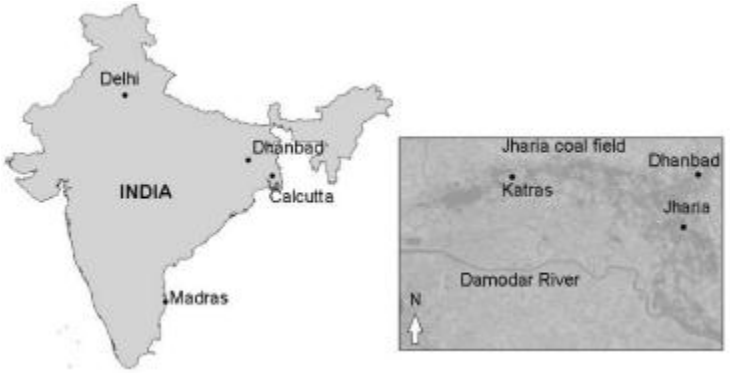

- 4 Scenes: Feb 2005 (morning, afternoon, evening, predawn)

- band 20 (3,66-3,84µm) and 32 (11,77-12,27µm), furthest apart = good contrast between 20 (outstanding hot spot signals, few reflected and mainly emitted components) and 32 (representing temp. pattern in common thermal domain, only emitted components)

- Creation of ratio band: 20/32. à pixels with similar emission in both bands = values close to 1. Pixels with relatively greater radiance in 20 yield values > 1. à Ratio of 20/32 enhances very strong hot spots

- Automated algorithm for the detection of relative thermal anomalies

Thermal Infrared

The capability of MODIS diurnal thermal bands observations

MODIS band 20/32 Ratio Images

- Predawn, 17. Feb. 2005
- b, c: background temp. strong var. Lighter pixels = higher temps.
- Ratio image enhances hot thermal anomalies as high pixel values and suppresses background variation

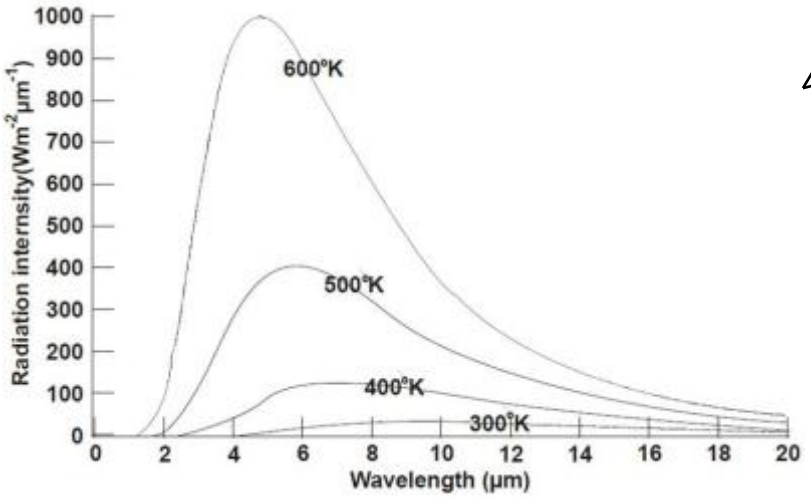

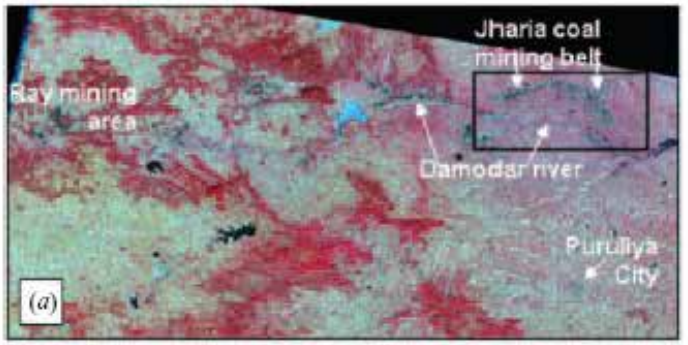

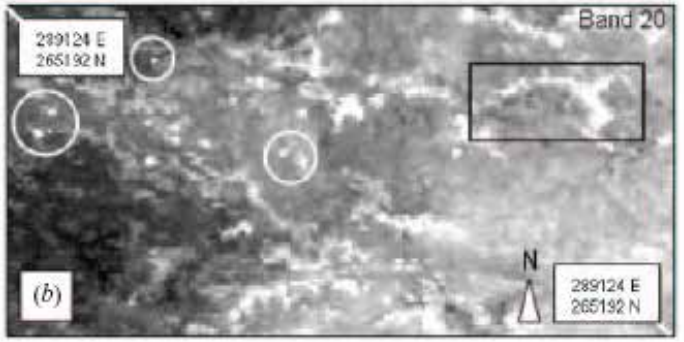

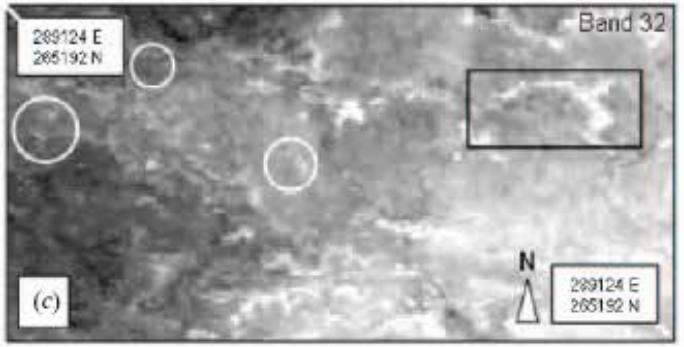

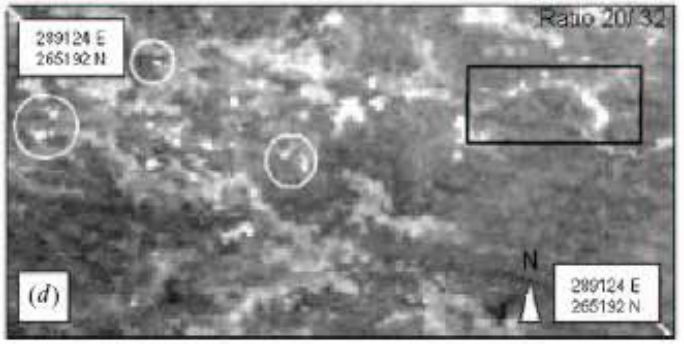

The capability of MODIS diurnal thermal bands observations

Application of the Algorithm to MODIS

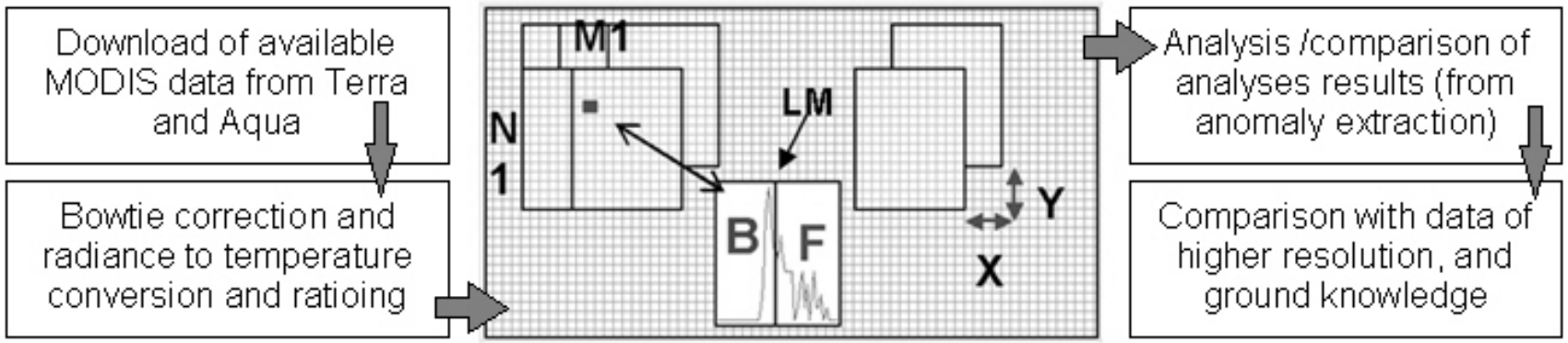

- 20, 32 and ratio underwent algorithm

- Output:
  - Background = black, 0;
  - Regional anomalies counted 70%-85% of times = grey, 1
  - Anomalies counted > 85% of times = white, 2.

Thermal Infrared

The capability of MODIS diurnal thermal bands observations

Result of Anomaly Extraction

(20, 32, ratio from predawn)

- **R**esult overlain on a Landsat scene
- **b:** anomalies from band 20, c: anomalies from band 32, d: anomalies from ratio
- **B**lack = non-anomalous, grey: 70-85% counted, white: > 85% counted
- **J**haria: most outstanding cluster
- **2**0, 32: +/- same amount of clusters, but more in South of 32 ß clusters not warm enough to stick out in 20
- **R**atio: overall fewer anomalies, surpression of background, very strong hotspots. Major hot spots also within coal fire area.

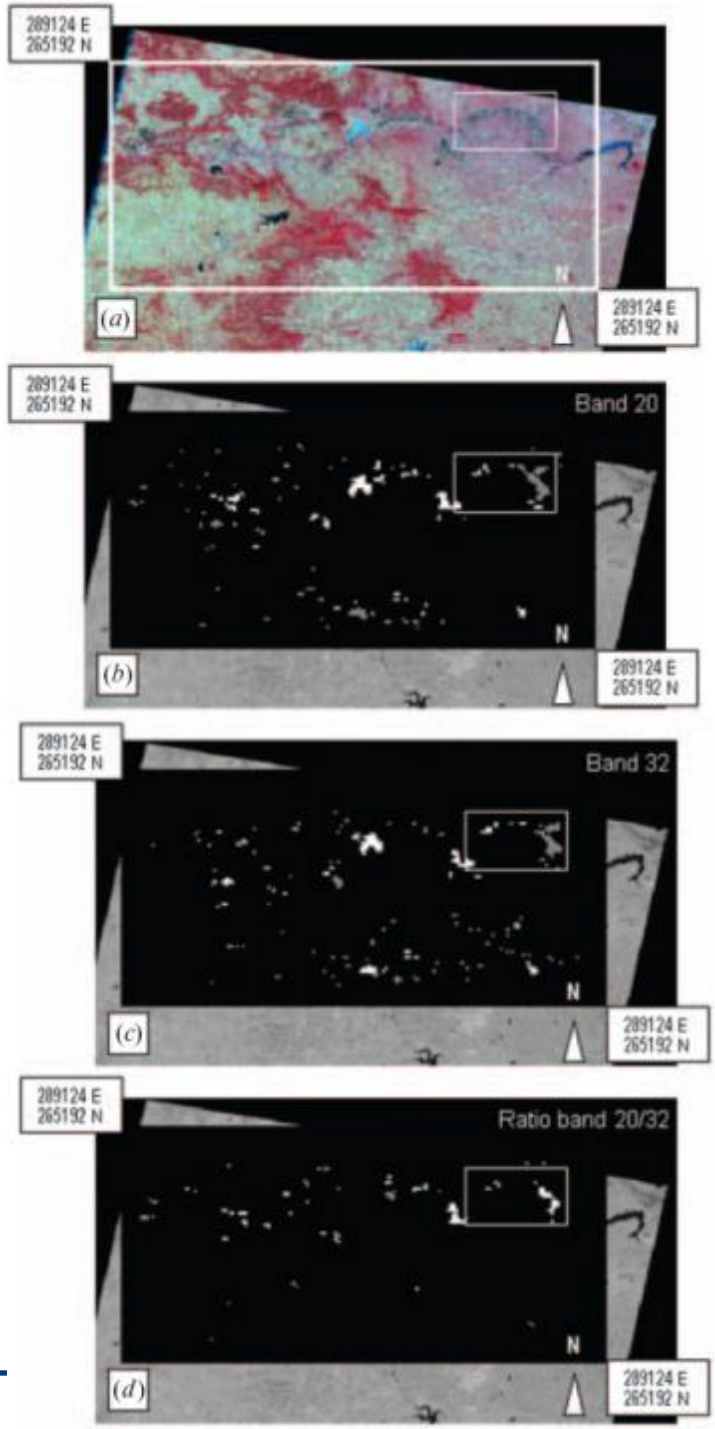

Extraction from Ratio Band

(morning, afternoon, evening, predawn)

- a: morning, b: afternoon, c: evening,
  d: predawn
- Jharia most prominent cluster
- Opposite to band 32 here only the hottest spots of the coalfire zone extracted
- Further hotspots from industry, humans
- Comparing 32 and Ratio: allows to draw conclusion on strength of anomaly
- Statistical calculations: in all images: decrease in anomalies towards afternoon, increase again towards predawn, cluster size largest during predawn (but here human influence)

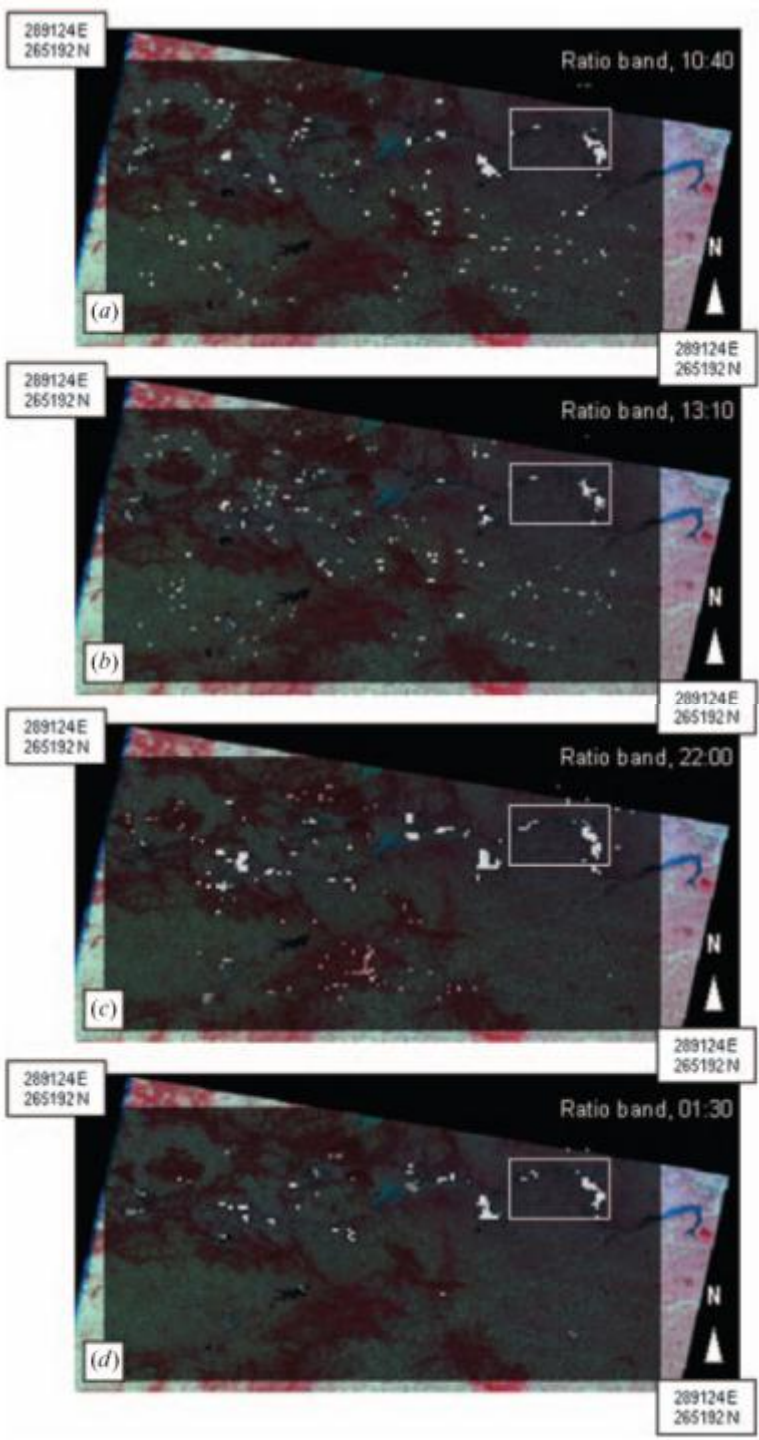

Comparison with High-Res. TIR Data and Ground Truth

- **A**STER night-time band 15 (10,95–11,65µm) = comparable to 32
- anomalous clusters extracted from ASTER = orange, MODIS 32 anomalies = grey, hottest zones from ratio image = white. All extracted ASTER hot spots directly on top of or adjacent to MODIS anomalies (slight shift due to rough geolocation?). No clusters outside coalfire area or settled region.
- **B**: Landsat-5 TM based extraction (manually) Chatterjee (2006) from 1992 data, confirmed in 2003
- **C**: in-situ mapping result of Michalski (2004)

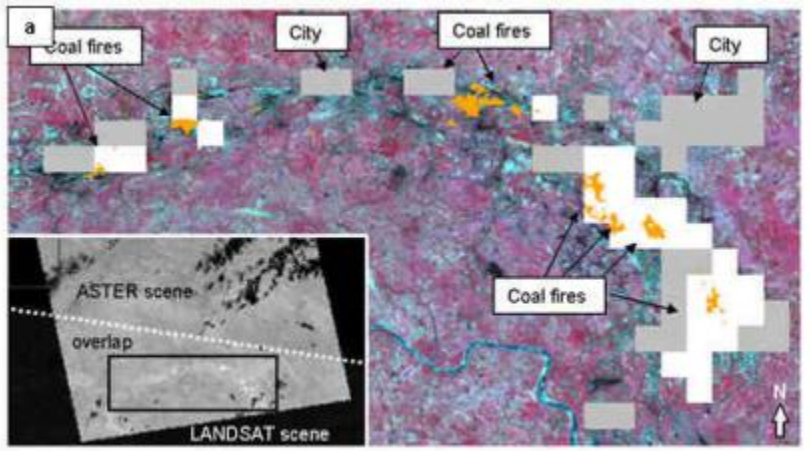

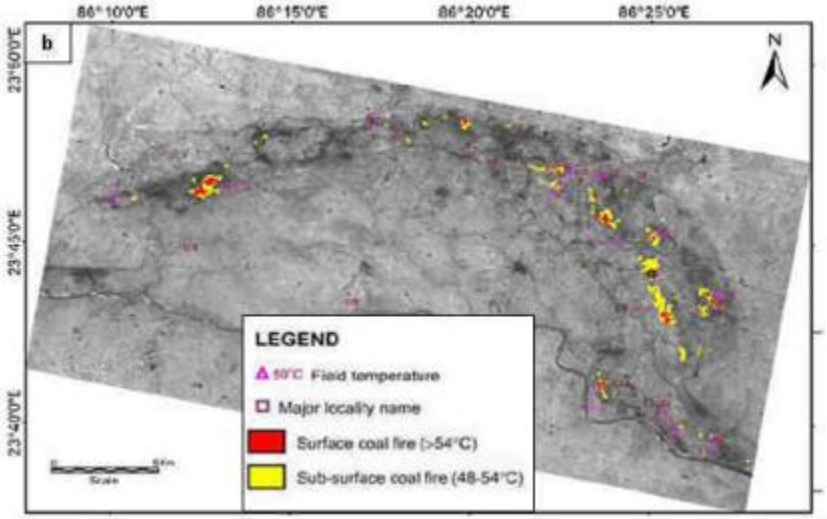

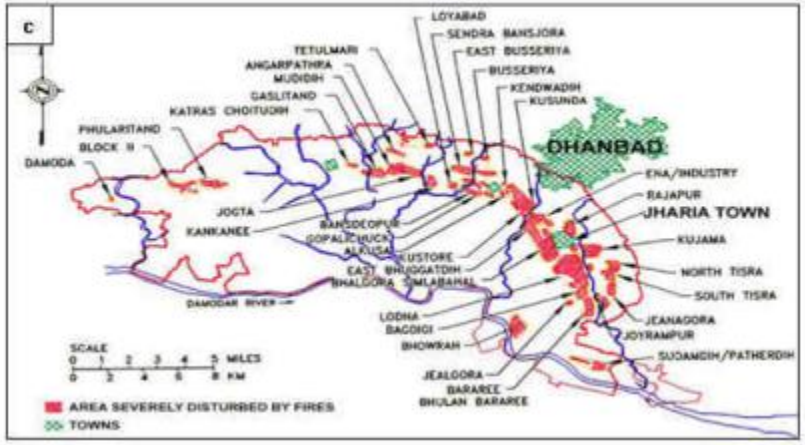

Summary: multi-diurnal and multi-band Analyses

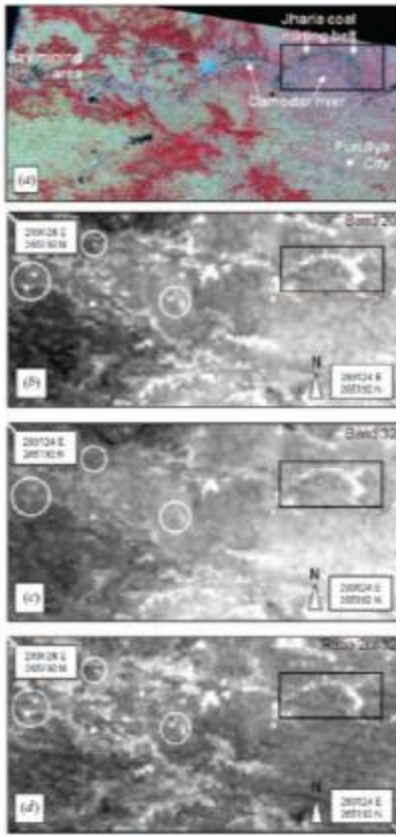

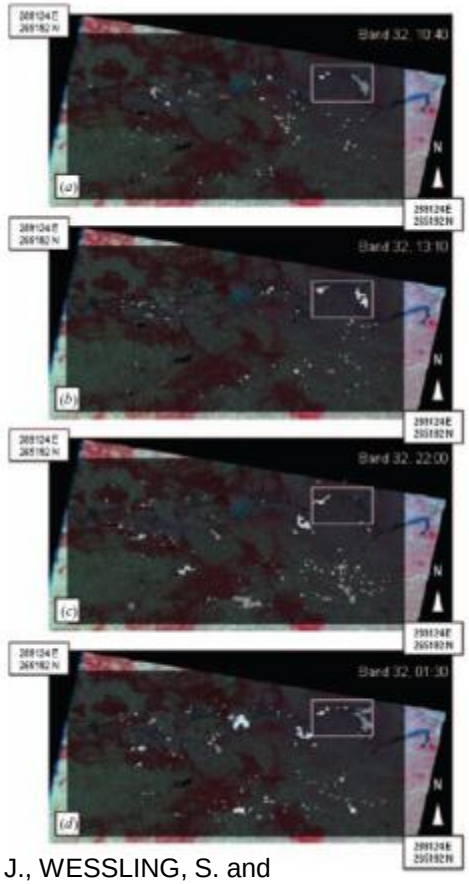

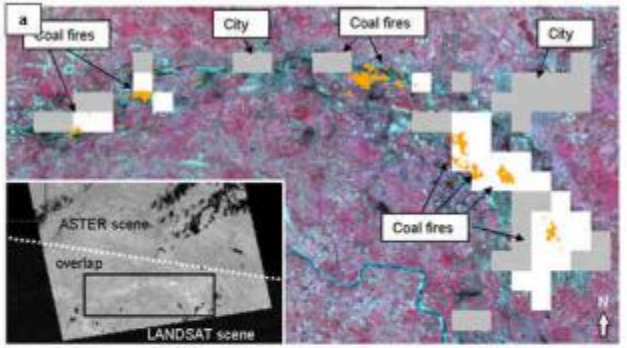

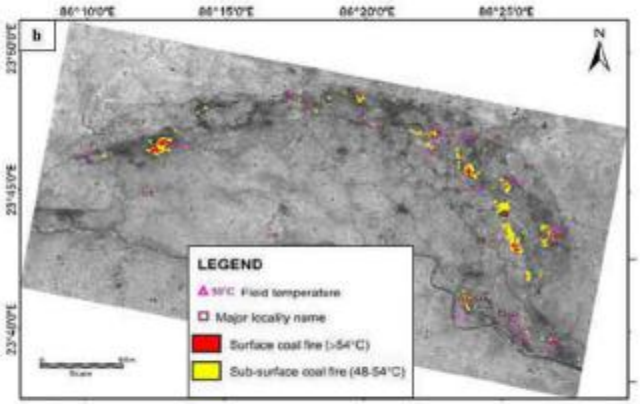

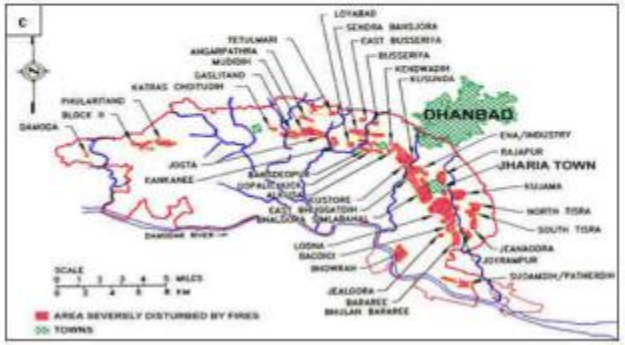

KUENZER, C., HECKER, C., ZHANG, J., WESSLING, S. and WAGNER, W., 2008: The potential of multi-diurnal MODIS thermal bands data for coal fire detection. In: International Journal of Remote Sensing, Vol. 29, 923-944, DOI: 10.1080/01431160701352147

Conclusion

- **Weak thermal anomalies cannot be extracted with simple thresholding; but moving window algorithm presented is suitable**
- **Sensors Landsat, Aster, and MODIS suitable. Thermal MODIS bands allow for multi-diurnal dense observation = optimal thermal monitoring at low cost**
- **Ratio images of 20/32 à extraction of outstanding hotspots**
- **Automated thermal anomaly extraction = little bias, no manual “thresholding”, and “twisting until it fits”**
- **Diurnal approach interesting for forest fire activity monitoring (changes in energy release), industry observation, urban heat pattern analyses, thermal pollution along rivers and coasts, observation of geothermal phenomena, etc.**

EARSEL Special Interest Group: Thermal Remote Sensing

- Visit: www.itc.nl/sigtrs

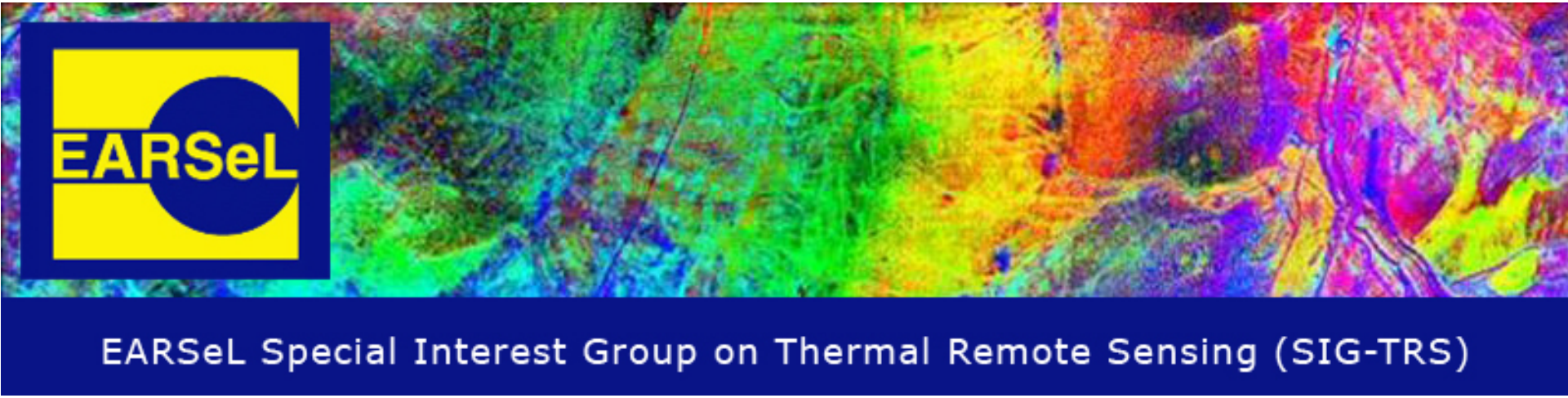

Thermal Infrared Remote Sensing